University of Windsor
Scholarship at UWindsor

Electronic Theses and Dissertations

1993

Onset and cessation of nucleate boiling.

Ignacio Ramiro. Martin Dominguez
University of Windsor

Follow this and additional works at: http://scholar.uwindsor.ca/etd

Recommended Citation
Martin Dominguez, Ignacio Ramiro., "Onset and cessation of nucleate boiling." (1993). *Electronic Theses and Dissertations.* Paper 2930.

This online database contains the full-text of PhD dissertations and Masters' theses of University of Windsor students from 1954 forward. These documents are made available for personal study and research purposes only, in accordance with the Canadian Copyright Act and the Creative Commons license—CC BY-NC-ND (Attribution, Non-Commercial, No Derivative Works). Under this license, works must always be attributed to the copyright holder (original author), cannot be used for any commercial purposes, and may not be altered. Any other use would require the permission of the copyright holder. Students may inquire about withdrawing their dissertation and/or thesis from this database. For additional inquiries, please contact the repository administrator via email (scholarship@uwindsor.ca) or by telephone at 519-253-3000ext. 3208.

National Library
of Canada

Acquisitions and
Bibliographic Services Branch

395 Wellington Street
Ottawa, Ontario
K1A 0N4

Bibliothèque nationale
du Canada

Direction des acquisitions et
des services bibliographiques

395, rue Wellington
Ottawa (Ontario)
K1A 0N4

Your file Votre référence

Our file Notre référence

NOTICE

The quality of this microform is heavily dependent upon the quality of the original thesis submitted for microfilming. Every effort has been made to ensure the highest quality of reproduction possible.

If pages are missing, contact the university which granted the degree.

Some pages may have indistinct print especially if the original pages were typed with a poor typewriter ribbon or if the university sent us an inferior photocopy.

Reproduction in full or in part of this microform is governed by the Canadian Copyright Act, R.S.C. 1970, c. C-30, and subsequent amendments.

AVIS

La qualité de cette microforme dépend grandement de la qualité de la thèse soumise au microfilmage. Nous avons tout fait pour assurer une qualité supérieure de reproduction.

S'il manque des pages, veuillez communiquer avec l'université qui a conféré le grade.

La qualité d'impression de certaines pages peut laisser à désirer, surtout si les pages originales ont été dactylographiées à l'aide d'un ruban usé ou si l'université nous a fait parvenir une photocopie de qualité inférieure.

La reproduction, même partielle, de cette microforme est soumise à la Loi canadienne sur le droit d'auteur, SRC 1970, c. C-30, et ses amendements subséquents.

Canada

ONSET AND CESSATION

OF

NUCLEATE BOILING

Dissertation

Submitted to the Faculty of Graduate Studies through the

Department of Mechanical Engineering.

In Partial Fulfillment of the Requirements for the Degree of:

Doctor of Philosophy

at the

University of Windsor

by

Ignacio Ramiro Martín Domínguez

Windsor, Ontario, Canada.

1993

© 1993 I. R. Martín-Domínguez

National Library of Canada
Acquisitions and Bibliographic Services Branch
395 Wellington Street
Ottawa, Ontario
K1A 0N4

Bibliothèque nationale du Canada
Direction des acquisitions et des services bibliographiques
395, rue Wellington
Ottawa (Ontario)
K1A 0N4

Your file Votre référence

Our file Notre référence

The author has granted an irrevocable non-exclusive licence allowing the National Library of Canada to reproduce, loan, distribute or sell copies of his/her thesis by any means and in any form or format, making this thesis available to interested persons.

L'auteur a accordé une licence irrévocable et non exclusive permettant à la Bibliothèque nationale du Canada de reproduire, prêter, distribuer ou vendre des copies de sa thèse de quelque manière et sous quelque forme que ce soit pour mettre des exemplaires de cette thèse à la disposition des personnes intéressées.

The author retains ownership of the copyright in his/her thesis. Neither the thesis nor substantial extracts from it may be printed or otherwise reproduced without his/her permission.

L'auteur conserve la propriété du droit d'auteur qui protège sa thèse. Ni la thèse ni des extraits substantiels de celle-ci ne doivent être imprimés ou autrement reproduits sans son autorisation.

ISBN 0-315-93294-5

Canada

ABSTRACT

ONSET AND CESSATION OF NUCLEATE BOILING

by

Ignacio R. Martín Domínguez

A model for nucleate boiling inception and cessation is presented which provides a rational unified explanation of the following experimentally observed phenomena:

- the *wall superheat* at the *onset of nucleate boiling* is dependent upon the working fluid and past thermal history of the fluid-solid surface.
- for most fluids other than water, a large difference exists between the wall superheat at the onset and at the cessation of nucleate boiling.
- fluid flow has a negligible effect on the incipient boiling wall superheat for most fluids. Water is a notable exception.

In this study fluids R-11 and water are used to illustrate the behaviour of well and poor wetting liquids respectively. The analysis allowed the following conclusions to be drawn:

- only *re-entrant* cavities can retain vapour bubble embryos during a non-boiling period. As subcooling of a site fluid increases, cavities with the largest embryos are quenched first. Dormant site

radii are of the order of 1 μm.

- at incipient boiling conditions, stable bubble embryos of well wetting substances can only exist attached to the mouth of a re-entrant (sub) cavity.
- under certain conditions stable bubble embryos of a poor wetting substance can also attach at the mouth of a conical cavity.

Since incipient boiling is a function only of the wall superheat surrounding the bubble embryo, it can be affected by fluid flow only if the bubble protrudes into a non isothermal boundary layer or is physically deformed by the flow or the cavity pressure is affected by the flow. This is unlikely to occur with well wetting liquids and is very likely to occur for water.

The common version of the integrated *Clapeyron* equation predicted liquid superheats which were very sensitive to the temperature at which the properties were evaluated. A comparison of these liquid superheats with those obtained using tabulated data showed errors of as much as 400%, for the small radius of curvature of the bubble embryos associated with dormant nucleation sites.

DEDICATION

To my wife:

María Teresa

for her love, patience and encouragement.

To my children:

Daniel Alberto, Leonardo and ***Dafne Carolina***

for the joy and motivation they brought to our lives.

To my parents:

Ignacio and ***Silvia***

for their love and confidence in me.

To my brother and sisters:

Raúl Antonio, Alejandra and ***Laura***

for their continuous support.

ACKNOWLEDGEMENTS

The author is greatly indebted to **Dr. Thomas W. McDonald** for his guidance and suggestions throughout the development of this dissertation. Without his timely advice this work could have never been completed.

Thanks are due to **Dr. Witold T. Kierkus** for his sharp comments and pleasing discussions whenever the author encountered difficulties.

Special thanks to **Dr. Robert G. Gaspar** for his advice and support in computer related matters.

Technicians **R. H. Tattersall** and **W. Beck** also merit the authors gratitude for their assistance during this work.

The National Council of Science and Technology of México (**Consejo Nacional de Ciencia y Tecnología CONACyT**) is acknowledged for the scholarship given to the author, which made the initiation of this work possible.

Financial support for this work through **NSERC** operating grant A0877 is thankfully acknowledged.

The **Department of Mechanical Engineering** and the **Faculty of Graduate Studies and Research** are thankfully acknowledged for their support through assistantships and scholarships.

TABLE OF CONTENTS

LIST OF FIGURES

LIST OF TABLES

NOMENCLATURE

ALS	=	Actual liquid superheat		K
Bo	=	Boiling number	$\frac{q''}{\dot{m}\ h_{fg}}$	
C_1, C_2	=	Constant coefficients		
Cp	=	Specific heat at constant pressure		kJ/kg-K
CNB	=	Cessation of nucleate boiling		
C_s	=	Coefficient in Rohsenow correlation		
D	=	Diameter		m
D_h	=	Hydraulic diameter		m
g	=	Gibbs free energy		kJ/kg
g	=	Gravitational acceleration		m/s^2
h	=	Enthalpy		kJ/kg
IWS	=	Incipient wall superheat		
Ja	=	Jakob number	$\frac{Cp_f (T_s - T_i)}{h_{fg}}$	
Ja_{mod}	=	Modified Jakob number	$\frac{h_s - h_i}{h_{fg}} \frac{\rho_f - \rho_g}{\rho_g}$	
$\dot{m}''$	=	Mass flux		$kg/s\text{-}m^2$
Nu	=	Nusselt number	$\frac{h\ D_h}{\kappa_f}$	
ONB	=	Onset of nucleate boiling		
P	=	Pressure		Pa
P_c	=	Critical pressure		Pa
Pr	=	Prandtl number	$\frac{Cp\ \mu}{\kappa}$	
P_r	=	Reduced pressure	$\frac{P}{P_c}$	

q	=	Heat rate	W
q"	=	Heat flux	W/m^2
r	=	Bubble radius of curvature, radius	m
R	=	Radial distance	m
Re	=	Reynolds number $\frac{\rho V D}{\mu}$	
RLS	=	Required liquid superheat	K
s	=	Entropy	kJ/kg-K
T	=	Temperature	°C or K
T_c	=	Critical temperature	K
TOS	=	Temperature overshoot	K
T_r	=	Reduced temperature $\frac{T}{T_c}$	
v	=	Specific volume	m^3/kg
X	=	Parameter in Hodgson equation	
Z	=	Parameter in Hodgson equation	

GREEK LETTERS

ß	=	Contact angle	°
ϕ	=	Angle	°
γ	=	Angle	°
κ	=	Thermal conductivity	W/m-K
μ	=	Dynamic viscosity	Pa-s
π	=	3.14159....	
ψ	=	Coefficient in Marsh and Mudawar equation	
ρ	=	Density	kg/m^3
σ	=	Surface tension	N/m
Θ	=	Angle	°

SUBSCRIPTS

b	=	Bulk
f	=	Saturated liquid
fg	=	Difference between saturated liquid and saturated vapour
g	=	saturated vapour
i	=	Inlet, inner
m	=	At the cavity mouth
max	=	Maximum value
min	=	Minimum value
n	=	At the re-entrant neck
o	=	Outlet, outer
s, sat	=	saturation
sup	=	Superheated
w	=	Wall

Chapter I

INTRODUCTION

A. The Boiling Phenomenon.

Heat transfer from a hot solid surface to a cooler liquid commonly occurs in heat exchangers. When the liquid undergoes a phase change with the appearance of vapour bubbles the phenomenon is called nucleate boiling.

Nucleate boiling is a very efficient heat transfer mechanism because the liquid absorbs large amounts of energy to change its phase, essentially at constant temperature, and this energy is rapidly removed from the wall neighbourhood when the bubble departs. This departure increases the turbulence in the zone close to the solid surface which, in turn, provides enhanced mixing and an increase in the heat transfer coefficient.

Boiling is one of the most common and most perplexing of the heat transfer phenomena. Although it has never been fully explained, it is usually characterized by an empirical relationship between the wall superheat (the difference between the temperature of the surface and the saturation temperature of the liquid).

In the absence of nucleate boiling, convective heat transfer governs the relationship. The transition between the convective process and nucleate boiling is even less well understood and is the topic of interest in this study.

Figure I.1 illustrates the transition region for a typical refrigerant. As the surface heat flux increases, the relationship is that of convective heat transfer, curve A → B, until

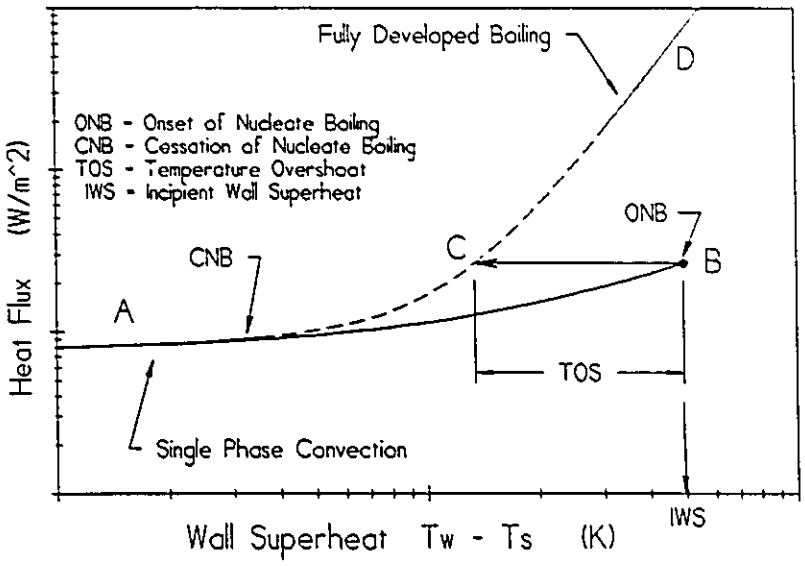

Figure I.1. Transition between convection and boiling heat transfer.

the *onset of nucleate boiling* (ONB) occurs at B, when bubbles first appear on a heated surface. The superheat at the ONB is called the *incipient wall superheat* (IWS). The transition from convection to nucleate boiling is usually very abrupt, occurring in an explosive burst of bubbles somewhere on the surface, and rapidly spreads over the surrounding surface. When this occurs, at constant wall heat flux, the wall superheat drops from B to C. This temperature drop is referred to as the *temperature overshoot* (TOS). Any further increase in the wall heat flux will result in the relationship following the nucleate boiling portion of the curve, C → D and beyond. If the wall superheat is held constant at the point of boiling incipience, an even more vigorous explosion of bubbles will occur and the heat flux will jump to D. Additional increases will be characterized by the boiling curve.

When a surface subject to fully developed nucleate boiling is cooled, the path

followed by the system is described by D → C → A. The transition between convection and nucleated boiling is thus a *hysteretic* process.

The condition when the last bubble disappears from the heat transfer surface during the cooling process, D → C → A, is termed *cessation of nucleate boiling* (CNB) and occurs where the transition (dashed line) correlation merges with that of single phase convection. Although one might expect that incipience and cessation would be synonymous, it is not generally true.

B. Industrial Applications of Boiling.

Many industrial systems such as boilers, air conditioners and nuclear reactors rely on the boiling mechanism in order to operate. A wide variety of working fluids are used:

- boiling water for steam generation in the power industry and in many industrial processes.
- hydrogen, nitrogen or argon in cryogenic processes.
- water and liquid metals (sodium and potassium) in the nuclear industry.
- halocarbons and fluorinated refrigerants in the refrigeration and air conditioning industry.
- halocarbon refrigerants in heat pipes, two-phase thermosyphons and in microelectronic cooling applications.

In industrial applications that rely on nucleate boiling to achieve the desired heat transfer rates at the prescribed temperature differences, it is of vital importance to know accurately when the ONB will occur. Two examples of such systems are described:

- *Two-phase thermosyphons*. In these systems the available temperature differences are restricted to a certain limit imposed by the heating media, and if the condition for the ONB is not achieved the apparatus will not work.
- *Cooling of micro-electronic* components. Modern electronic chips used in high performance computers require the dissipation of enormous heat fluxes. Cooling by immersion boiling in chemically inert coolants of high dielectric strength and low boiling point is one of the most promising heat transfer methods. Boiling on the surface of the components must initiate at relatively low temperatures ($T_w < 85°C$) to prevent damage of the electronic components.

The phenomenon of TOS occurs in applications with working fluids like halocarbon and fluorinated commercial refrigerants, liquid metals and cryogenic substances, and only rarely with water. The principal problem introduced by temperature overshoots in industrial applications is its apparent randomness. To date its occurrence and magnitude cannot be predicted accurately . Even under reasonably well controlled laboratory conditions, large variations in the values of the wall superheat at the ONB

have been observed **Bar-Cohen and Simon** (1988), **You et al.** (1990a and 1990b). This inability to reliably predict or control the TOS limits the use of boiling, for example in immersion cooling of micro-electronic components. For such cases, the overshoot at the ONB can produce two damaging effects. High temperatures can damage the chip, and the sudden temperature drop which occurs after the ONB can cause thermal stresses that affect the chip structure.

The ability to predict the ONB is of vital importance also for those industrial applications where boiling should not occur for safety reasons, such as some nuclear reactor designs. For these systems, the conditions for the ONB define an upper performance limit.

C. Description of the Problem to be Analyzed.

Much research in boiling has been carried out to explain and mathematically describe the process. Specific topics of interest include:

- for a given temperature difference between the wall and the liquid, what is the rate of heat transfer?.
- what is the effect on the heat transfer coefficient of parameters like: mass flow rate, liquid-solid combination, solid surface characteristics and subcooling (where the temperature of the liquid is lower than its saturation value at the working pressure)?.
- what will be the effect of the above parameters on the ONB?.

- what is the highest achievable surface temperature during nucleate boiling, beyond which a vapour film covers the solid surface and isolates the surface from the liquid?. This condition is known as film boiling and the point where the transition occurs is referred to as the *boiling crisis*.

The primary objectives of this dissertation are to investigate the questions:

- "Under what conditions will the onset of nucleate boiling occur?".
- "What factors influence it?".

D. Objectives of the Present Study.

The objectives of this study are to:

- analyze the conditions that cause the TOS at the ONB.
- identify the parameters involved in the phenomenon.
- model the mechanism of nucleate boiling inception to explain how a boiling site becomes active and what causes it to become dormant and finally extinct.

Chapter II

NUCLEATE BOILING BASIC THEORY

A. Boiling.

Boiling heat transfer is traditionally divided into two parts: *Pool Boiling* and *Flow Boiling*. In pool boiling evaporation occurs on the interface between a liquid phase and a heated solid surface in a pool of otherwise quiescent liquid. Flow boiling, as the name implies, refers to the process in which there is a bulk motion of the liquid past the heated surface, either by natural or forced circulation during evaporation.

Convective heat transfer rate can be predicted in terms of parameters like thermal conductivity, density, viscosity and geometric characteristics. The boiling heat transfer process depends on the same parameters plus those linked with the change of phase, such as vaporization enthalpy, saturation temperature, surface tension and vapour density. In addition, the micro structure and material of the heat transfer surface also influence boiling nucleation, as will be shown later.

A.1. Pool Boiling.

Pool boiling is the traditional starting point for a discussion of heat transfer in boiling systems, since the number of involved variables is smaller. The first complete characterization of pool boiling was reported by **Nukiyama** (1934), and his *Boiling Curve*

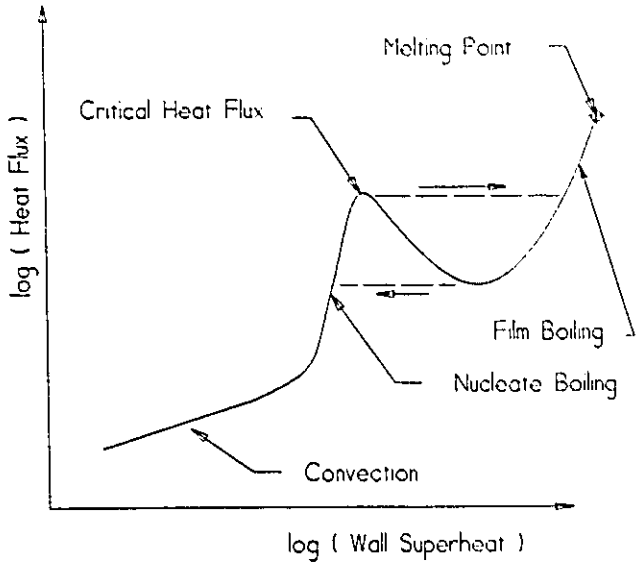

Figure II.1. Typical boiling curve for saturated pool boiling, (log scales).

is still the most used graphical representation of the phenomenon.

The complete boiling curve can be generated using an apparatus which can provide a controlled constant wall temperature. If a controlled constant wall heat flux is used, the curve follows the dashed lines shown in Figure II.1 and is no longer unimodal.

Figure II.2 shows a typical average temperature distribution in pool boiling for water at atmospheric pressure, subjected to a heat flux of 22.44 kW/m^2, **Stephan** (1988). Over the heated surface at a wall temperature of about 109°C, a thin layer ($\approx$ 1 mm) of superheated liquid forms where a large temperature drop takes place. In the liquid, the bulk temperature is almost constant over the depth of the pool at about 100.4°C . At the water surface the temperature drops slightly to reach the saturation temperature value.

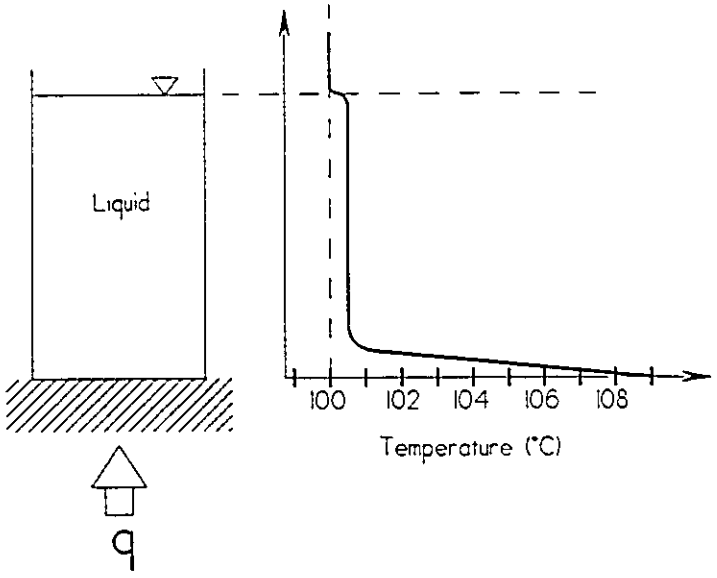

Figure II.2. Temperature distribution in saturated pool boiling water over a horizontal surface.

A.2. Flow Boiling.

In pool boiling, the only *flow* is natural convection of bubbles and warm liquid near the hot surface. If a bulk velocity is superimposed, as is the usual case for flow in a tube, then the convective heat flux increases as shown schematically in Figure II.3. The transition from forced convection to fully developed nucleate flow boiling is known as the *knee* of the boiling curve.

As shown in Figure II.3, increasing the mass flow rate causes the convective part of the *boiling* curve to be shifted to higher heat fluxes, for a given wall superheat, but the fully developed nucleate boiling curve is not affected. The flow boiling process can occur outside or inside tubes, with the latter being the more common.

The subject of in-tube flow boiling is normally divided into two separate geometries: *vertical tubes* and *horizontal tubes*. The corresponding characteristics for

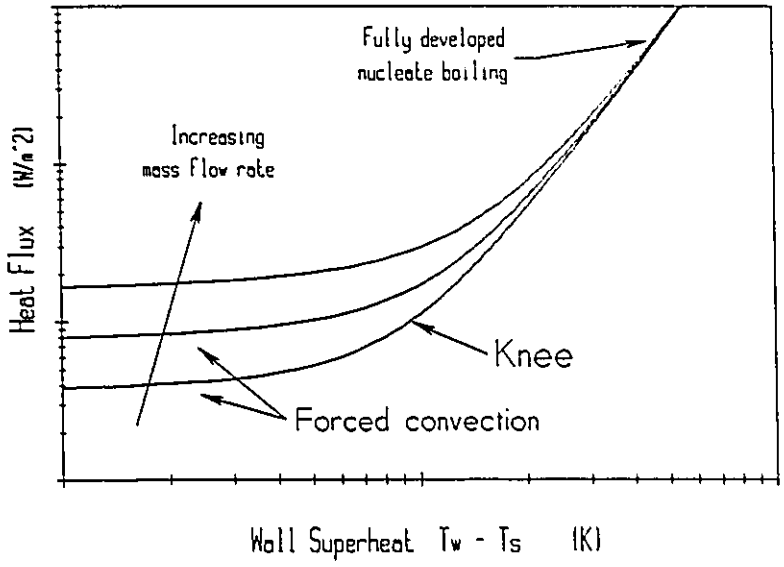

Figure II.3. Effect of mass flow rate on the forced convection branch of the boiling curve.

these orientations are sufficiently different to require different design correlations for each of them.

Boiling inside vertical tubes is utilized in thermosyphon reboilers and some steam generators, and boiling inside horizontal tubes is common to refrigeration evaporators and the convection sections of steam generators.

To better appreciate the much more complicated process of flow boiling, compared with pool boiling, note that in flow boiling all the states described by the boiling curve can exist simultaneously, spread along the length of the heated tube as illustrated schematically in Figure II.4.

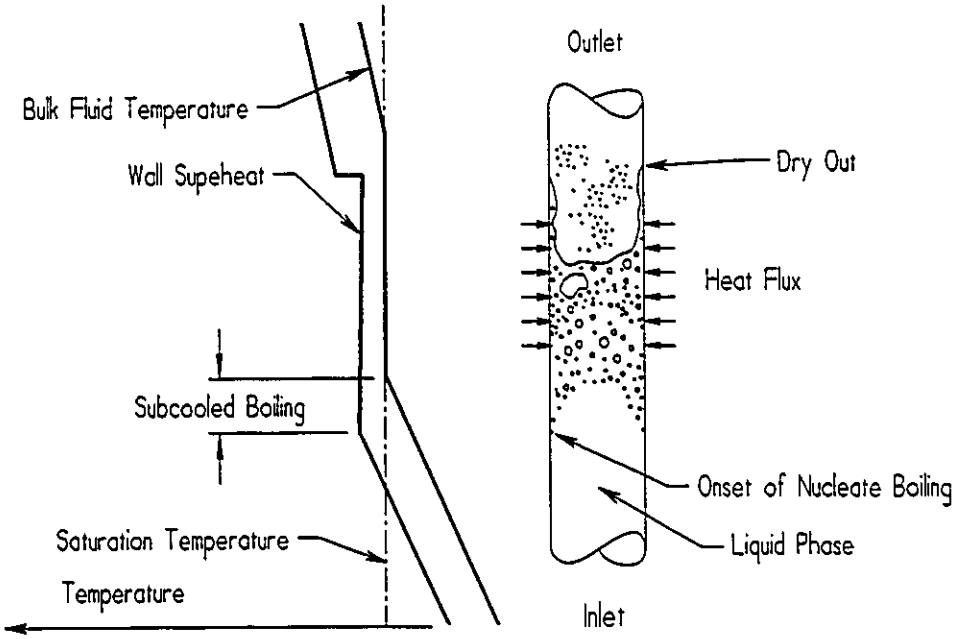

Figure II.4. Boiling in upward flow inside a uniformly heated vertical tube.

a. Boiling Models.

The single phase forced convection process for turbulent flow can be modeled by using the **Dittus and Boelter** (1930) correlation:

$$Nu = 0.023\ Re^{0.8}\ Pr^{0.33} \tag{II.1}$$

which yields:

$$q'' = 0.023\ Re^{0.8}\ Pr^{0.33}\ \frac{\kappa}{D}\left(T_w - T_b\right) \tag{II.2}$$

and fully developed nucleate boiling has often been modeled using the **Rohsenow** (1952) correlation for pool boiling:

$$q'' = \mu_f h_{fg} \left[\frac{g(\rho_f - \rho_g)}{\sigma} \right]^{\frac{1}{2}} \left[\frac{Cp_f (T_w - T_s)}{C_s h_{fg} Pr_f^n} \right]^3 \qquad \text{(II.3)}$$

where the C_s and n coefficients depend on the surface-liquid combination. It has been common practice to model the transition (knee) region by adding both expressions

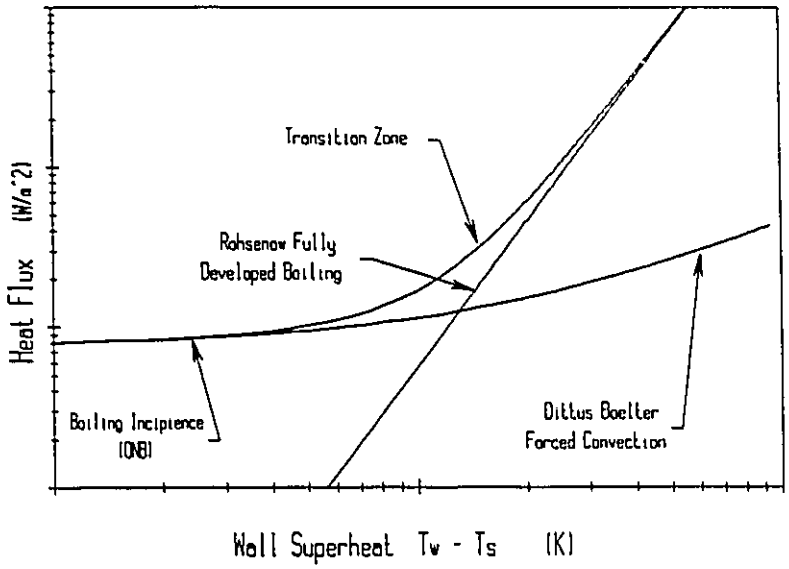

Figure II.5. Dittus and Boelter (1930) and Rohsenow (1952) correlations.

for q". Such a model is shown in Figure II.5.

B. Nucleation.

The process of nucleate boiling consists of two separate mechanisms, the formation of the bubbles or nucleation, and the subsequent growth and motion of these bubbles. Nucleation may occur inside the liquid phase, which is named *Homogeneous*

Nucleation, or at the interface between the liquid and a solid and called *Heterogeneous Nucleation.*

B.1. Homogeneous Nucleation.

In a homogeneous medium, such as the bulk of a fluid without an interface with another phasc, there are local fluctuations of densities according to the kinetic theory for pure gases and liquids. These fluctuations can be caused in a liquid by high energy molecules colliding to form a vapour nucleus, which constitutes a bubble embryo that can then grow, leading to homogeneous nucleation. **Lienhard** (1982) proposed a model to estimate the required liquid superheats to initiate homogeneous nucleation. The resulting values are extremely high. For many organic substances at 100 kPa the homogeneous nucleation occurs at about 0.89 of the critical temperature (T_c) and for water at about 0.92 T_c.

B.2. Heterogeneous Nucleation.

Experiments have shown that nucleation does not occur in the bulk liquid, but rather at the liquid-solid interface **Clark et al.** (1959). This phenomenon is called heterogeneous nucleation.

Bankoff (1957) studied the theoretical thermodynamic aspects of the nucleation process, and found that the minimum energy required to cause a phase change on the interface with the solid phase can be smaller than, equal to, or larger than for the

homogeneous phase, depending on whether the solid geometry is a cavity, a perfectly flat surface, or a protruding point. The energy required was predicted to be a minimum for the case of a cavity, and subsequent experimental microscopic photographic studies, **Clark et al.** (1959), showed that bubbles did indeed form only on small pits and scratches on the heat transfer surface.

B.3. Bubble Equilibrium in a Uniform Temperature Fluid.

As a starting point, the parameters affecting the growth or collapse of a bubble will be analyzed for the simple case of an already existent single component bubble nucleus immersed in a fluid of uniform temperature.

The forces acting on a bubble hemisphere are shown in Figure II.6, and are due

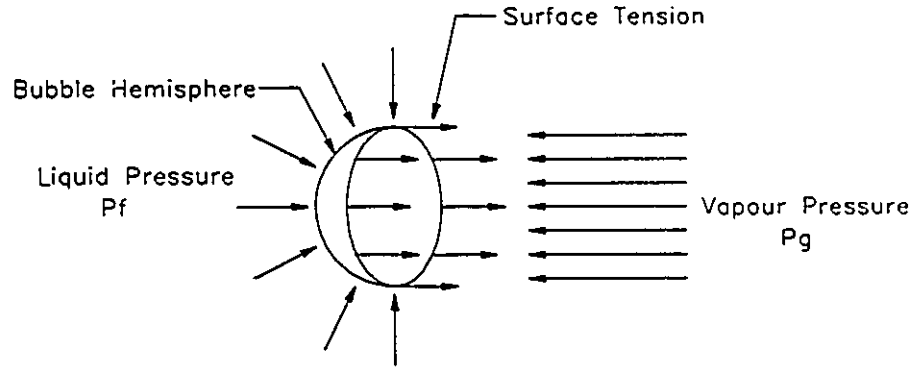

Figure II.6. Forces acting on a bubble in a constant temperature fluid.

to the internal and external pressures and the surface tension of the gas-liquid interface. (buoyancy forces are neglected).

Thermal and mechanical equilibrium exist between the gas and the liquid phase. The mechanical equilibrium condition necessary to maintain the size of the bubble is given by:

$$\pi\, r^2\, P_g = \pi\, r^2\, P_f + 2\,\pi\, r\,\sigma \qquad \text{(II.4)}$$

Therefore the internal pressure in the bubble is higher than that in the external liquid phase:

$$P_g = P_f + \frac{2\,\sigma}{r} \qquad \text{(II.5)}$$

Thermal equilibrium requires that the temperatures inside and outside the bubble be the same. Equilibrium thermodynamics leads one to the conclusion that since liquid and vapour are in contact at the bubble interface, then both phases *should* be in a saturated state and the temperature is governed only by the local pressure. Thus:

$$T_g = T_s(P_g) \qquad \textit{and} \qquad T_f = T_s(P_f) \qquad \text{(II.6)}$$

From equation (II.5) we note that:

$$P_g > P_f \quad \therefore \quad T_g > T_f \qquad \text{(II.7)}$$

which appears to be inconsistent with the requirement of thermal equilibrium between the liquid and the vapour phases.

This raises the question of the nature of the thermodynamic state of the substance on either side of the curved interface. To help clarify this situation, Figure II.7 shows a capillary tube partially immersed in a pool of saturated liquid. The meniscus at the top

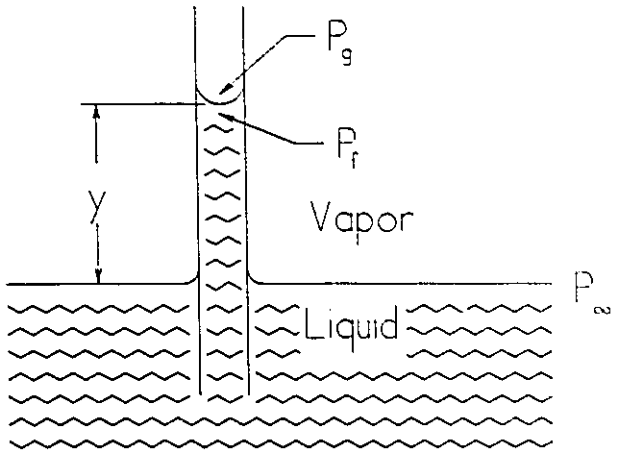

Figure II.7. Capillary tube analogy to a hemispherical bubble.

of the liquid column inside the tube corresponds to a portion of a hemispherical bubble like the one depicted in Figure II.6.

The system is in a uniform temperature field and the pressure at the flat interface (P_∞) is the saturation pressure that corresponds to that temperature. Pressures P_g and P_f are those of the gas and the liquid on either side of the curved interface. They can be related to the saturation pressure P_∞ as:

$$P_\infty = P_f + \rho_f g y \qquad \text{(II.8)}$$

and

$$P_\infty = P_g + \rho_g g y \qquad \text{(II.9)}$$

From these equations we can observe that both P_f and P_g are below the saturation pressure for the given temperature and hence both the liquid and gas are in a *superheated* condition. Since the density of the vapour phase is much smaller than that of the liquid, the vapour is much less superheated than the liquid.

It is desirable to relate the pressures P_f and P_g to P_∞ using the surface tension rather than the unknown height y. This may be done as follows:

$$\frac{P_\infty - P_f}{\rho_f g} = y = \frac{P_\infty - P_g}{\rho_g g} \qquad \text{(II.10)}$$

or

$$P_\infty (\rho_g - \rho_f) = \rho_g P_f - \rho_f P_g \qquad \text{(II.11)}$$

Eliminate P_g by using equation (II.5), to get

$$P_\infty - P_f = \left(\frac{\rho_f}{\rho_f - \rho_g} \right) \frac{2\sigma}{r} \qquad \text{(II.12)}$$

Similarly, eliminate P_f to get

$$P_\infty - P_g = \left(\frac{\rho_g}{\rho_f - \rho_g} \right) \frac{2\sigma}{r} \qquad \text{(II.13)}$$

Since $\rho_f \gg \rho_g$, equation (II.12) can be approximated as:

$$\left(\frac{\rho_f}{\rho_f - \rho_g} \right) \to 1 \quad \therefore \quad P_\infty - P_f \approx \frac{2\sigma}{r} \qquad \text{(II.14)}$$

and equation (II.13) as:

$$\left(\frac{\rho_g}{\rho_f - \rho_g} \right) \to 0 \quad \therefore \quad P_\infty \approx P_g \qquad \text{(II.15)}$$

Therefore we can conclude that the vapour inside the bubble is in a saturated state while the liquid just outside the bubble is in a metastable *superheated* condition, when thermal and mechanical equilibrium between the bubble and the liquid exists.

Although difficult, the *superheated* liquid can be shown on equilibrium phase diagrams as shown in Figure II.8, where the dashed line represents metastable states that

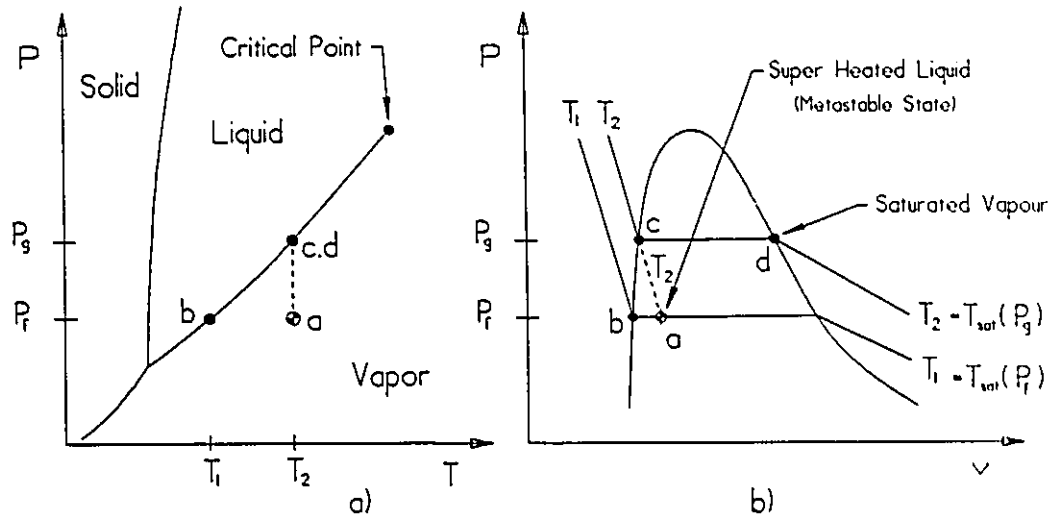

Figure II.8. *Thermodynamic states of the liquid and vapour phases in a bubble.*

are not in thermodynamic equilibrium and therefore off of the normal P-v-T surface.

The important question here is, what will be the degree of liquid superheating, (T_a - T_b in Figure II.8), required for thermo-mechanical equilibrium of the bubble to exist. The fact that the liquid is in a metastable state, "a", where the pressure is P_f even though the temperature is T_2, invalidates the use of any tool based in the assumption of thermodynamic equilibrium to directly analyze such a condition. The required liquid

superheat can be obtained from the two states "b" and "c" which are in thermodynamic equilibrium.

$$T_a - T_b = T_c - T_b = T_2 - T_1 \qquad \text{(II.16)}$$

In order to derive an expression for the pressure-temperature dependence for the equilibrium states between the liquid and the vapour phases consider a one component

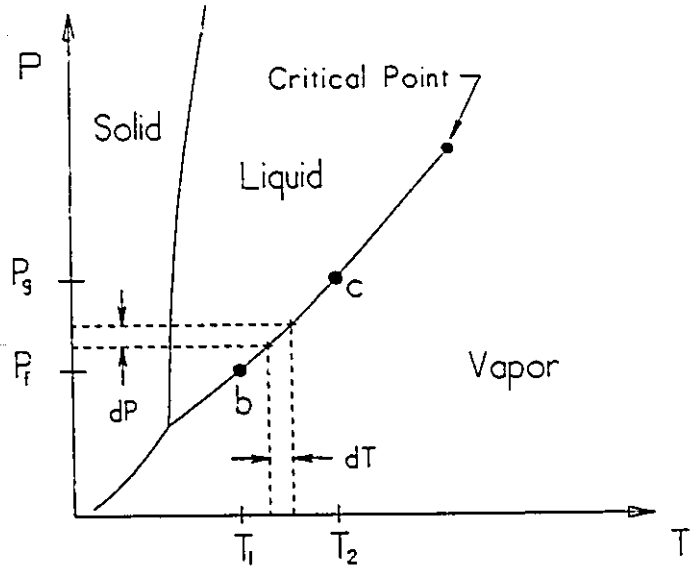

Figure II.9. Simple substance solid-liquid-vapour diagram.

system that undergoes an infinitesimal pressure and temperature change on the *phase coexistence curves* of Figure II.9.

The condition for equilibrium is that the Gibbs free energy change in the liquid should be equal to that in the vapour phase.

$$dg_f = dg_g \qquad \text{(II.17)}$$

the definition of the Gibbs free energy is

$$dg = v\,dP - s\,dT \tag{II.18}$$

and for the saturated liquid and vapour along the coexistence curve, we can write

$$v_f\,dP - s_f\,dT = v_g\,dP - s_g\,dT \tag{II.19}$$

and

$$\frac{dP}{dT} = \frac{s_g - s_f}{v_g - v_f} = \frac{s_{fg}}{v_{fg}} \tag{II.20}$$

From the $T\,ds$ equations we have

$$dh = Tds + v\,dP \tag{II.21}$$

For a phase change, from saturated liquid to saturated vapour at constant temperature, the pressure also remains constant and the previous equation reduces to

$$dh = Tds \tag{II.22}$$

If integrated over the phase change this gives

$$s_g - s_f = s_{fg} = \frac{h_{fg}}{T_s} = \frac{h_g - h_f}{T_s} \tag{II.23}$$

Introducing this result into equation (II.20) gives the *Clapeyron* equation

$$\left(\frac{dP}{dT}\right)_{sat} = \frac{h_{fg}}{T_s\,v_{fg}} \tag{II.24}$$

To integrate this equation along the saturation line, several assumptions have been made, **Bergles and Rohsenow** (1964) and **Davies and Anderson** (1966) assumed that

the vapour behaves as a perfect gas and that:

$$v_g > v_f \quad \rightarrow \quad v_g = v_{fg} \tag{II.25}$$

Thus:

$$\left(\frac{dP}{dT}\right)_{sat} = \frac{P\, h_{fg}}{R\, T_s^2} \tag{II.26}$$

To integrate equation (II.26) they further assumed that the vaporization enthalpy is constant over the integration range:

$$h_{fg} = constant \tag{II.27}$$

The resulting equation is known as the *Clausius-Clapeyron* equation.

$$T_s(P_g) - T_s(P_f) = \frac{R\, T_s(P_g)\, T_s(P_f)}{h_{fg}} \ln\left(1 + \frac{2\,\sigma}{r\, P_f}\right) \tag{II.28}$$

Frost and Dzakowic (1967), argued against the use of the ideal gas assumption and proposed, for small pressure variations:

$$\frac{h_{fg}}{T_s\, v_{fg}} = constant \tag{II.29}$$

They also assumed that the saturation temperature was constant. Based on these assumptions equation (II.24) can be integrated to yield:

$$\frac{P_g - P_f}{T_s(P_g) - T_s(P_f)} = \frac{h_{fg}}{T_s(P_f)\, v_{fg}} \tag{II.30}$$

They then eliminated P_g - P_f in equation (II.30) using the equation for bubble mechanical equilibrium (II.5), to get:

$$\Delta T_{w,sup} = T_s(P_g) - T_s(P_f) = \frac{2\ \sigma\ T_{sat}\ v_{fg}}{h_{fg}\ r} \qquad \text{(II.31)}$$

They suggested that T_{sat} be evaluated at $T_s(P_f)$.

An important fact to note in both equations (II.28) and (II.31) is that the liquid superheat required to maintain the bubble thermal and mechanical equilibrium increases with decreasing radius of the bubble, therefore the smaller the radius the higher the superheat required to maintain mechanical equilibrium. As a consequence, incipience of bubbles in an homogeneous liquid is not likely to occur because of the extremely high liquid superheats required to initiate the bubble (negligible radius).

B.4. Nucleation at a Solid Surface.

Mechanical equilibrium equation (II.5), derived in the previous section is still valid for a bubble in contact with a solid surface, but the situation is now somewhat different. The gas-liquid interface still is a spherical segment, but the curvature radius is not just a function of the trapped vapour volume as it also depends upon the interaction between the solid and the liquid. The required superheat to initiate the nucleation process depends also on this new factor.

a. The Contact Angle.

When the liquid and vapour phases interact with the solid surface, a new important parameter must be considered, the *contact angle* formed by the liquid phase with respect to the solid surface at the interface of the three phases. This important parameter depends on the liquid-solid-gas combination and on the "*cleanness*" of the solid surface.

Figure II.10 illustrates the bubble shapes and resulting radius of curvature for three example cases. Note that, for a given volume of vapour in contact with a *flat* solid surface the corresponding curvature radius will vary from a minimum equal to the radius of a sphere for a *well wetting* substance up to a very large radius for a *non wetting* fluid, where the contact angle approaches 180°.

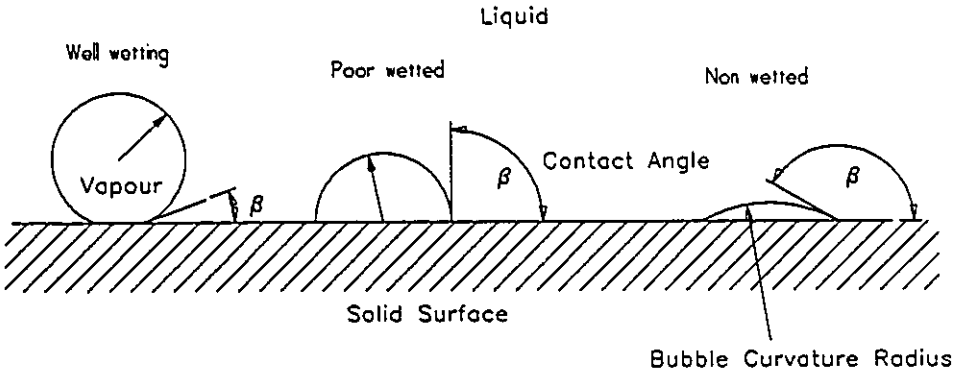

Figure II.10. *Contact angle at the triple interface.*

For all contact angles, if the liquid phase superheat temperature decreases below its equilibrium value then the vapour phase will collapse by condensation, or, if the temperature rises, the bubble will grow and depart from the surface leaving no nucleus

for another bubble. It thus becomes clear that the presence of a solid surface is not the sole explanation for nucleate boiling. Some other condition is necessary. The other necessary, but not sufficient, condition is the presence of cavities on the solid surface.

b. Cavities.

Cavities do not, by themselves, constitute nucleation sites for bubbles. They must contain either vapour or pockets of gas trapped when the surface was flooded by the liquid.

When a bubble is inside of a cavity, the liquid-vapour interface is a *spherical segment* with a radius of curvature which depends upon the contact angle, the cavity

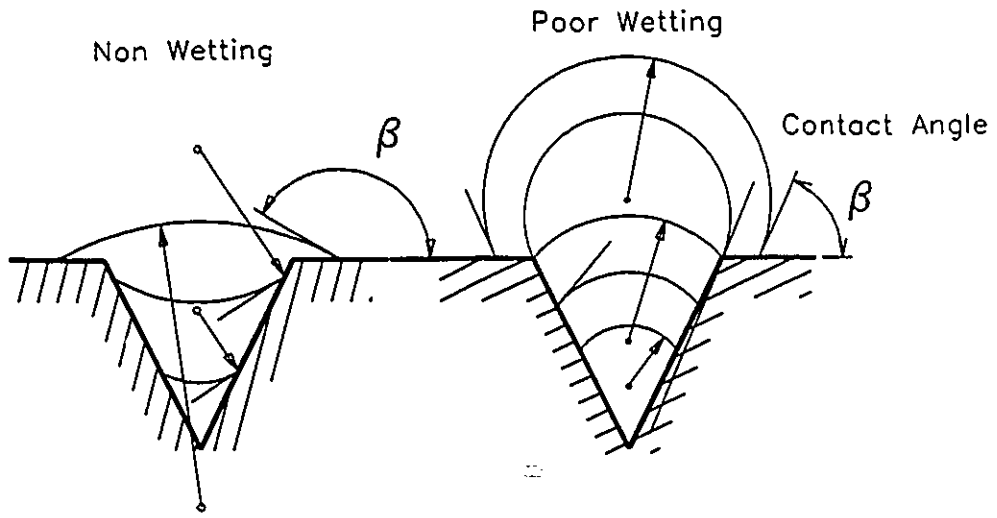

***Figure II.11.** Effect of the liquid contact angle on the bubble curvature radius, non and poor wetting fluids.*

geometry and the location of the bubble within the cavity. Figure II.11 shows how the

bubble curvature radius can become negative (convex towards the vapour) inside of a conical cavity when the contact angle has a large value (non-wetting substance), while for the same cavity angle it remains positive (concave) with a smaller contact angle (poor-wetting substance). Thus, for such a *non wetting* substance, the vapour trapped in the cavity is been *helped* by the surface tension to resist the push of the liquid phase, and that such help becomes stronger as the interface shrinks inside the cavity since the curvature radius attains smaller *negative* values. Such bubble nucleii are stable and could resist any liquid subcooling without collapsing.

In the case of a *poor-wetting* substance the contrary is true. The bubble nucleii are unstable inside of the cavity since the surface tension is acting against the vapour phase and any reduction in the liquid temperature will produce a reduction in the volume of each nucleus and a further reduction in the curvature radius. Therefore, once equilibrium is lost, the nucleus will simply collapse inside the cavity.

Figure II.12 shows the case of bubbles of a well-wetting substance over the same cavity as in Figure II.11. The same unstable situation as with the poor-wetting substance applies in this case, but note the strong effect that the contact angle has on the curvature radius when the bubble outgrows the cavity mouth. Inside the cavity, at the same depth, the curvature radius will be smaller with the well-wetting substance compared to the poor-wetting substance, as can be appreciated by comparing Figures II.11 and II.12.

The cavity angle-effect on the curvature radius is shown in Figure II.13 for a poor-wetting substance. It can be appreciated that the curvature radius increases as the

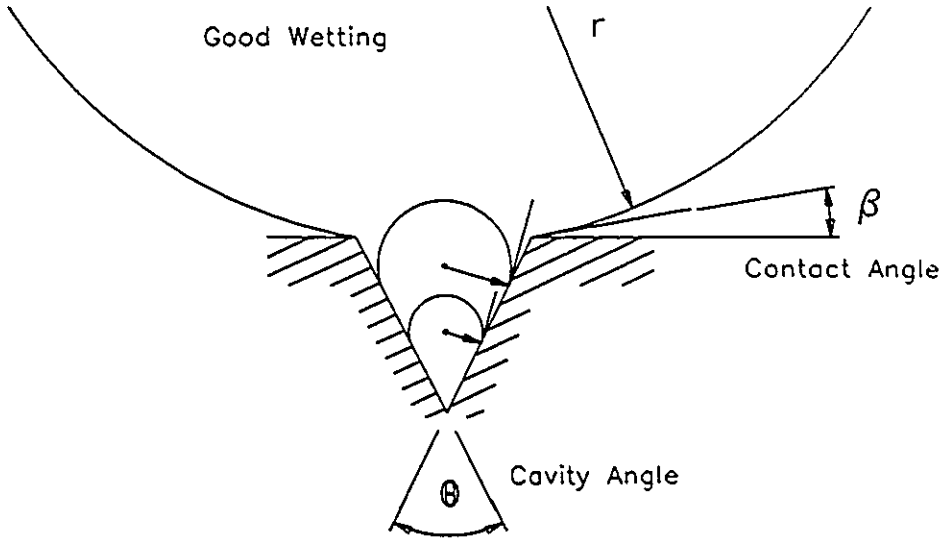

Figure II.12. Effect of the liquid contact angle on the bubble curvature radius, well wetting fluid.

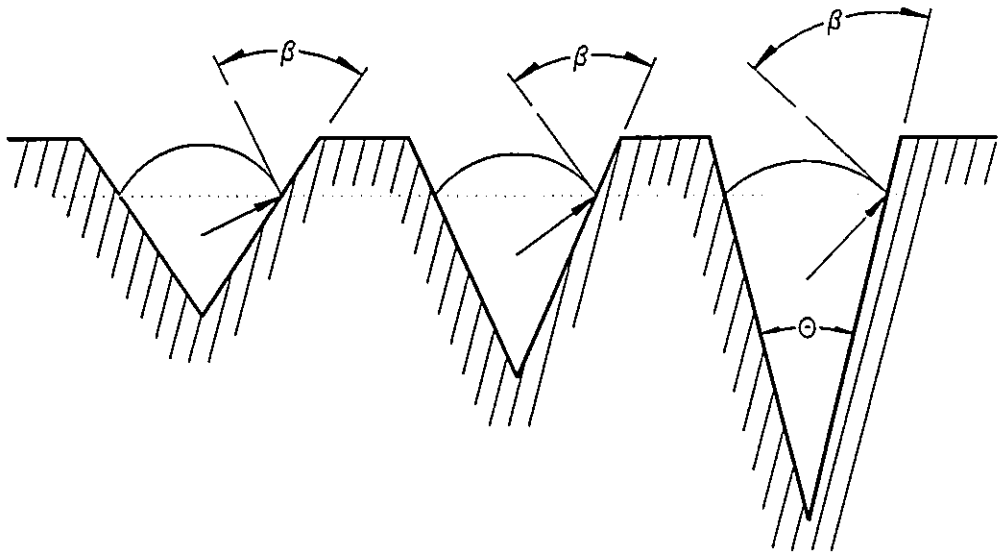

Figure II.13. Effect of the cavity angle on the bubble curvature radius.

cavity angle gets smaller. This effect becomes less important with smaller contact angles.

From geometrical considerations it can be shown that the bubble radius of

curvature becomes infinite when:

$$\theta = 2\,(\beta - 90°) \tag{II.32}$$

For most common substances which have contact angles varying from zero to 90°, it is evident that conical cavities cannot contain bubble nucleii after having been cooled below their equilibrium temperature. Some other mechanism must exist to permit the survival of nucleii in cavities.

Chapter III

POSTULATION AND LITERATURE REVIEW

A. Introduction.

An extensive literature review has been made of the onset of nucleate boiling, covering works from 1955 to 1992. Appendix A outlines, in chronological order, material found in the literature which is relevant to this study.

In this chapter, a postulation is made about the nature of the problem here analyzed, followed by an analysis of the theories and data published in the literature that relate to the postulation.

B. Postulation.

Based on an analysis of the relevant literature, the following is postulated for the parameters which govern the incipience and quenching of nucleate boiling sites in cavities. For a given fluid-solid combination:

- the equilibrium of a vapour bubble in a cavity is governed by the local pressure and temperature, the bubble radius of curvature, and the surface tension.
- the bubble radius of curvature depends on the contact angle

between the liquid-vapour surface and the solid wall of the cavity and on the cavity geometry and size.

- a vapour bubble embryo can exist in equilibrium within a cavity *above* the local saturation temperature only if the vapour-liquid interface is *concave* relative to the vapour and of a shape such that further *superheating* causes a reduction in the surface radius of curvature.
- a vapour bubble embryo can exist in equilibrium within a cavity *below* the local saturation temperature only if the vapour-liquid interface is *convex* relative to the vapour and of a shape such that further *subcooling* causes a reduction in the surface radius of curvature.
- the degrees of subcooling required to quench a site is dependent upon the cavity geometry and the contact angle. If the quench subcooling requires a temperature below the triple point temperature of the fluid, the site cannot be quenched.

C. Literature Review.

This literature review is structured by topic citation along with a brief comment on their findings. More complete details of the works cited are given in Appendix A. This method provides an overview of the details of numerous research works to be

presented in a relatively compact format.

D. Historic Perspective.

The earliest works analyzed in this literature review are from the 1950's, and constitute the foundations of many of the subsequent research paths followed during the next decades. The most relevant topics analyzed are classified here.

D.1. Conditions Required to Initiate Nucleation.

Bankoff (1957) demonstrated theoretically that homogeneous nucleation within a liquid, or nucleation on flat or projecting surfaces was not possible. He concluded that only a non-well-wetted cavity where vapour or some other gas is trapped, could possibly serve as a nucleation site.

D.2. Gas and Liquid Entrapment in Cavities.

Bankoff (1958) analyzed, by geometric considerations, the conditions for gas and liquid entrapment in cavities during advancing and receding liquid fronts.

D.3. Photographic Observations.

Clark et al. (1959) conducted a photographic study of boiling and observed that all the boiling sites were pits or scratches in the solid surface.

D.4. Bankoff Model to Predict the Onset of Nucleate Boiling.

Bankoff (1959) starts his paper by saying that "It will be very desirable to be able to predict the degree of wall superheat which will initiate steady boiling with a particular liquid in contact with a particular surface at a given pressure". He then developed a semi-empirical equation to predict the wall superheat at the onset of boiling for a bubble in a cylindrical cavity.

E. Observed Facts that Lead to the Development of the New Model Postulated Here.

From a review of literature relevant to this work, a number of facts related to the occurrence of temperature overshoots at the onset of nucleate boiling were observed which lead to the development of the model postulated here.

E.1. Effect of the Contact Angle on the Onset of Nucleate Boiling.

The simplest method of studying the effect of contact angle on the ONB is by using mixtures of liquids in which the contact angle is a function of composition. Since the composition of the mixture can be accurately controlled, the contact angle and hence the effect on the ONB may be varied gradually.

Eddington and Kenning (1979) observed that the number of active nucleation sites decreased as the contact angle of a water-ethanol mixture decreased by increasing the ethanol content in the mixture.

Thome et al. (1982) studied the effect of mixture composition on the wall superheat at the onset of nucleate boiling. They observed that:

- with fluids having the same contact angle, nitrogen and argon, the wall superheat required to initiate nucleate boiling was not affected by the mixture composition.
- with mixtures of fluids having different contact angles, water and ethanol, the wall superheat showed large dependency on the mixture composition varying from TOS $\approx$ 7 K with pure water ($\beta \approx 80°$), to TOS $\approx$ 44 K at 50% composition ($\beta \approx 30°$), and to TOS $\approx$ 25 K with pure ethanol ($\beta \approx 0°$).

For pure fluids, the effect of the contact angle on the wall superheat at the onset

of nucleate boiling can be observed by comparing the behaviour of common working fluids reported in the literature according to their contact angle. Fluids commonly used as working media in heat transfer applications can be classified as either poor wetting and well wetting.

a. Poor Wetting Substances.

Water (ß ≈ 85 degrees) is the only substance with characteristics of poor wettability reported in the literature related with the study of boiling incipience.

The observation of a temperature overshoot and hysteresis while using water as a working fluid is rare. When it happens the magnitude of the overshoot is usually small. **Turton** (1968) reported a temperature overshoot of 2.8 K, using a stainless steel surface, **Bergles and Chyu** (1982) reported a temperature overshoot of 3 K using a porous surface and **Sudo et al.** (1986) reported one case with an overshoot of 2 K.

b. Well Wetting Substances (ß < 10 degrees).

Test on several groups of substances having small contact angles indicate that temperature overshoots frequently occur and are of larger magnitude than those for poor wetting substances.

i. Refrigerants (ß < = 10 degrees).

The occurrence of temperature overshoots when using refrigerants has been reported by:

- **Turton** (1968) in all his experiments with R-11, the TOS varied between 5 K and 40 K using stainless steel.
- **Murphy and Bergles** (1972) observed a TOS of approximately 12 K with R-113 on a stainless steel tube.
- **Yin** (1974) observed TOS values between 18 K and 24 K using R-11 on stainless steel tubes.
- **Joudi and James** (1977) in all their experiments with R-113 on stainless steel observed values of TOS between 12 K and 19 K.
- **Bergles and Chyu** (1982) observed TOS with values of 7.5 K with R-113 on porous metallic surfaces.
- **Marto and Lepere** (1982) observed TOS of approximately 13 K with R-113 and ≈ 8 K with FC-72 on copper surfaces.
- **Hino and Ueda** (1985) observed TOS of approximately 23 K with R-113 on stainless steel tubes.
- **Park and Bergles** (1986) observed TOS of 11 K to 19 K with R-113 on copper plates.
- **Kim and Bergles** (1988) observed TOS with values between 30 K to 40 K on a plain copper surface and from 20 K to 30 K on

sintered porous surfaces (copper powders), using R-113.

- **Maddox and Mudawwar** (1988) observed TOS of up to 7.5 K with FC-72 on copper surfaces.
- **Bräuer** (1988) reported TOS with values between 3.5 K and 4.5 K with R-12 on stainless steel.
- **Ayub and Bergles** (1988) observed TOS with values between 1.5 K and 3.3 K on smooth and enhanced copper surfaces, with R-113.
- **Anderson and Mudawwar** (1988) reported TOS with values up to 10.4 K, with FC-72 on plain and enhanced copper surfaces.
- **Park and Bergles** (1988) reported TOS with values between 9 K and 19 K on nichrome surfaces using R-113.
- **McDonald and Shivprasad** (1989) observed TOS of up to 26 K, with R-11 on copper tubes.
- **Lee and Simon** (1989) observed TOS of up to 16 K with FC-72 on platinum surfaces.
- **You et al.** (1990a) reported TOS from 10 K to 23 K on a chromel wire and from 29 K to 53 K on a thin platinum film using R-113.
- **You et al.** (1991) measured TOS of up to $\approx$ 10 K using FC-72 on platinum surfaces.
- **Marto and Anderson** (1992) reported TOS of $\approx$ 6 K using R-113

on copper tubes.

ii. Organic Fluids (ß ≈ 0 degrees).

Organic fluids have small contact angles and therefore their behaviour at the onset of nucleate boiling is similar to that of refrigerants. Some of the reported occurrences of temperature overshoots are: **Corty and Foust** (1955) observed TOS ≈ 10 K with diethyl ether on copper, TOS ≈ 11 K with n-pentane on copper and TOS ≈ 17 K with n-pentane on nickel, **Joudi and Janies** (1977) observed TOS ≈ 15 K with methanol on stainless steel surfaces, **Jemison et al.** (1982) with methanol on a copper surface, **Thome et al.** (1982) measured TOS of up to 35 K with methanol-water mixtures on copper surfaces.

iii. Cryogenic Fluids (ß ≈ 0 degrees).

Temperature overshoots using cryogenic fluids have been found by **Coeling and Merte** (1969) of the order of 2.5 K for hydrogen on a polished copper surface and of the order of 12 K for hydrogen on a stainless steel surface. **Robertson and Clarke** (1981) mention having observed temperature overshoots with nitrogen but does not report the magnitude. **Thome et al.** (1982) report the occurrence of TOS with nitrogen-argon mixtures when their system suffered even small pre-pressurizations. **Clarke and Robertson** (1984) also observed a TOS with nitrogen boiling on an aluminium surface.

iv. Liquid Metals (ß ≈ 0 degrees).

Liquid metals were of much interest because of their application in nuclear reactors. Some of the works where temperature overshoots were reported are by: **Marto and Rohsenow** (1966) with sodium and by **Dwyer et al.** (1973) who report a TOS ≈ 20 K with sodium.

E.2. Effect of Pre-pressurization on TOS.

Although water normally has a small or negligible temperature overshoot, when subjected to a high pressure prior to the heating process a temperature overshoot does occur. Two works were found where the test surfaces were deliberately subjected to a high pressure prior to initiating nucleate boiling. **Sabersky and Gates** (1955) reported temperature overshoots of up to 47 K in experiments with platinum and nichrome wires, on water at atmospheric pressure, which had been pre-pressurized up to 100,000 kPa for periods of 15 min. **Van Vleet** (1985) reported temperature overshoots of up to 13 K in experiments with pure platinum wires on water at atmospheric pressure, which had been pre-pressurized up to 1,400 kPa. In both works it was also mentioned that once boiling has occurred on the surface and the surface is then cooled until boiling ceased, any subsequent boiling incipiencies occur with normal wall superheat. These results show that even water can exhibit large temperature overshoots, at the onset of nucleate boiling, if it is subjected to pre-boiling pressurization.

Thome et al. (1982) report that even small pre-pressurizations on their nitrogen-

argon system caused a substantial increase in the wall superheat at the ONB, which was negligible otherwise.

Note that pressurization of a liquid-solid system produces an increase in the saturation temperature of the liquid. For a given fluid temperature, as the pressure increases, the thermodynamic state of the liquid at the bubble interface becomes less superheated and eventually subcooled. For water at 100°C and 1,400 kPa the subcooling is $\approx$ 95 K.

The model postulated predicts that increasing the liquid subcooling will cause larger vapour nucleation sites to quench. Since the remaining smaller site require a greater wall superheat to initiate boiling, a larger TOS occurs.

E.3. Effect of a Controlled Cooling and Reheat Process in the Vicinity of CNB.

When a surface where a well wetting substance is in fully developed nucleate boiling is cooled, it has been observed by **Corty and Foust** (1955) with ether, pentane and R-113, **Marto et al.** (1968), **McDonald and Shivprasad** (1989) with R-11, **You et al.** (1990a) with R-113 that more and more of the active sites become inactive as the superheat decreases. All sites become inactive when (or before) the wall superheat reaches zero. Depending upon the wall superheat (subcooling) reached, a subsequent increase in the surface temperature will reactivate some of the sites without any wall temperature overshoot. This is in agreement with the model which predicts that nucleus

survival in a cavity is a function of the degree of superheating (or subcooling) attained at the nucleus.

E.4. Location of Nucleation in Cavities with Well Wetting Fluids.

Several authors have suggested that the nucleation process starts inside the cavities, for well wetting fluids. **Cornwell** (1982) proposed that the micro-roughness of the cavity's internal walls inverts the shape of the bubble embryo's surface deep inside of the cavity. **Marsh and Mudawwar** (1988) observed that since their results with FC-72 were independent of flow subcooling, flow rate or heat flux, they conclude that the bubble embryos must be located inside the cavities. **Marsh and Mudawwar** (1989) also found that the wall superheat at the ONB, in their experiments with FC-72, was independent of the flow conditions and concluded that the nucleation process must then start inside the cavity. **Tong et al.** (1990) analyzed the effect of the contact angle hysteresis (the difference in contact angle of a moving liquid front between advancing and receding conditions) and concluded that for well wetting substances, bubbles at the *critical radius* (the bubble radius of curvature at the ONB) always occur inside the cavities. **You et al.** (1990a) concluded that, for highly wetting fluids, the minimum radius of bubble embryos is attained within the cavity, after observing that a controlled partial cooling of a boiling surface produced selective site quenching. **Hahne et al.** (1990) observed that if cavity size data, reported by others, was introduced in an

equation developed to predict the wall superheat at the ONB, the bubble temperature predicted was equal to the wall temperature, therefore they conclude that the bubble should be located within the cavity. **Mizukami et al.** (1990) analyzed the mechanical equilibrium of bubbles in cavities (without regard for thermal conditions) and concluded that conical and cylindrical cavities cannot trap vapour during liquid subcooling, only re-entrant cavities could, and that nucleation should start from inside such cavities. **You et al.** (1991) analyzed the behaviour of the bubble curvature radius as a result of the cavity geometry, a sketch of the inverse of the bubble curvature radius vs. bubble volume is presented and they observe from the curves that for well wetting fluids the incipient bubble is probably far inside the cavity.

The proposed model supports the concept that nucleation occurs from within most cavities.

E.5. Relationship Between Wall Superheat at the Onset of Nucleate Boiling and Flow Conditions.

Any bubble which attains a stable steady state condition sitting at an isothermal cavity mouth would typically protrude into the boundary layer. For such a bubble, the flow conditions, flow rate, and temperature gradient in the fluid would certainly affect its stability. However, a steady state bubble that is located inside of an isothermal cavity is unlikely to be affected by the flow outside of the cavity.

The dependence or independence of the wall superheat at the ONB respect to the

flow conditions should then be an indication of the position of the bubble at the time of incipient boiling. Some of the experimental results found in the literature on this subject can be classified as follows:

- *Poor wetting fluids*. Experimental results with poor wetting fluids show that the wall superheat at the onset of nucleate boiling does depend on the flow rate and on the subcooling. Some of the reported results are: **Sudo et al.** (1986) with water, **Marsh and Mudawwar** (1989) with water.
- *Well wetting fluids*. Experimental results with well wetting fluids show that the wall superheat at the ONB does not depend on the flow rate and/or on the degree of subcooling. Some of the reported results are: **Abdelmessih et al.** (1974) with R-11, **Hino and Ueda** (1985) with R-113, **Bräuer** (1988) and **Bräuer and Mayinger** (1988) with R-12, **Spindler and Hahne** (1988) with R-11, **Marsh and Mudawwar** (1989) with FC-72, and **You et al.** (1990b) with FC-72. However, **Lee and Simon** (1989) report a different behaviour based on their experiments with small platinum heaters and FC-72. (Some doubts exist about this work, since the hysteretic graphs shown in the paper follow a *reversed* direction with respect to that observed by every other author).

The model indicates that only poorly wetting fluids can have bubbles attached at

a cavity mouth which can protrude into the fluid boundary layer and be affected by flow conditions.

E.6. Gas versus Vapour as a Nucleation Site Embryo.

You et al. (1991) proposed that the existence of a non condensable gas, dissolved in the liquid, is essential to prevent the complete disappearance of bubble embryos in cavities, and hence affects the magnitude of TOS. **Marto et al.** (1968) measured temperature overshoots with liquid nitrogen and greased copper and teflon surfaces, even when the system had been previously degassed by boiling. In a cryogenic liquid, only substances with lower molecular masses could still be in the gaseous phase at the working temperature of the liquid. Therefore, the presence of a dissolved gas in this experiments is unlikely, and one may conclude that some other mechanism must exist that permits a bubble embryo to survive inside a cavity.

The model proposes that re-entrant cavities permit the survival of bubble embryos during non boiling periods.

E.7. Question the Use of the Integrated *Clapeyron* Equation.

Lee and Simon (1989), **Tong et al.** (1990), **You et al.** (1990a) have questioned

the validity of the way in which some authors have integrated the Clapeyron equation to calculate the required liquid superheat with refrigerants, when the temperature overshoot is large. The non-linearity of the P-T curve introduces errors in the calculations for most of the assumptions made to perform the integration.

F. Models Proposed for the Onset of Nucleate Boiling.

Several models have been proposed in the literature to predict the onset of nucleate boiling. They can be classified according to their main characteristics as shown in the following subsections:

F.1. Based on a Bubble Sitting at the Cavity Mouth.

The earliest models developed assumed that a bubble already exists and is sitting attached to the cavity mouth where it is subject to the influence of the temperature distribution in the thermal boundary layer. Later modifications included different criteria for the required size of the bubble to induce bubble growth, relative to the temperature profile in the boundary layer. It has become customary to classify these models in two categories:

- the *tangency* (r_{tan}) criterion. A relationship between the cavity

mouth radius and the curvature radius of a bubble sitting at the mouth of the cavity is established, then a curve of required liquid superheat as a function of cavity mouth radius is plotted. The temperature profile in the boundary layer near the boiling surface is a function of the heat flux, for a given mass flow rate and subcooling. It is usually assumed linear. During the heating process prior to boiling, the wall superheat increases and the temperature profile approaches the required liquid superheat curve. This is the point where the temperature profile line becomes tangent to the required wall superheat line and defines the size of the first cavity where nucleation can start. A further increase in the wall superheat could activate a range of cavities, delimited by the intersections between the temperature profile and the required liquid superheat curve. (Figure A.1 and Figure A.2 show this criteria). The models that follow this criterion are: **Hsu** (1962), **Bergles and Rohsenow** (1964), **Sato and Matsumura** (1964), **Han and Griffith** (1965), **Davies and Anderson** (1966), **Howell and Siegel** (1966), **Frost and Dzakowic** (1967), **Chen** (1968), **Murphy and Bergles** (1972), **Yin and Abdelmessih** (1974), **Lee et al.** (1988), **Bräuer** (1988), **Bräuer and Mayinger** (1988), **Marsh and Mudawwar** (1989).

- the *maximum available cavity radius* (r_{max}) criterion. The failure of the *tangency* criterion to correctly predict the onset of nucleate boiling, particularly with well wetting fluids, led **Hino and Ueda** (1985) to contemplate the possibility that the cavity size predicted by the *tangency* criterion may not be available in the solid surface. This could happen if the cavity size distribution in the solid surface consisted only of small sizes, and therefore the surface must reach a higher temperature than that predicted by the tangency criterion before the largest cavity available could be activated. They modified the equation developed by **Sato and Matsumura** (1964) by introducing the maximum available cavity radius as a limiting factor. (Figures A.6 and A.7 illustrate this model).

F.2. Empirical Models.

Some models have been developed based on a traditional dimensional analysis. Others have presented dimensional equations. In both cases the required coefficients were obtained by correlating experimental results.

Hodgson (1968) selected those variables thought important, developed a model by dimensional analysis, and evaluated the empirical coefficients using water data. **Bucher** (1979) developed a model by dimensional analysis based on heat transfer laws,

and fitted his equation to water data. **Bräuer** (1988) and **Bräuer and Mayinger** (1988) fitted the equation developed by **Bucher** (1979) to their own R-12 data. **Belhadj et al.** (1988) proposed an empirical correlation, valid for a single geometry and fluid for a restricted operational range.

F.3. Effect of Dissolved Gas.

In some models the dissolved gas content of the liquid has been included. **Chen** (1968) proposed an equation based on **Hsu**'s (1962) model that includes the effect of inert gas trapped inside the cavity. **Torikai et al.** (1970) introduced the dissolved gas content term into the mechanical equilibrium equation for a spherical bubble. **Murphy and Bergles** (1972) included an adjusted or "gassy" saturation temperature into **Bergles and Rohsenow** (1964) model, where the pressure in the vapour phase includes the partial pressure of the dissolved air. **Tong et al.** (1989) proposed an equation valid for spherical bubbles in a isothermal field.

G. Discrepancies and Problems Encountered.

When using the predictive models described in the previous section, the following discrepancies and problems have been encountered.

G.1. Models Predict Boiling Cessation, Rather than Incipience.

Models based on a bubble sitting at the cavity mouth trend to better predict the cessation of nucleate boiling rather than its incipience. This has been observed by: **Murphy and Bergles** (1972) with R-113, **Yin and Abdelmessih** (1974) with R-11 and by **Hino and Ueda** (1985) with R-113.

G.2. Inconsistent Results With the Maximum Available Cavity Radius Model.

Some authors report experimental results where the *maximum available cavity size* model proposed by **Hino and Ueda** (1985) produced inconsistent results. The inconsistencies observed were:

- microscopic observation of the test surface revealed the existence of cavities larger than the predicted maximum size, **Marsh and Mudawwar** (1988), **Marsh and Mudawwar** (1989), **You et al.** (1990a)
- for the same surface and fluid, the predicted maximum size varied with flow rate or subcooling, **Sudo et al.** (1986) with water, **Marsh and Mudawwar** (1989) with water
- boiling different fluids on the same test surface predicted different

maximum available sizes, **Marsh and Mudawwar** (1989) with FC-72 and water,

G.3. Non-repeatability of the Phenomena.

Low repeatability in the wall superheats at the onset of nucleate boiling have been observed in some experimental works with well wetting fluids where extreme care was taken to ensure exactly the same procedure and state were used in each test. Some of these works are: **Bar-Cohen and Simon** (1988) and **You et al.** (1990a) and (1990b)

H. Conclusions.

The problems and discrepancies reported to occur when using the existing models to predict the onset of nucleate boiling, indicate that a more comprehensive analysis of the conditions necessary for bubble formation and retention is required in order to better understand the phenomenon. As a result of this literature review, the postulation given in this chapter was developed. Based on that postulation the model detailed in the following chapters was developed.

Chapter IV

LIQUID SUPERHEAT AROUND SPHERICAL BUBBLES

A. Introduction.

In this chapter the prediction of the required liquid superheat around spherical bubbles will be analyzed.

The relationship between the pressure inside a bubble to the pressure outside as a function of its size and the surface tension may be easily derived using a force balance.

$$P_g = P_f + \frac{2\,\sigma}{r} \qquad \text{(II.5)}$$

In heat transfer applications, it is necessary to know the liquid superheat required to maintain such a metastable equilibrium state. The relationship between pressure and temperature at saturation conditions may be obtained by a curve fit of P vs. T for saturation conditions or by utilizing the *Clapeyron* differential equation.

$$\left(\frac{dP}{dT}\right)_{sat} = \frac{h_{fg}}{T_s\, v_{fg}} \qquad \text{(II.24)}$$

In order to use this equation to relate the pressure difference in equation (II.5) to a corresponding saturation temperature difference equation (II.24) must be integrated

over the corresponding pressure and temperature ranges. Since temperature dependent thermodynamic properties h_{fg}, v_{fg}, and the temperature itself are explicitly included in the *Clapeyron* equation, an exact integration requires the knowledge of their combined relationship vs. temperature. This information is usually not known. In order to provide a simple functional relationship, most heat transfer studies in this area assume that $h_{fg}/(v_{fg} T_s)$ is constant over the integration range (ie. that the slope of the P-T curve is constant). This yields the equation (II.31).

The errors introduced in the calculation of the required liquid superheat, by using this equation, will be demonstrated by comparison with tabulated data. In addition, the error due to the use of the saturated vapour specific volume v_g, rather than the vaporization volume v_{fg} equation, is also analyzed.

The following conclusions will be discussed:

- use of equation (II.31) to predict the liquid superheat can lead to serious error for bubbles with radii of curvature less than 1 μm.
- the approximation of using v_g rather than v_{fg}, introduces an error that is negligible for reduced temperatures (less than 0.8).
- the use of $T_s(P_f)$ instead of $T_s(P_g)$ to evaluate the temperature and the thermodynamic properties in equation (II.31) leads to a major error in the calculation of the wall superheat for bubbles with radii of curvature less than 1 μm.

- the saturation temperature vs. pressure curve fit correlation used to evaluate the liquid superheat is relatively insensitive to the choice of temperature used in the evaluation of the thermodynamic properties.

B. Methods for the Prediction of Liquid Superheat in Bubbles.

It was mentioned in Chapter II that the liquid surrounding a bubble is in a metastable superheated condition, and in thermal equilibrium with the vapour inside of the bubble. For a given substance and bubble radius, the pressures inside and outside a bubble are related by equation (II.5). In heat transfer applications, the independent variable is the temperature. Therefore we are normally more interested in knowing what liquid superheat will be required to maintain the thermo-mechanical equilibrium of the bubble, rather than knowing the bubble vapour pressure.

B.1. Using the *Clapeyron* Equation

The *Clapeyron* differential equation (II.24) provides the relationship between pressure and temperature at saturation. In order to simplify its integration a common practice in the literature is to assume $h_{fg} / (v_{fg} T_s)$ = constant. The saturation temperature T_s is usually evaluated at the liquid pressure P_f and this same temperature

is also used to calculate the properties. In addition, when v_g is much larger than v_f, v_f is often assumed negligible. The resulting relationship is given by equation (II.31).

The validity of such assumptions has been questioned by some researchers, such as **You et al.** (1990), based on the non-linearity of the P-T curve and on the fact that the observed liquid superheats could be very large, specially at the ONB and for well wetting fluids.

The error introduced in the estimation of the required liquid superheat using equation (II.31) both with and without the assumption that $v_{fg} = v_g$, will be analyzed in the following sections for the case of refrigerant R-11 and for water. The results obtained are presented as a function of the bubble radius.

B.2. Curve Fitted Correlations

The *required liquid superheat* surrounding a bubble (RLS) can be most accurately obtained, as a function of pressure, by using accurate curve-fitted correlations.

The thermo-mechanical equilibrium equation for a spherical bubble (II.5), can be used to estimate the pressure inside the bubble and therefore the RLS is obtained as:

$$RLS = T_s(P_g) - T_s(P_f) = T_s\left(P_f + \frac{2\,\sigma}{r}\right) - T_s(P_f) \qquad \text{(IV.1)}$$

The use of $T_s(P)$ curve fitted correlations presents the following obvious advantages over the use of the integrated *Clapeyron* equation with constant $h_{fg}/(v_{fg}\,T_s)$:

- its accuracy is independent of the magnitude of the RLS.

- it is simpler to use.

Accurate correlations for $T_s(P)$ and other thermodynamic and transport properties have been published elsewhere for R-11, R-113 and R-22 by **Martín-Domínguez and McDonald** (1992a, 1992b and 1993), based on **ASHRAE** data. Some correlations for R-11, together with unpublished similar ones for water, are presented in Appendix B.

C. The Slope of the P-T Curve.

In this section we will examine the slope of the P-T curve for R-11 and water, as a function of temperature.

The *Clapeyron* equation, which is a relationship between thermodynamic properties, can be used directly to obtain the slope of the P-T curve from tabulated h_{fg}, v_{fg} and T_s data.

The approximation $h_{fg} / (T_s v_g)$ can be also evaluated and compared with the exact slope to observe how they match or diverge.

The curve fitted correlation for $T_s(P)$ can be used to calculate its own slope numerically, by perturbing the pressure, for comparison with the exact values from the *Clapeyron* equation. Since we can use very small pressure increments, the results obtained will give a clear picture of how closely the slope of the fitted curves matches the true *Clapeyron* equation value. In this study the slope based on the curve fitted correlation was obtained by perturbing the pressure 0.1% above and below every given value at the same tabulated values used with the *Clapeyron* equation.

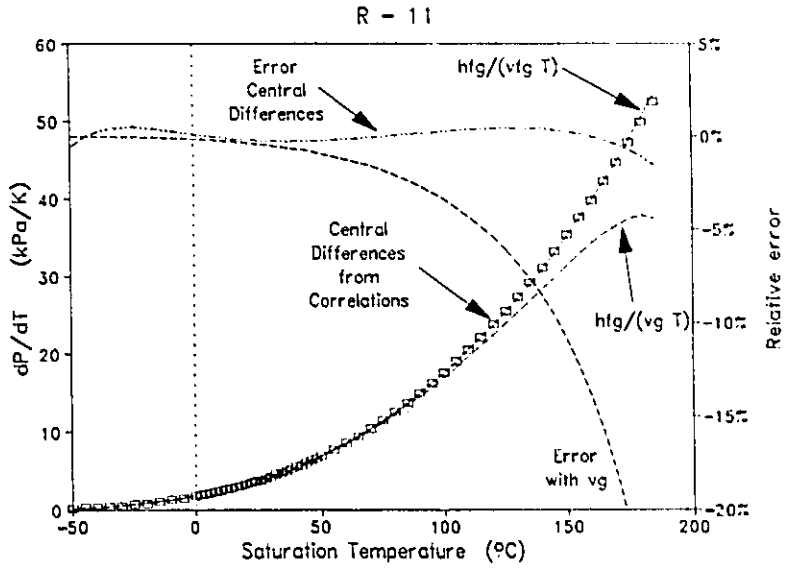

Figure IV.1. Slope of the P-T curve for R-11.

Data for refrigerant R-11 were obtained from the **ASHRAE Fundamentals Handbook** and the calculated results are shown in Figure IV.1. For water the data were

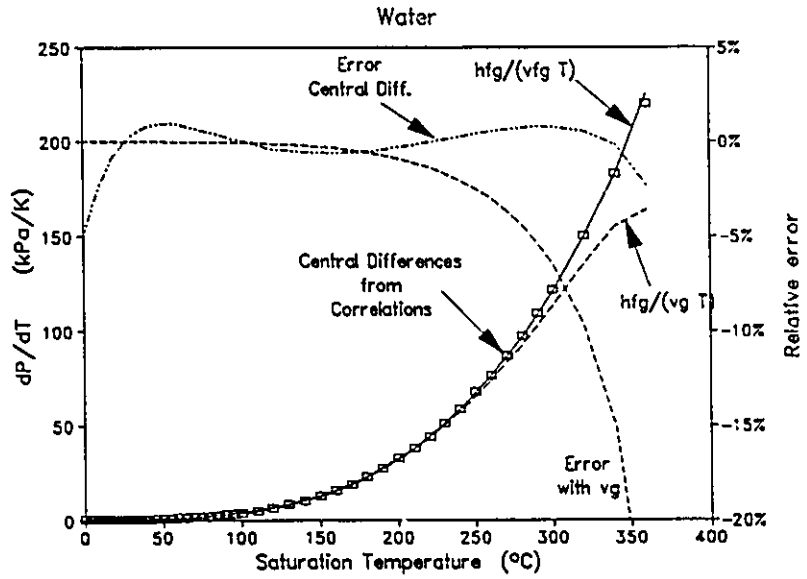

Figure IV.2. Slope of the P-T curve for water.

obtained from **Wark, K.** (1988), and the resulting graphs are shown in Figure IV.2.

Two important conclusions can be drawn from Figures IV.1 and IV.2:

- the use of v_g instead of the correct v_{fg} in the *Clapeyron* equation leads to increasing error as the reduced temperature increases beyond 0.8.
- the assumption that the slope of the P-T curve is constant, over the range of integration of the *Clapeyron* equation, can introduce significant errors in the predicted superheat when the superheat is large.
- the curve fitted correlations for $T_s(P)$, used in this study, closely reproduce the exact P-T curve slope values obtained with the *Clapeyron* equation.

D. Liquid Superheat Prediction for Small Bubbles.

The pressure difference across and hence the liquid superheat surrounding a bubble increases as the bubble curvature radius gets smaller, therefore it is important to know at what bubble size errors in the liquid superheat estimation become important for a given substance.

Figure IV.3 shows the predicted liquid superheat as a function of bubble radius of curvature for the integrated *Clapeyron* equation (II.31) and the fitted correlations. This case is for R-11 at a pressure of 101.3 kPa (T_s = 26.3°C). In both methods the

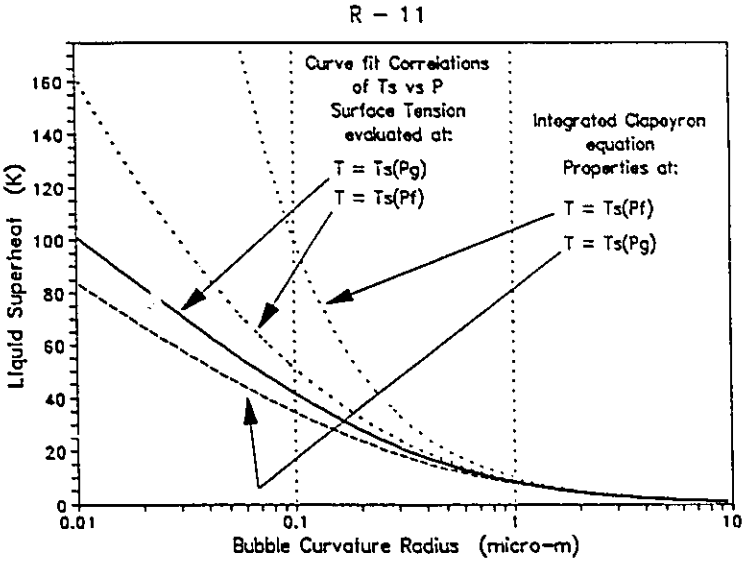

Figure IV.3. Required liquid superheat for a spherical R-11 bubble.

thermodynamic properties were evaluated using the vapour bubble temperature $T_s(P_g)$ and, to illustrate the error involved, also at the fluid saturation temperature $T_s(P_f)$.

In practice, the bubble temperature is known from wall temperature measurements and/or from an estimated temperature profile in the boundary layer, and the bubble size is the variable being calculated. In this analysis the independent variable is the bubble curvature radius and we want to obtain the bubble temperature. However, in order to calculate the required liquid superheat, we need to know the bubble temperature. This situation requires either an iterative or an approximate solution procedure.

The method used to generate the wall superheat curves using T_s vs. P_s correlations employed the following approximation. The calculation series started at a large bubble size, where the superheat was close to zero and progressed towards smaller bubble sizes, permitting in this way a very close approximation of the bubble temperature. Starting

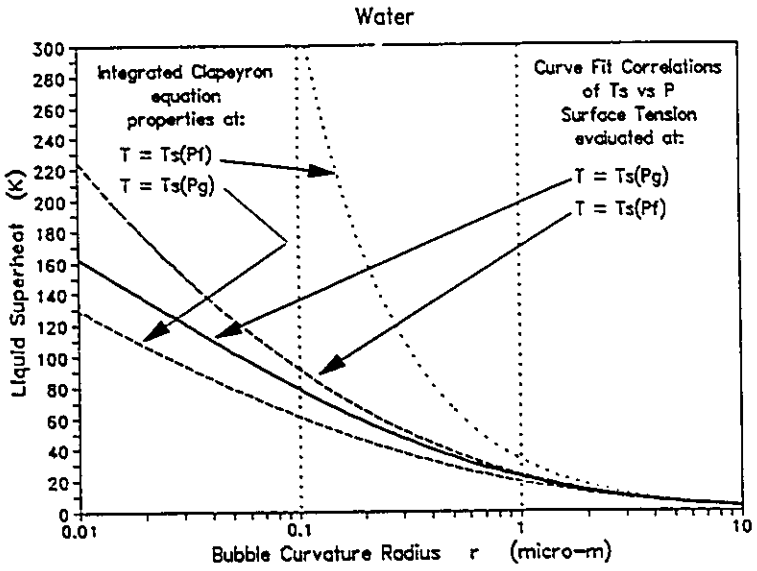

Figure IV.4. Required liquid superheat for a spherical water bubble.

with relatively large bubbles where $P_g \approx P_f$, and therefore $T_g \approx T_s(P_f)$, and evaluating the properties at $T_s(P_f)$, the required liquid superheat was calculated. Then this value for T_g was used to calculate the properties for the next smaller bubble size, employing progressively smaller step sizes. Figure IV.4 shows similar calculations for saturated water at 101.3 kPa. In the results presented on Figures IV.3 and IV.4, the curve obtained using the curve fitted correlations, with the temperature evaluated at the bubble pressure $T = T_s(P_g)$, represents the correct values. The results obtained with the approximation method were compared versus those obtained using an iterative procedure for selected bubble sizes. The maximum discrepancy observed, at $r = 0.01$ μm, were 0.89°C for R-11 and 1.04°C for water.

E. The Effect of Pressure on the Liquid Superheat.

The results presented in this chapter were produced by the simulation procedure developed in section D. The results obtained for R-11 and water are shown in Figures

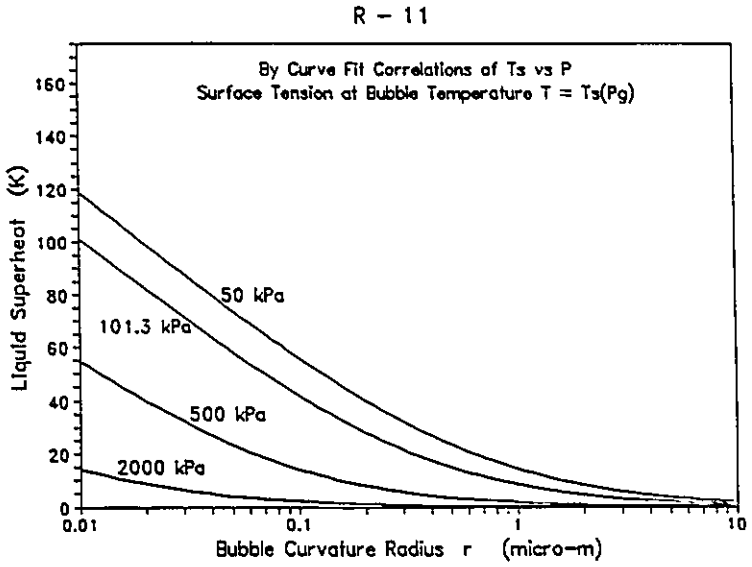

Figure IV.5. Effect of pressure on the required liquid superheat in R-11 spherical bubbles.

IV.5 and IV.6 respectively.

F. Conclusions.

These results show that the use of the *Clapeyron* equation can introduce a large uncertainty in the predicted values of the liquid superheat for small bubbles.

From these results is possible to conclude the following, for bubbles with radius of curvature smaller than 1.0 μm:

- the use of the liquid saturation temperature in evaluating equation

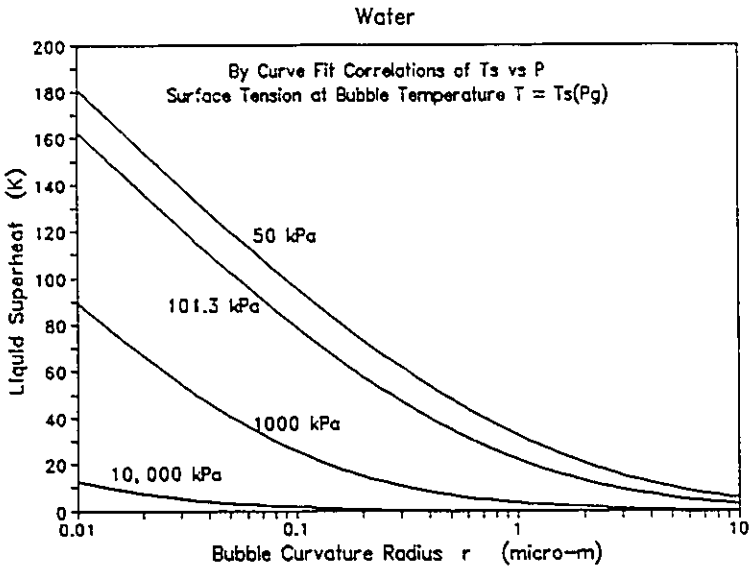

Figure IV.6. Effect of pressure over the required liquid superheat in water.

(II.31) introduces a major over prediction.

- when the correct temperature $T_s(P_g)$ is used, equation (II.31) underpredicts the superheat.
- the error introduced by using the incorrect temperature $T_s(P_f)$ in the curve fitted correlations to evaluate the surface tension results in a small overprediction of the liquid superheat.

Since the use of curve fitted correlations to evaluate the required liquid superheat is exact when the vapour temperature is chosen to evaluate the surface tension, it was used in the remainder of this study.

Care must be exercised in the use of equations based on equation (II.31) for small diameter applications, since improper evaluation of the properties can lead to serious errors.

Larger pressures (and saturation temperatures) reduce the surface tension and therefore the bubble pressure differences for a given bubble size. In addition, the slope of the $T_s(P)$ curve decreases at higher pressures. This also reduces the required liquid superheat. The combined effect is a large reduction in the required liquid superheat for a given bubble size.

Chapter V

BUBBLE EQUILIBRIUM

A. Introduction.

In the previous chapter we assumed that a bubble was in equilibrium with its surroundings at all times, in this chapter we will analyze the response of a bubble to pressure and temperature changes in its environment.

For a bubble in thermal equilibrium with the surrounding liquid, the relationship between the pressure inside to the pressure outside, required to maintain also a mechanical equilibrium, is given by:

$$P_g = P_f + \frac{2\sigma}{r} \qquad \text{(II.5)}$$

At this equilibrium condition it was shown in the previous chapter that the surrounding liquid is in a superheated thermodynamic state and that the degree of superheat, RLS, required in the liquid to maintain the bubble in equilibrium is given as:

$$RLS = T_s(P_g) - T_s(P_f) = T_s\left(P_f + \frac{2\sigma}{r}\right) - T_s(P_f) \qquad \text{(IV.1)}$$

For a bubble-liquid or a bubble-liquid-solid system, the independent (and controllable) variables are the fluid pressure and the system temperature. For the bubble

size range of interest in this analysis, the pressure and temperature inside the bubble will respond with minimal delay to every change on the external conditions, given the infinitesimal size of the bubble with respect to the bulk liquid and solid surface masses. The only restriction that the bubble vapour is able to impose is that its equilibrium thermodynamic state must always be that of a saturated vapour.

B. Bubble Unstable Equilibrium in the Bulk of a Fluid.

In this analysis remember that the surface tension is assumed to be a function of temperature only, and it decreases with increasing temperature.

If a bubble exists in equilibrium in the bulk of a liquid its shape in zero gravity is that of a sphere.

B.1. Isothermal Process.

The response of a bubble's volume to perturbations on the external pressure at constant temperature are as follows:

- if the liquid (system) pressure P_f decreases, the bubble internal pressure P_g decreases in the same amount, which drives the vapour thermodynamic state into the superheated region along the constant temperature line. The superheated condition induces liquid vaporization and an increase in volume. The increase in volume increases the bubble radius of curvature and further reduces the

internal pressure, causing even more liquid vaporization.

- if the liquid pressure P_f increases the bubble internal pressure increases in the same amount immediately, which initiates vapour condensation. This reduces the bubble radius of curvature and further increases the internal pressure, causing even more vapour condensation.

Consequently, any pressure perturbation will cause either the continuous growth or the continuous shrinkage of a bubble initially in thermo-mechanical equilibrium.

B.2. Isobaric Process.

The response of the bubble's volume to perturbations on the external temperature at constant pressure are as follows.

- if the liquid (system) temperature increases, the bubble temperature also increases in the same amount. This drives the vapour into the superheated region along the constant pressure line. The superheated condition induces liquid vaporization and an increase in the bubble's volume. The increase in volume increases the bubble radius of curvature and reduces the internal pressure, causing even more liquid vaporization.
- if the liquid temperature decreases, the bubble temperature also decreases in the same amount. This causes vapour condensation

and a reduction in the bubble radius of curvature. This shrinkage causes an increase in the bubble internal pressure and further vapour condensation.

Consequently, any temperature perturbation will cause either the continuous growth or the continuous shrinkage of a bubble initially in thermo-mechanical equilibrium.

C. Bubble Equilibrium at the Interface with a Solid Surface.

The only way in which a bubble can reach a stable state, after a pressure or temperature disturbance, is if the bubble radius of curvature somehow *decreases* as the volume *increases* or *increases* as the volume *decreases*. This could only occur when the bubble is in contact with a solid surface that could modify the bubble shape. Not every bubble-solid interaction would produce the desired behaviour on the bubble radius of curvature.

The following chapter focuses on how the geometry of a solid surface affects the bubble radius of curvature.

Chapter VI

CAVITY BUBBLE RADIUS OF CURVATURE

A. Introduction.

In this chapter the behaviour of bubbles in cavities will be geometrically analyzed. It will be shown that:

- the interface between the liquid and the vapour in a cavity forms a segment of a sphere.
- the magnitude of the bubble radius of curvature is a function of the liquid contact angle, cavity angle, cavity size and the location of the bubble inside of the cavity.
- when the contact circle between a bubble and the wall of a conical cavity increases, the radius of curvature of the bubble surface will always grow, regardless of the cavity angle and contact angle.
- when a growing bubble reaches the mouth of a cavity, the bubble radius of curvature can continue to grow or can first shrink and then grow again, depending on the contact angle and the cavity angle.

It is useful to keep in mind the significance of the radius of curvature. When it

increases, the pressure differential between the vapour and the liquid decreases and hence the corresponding superheat *required* for stability (RLS) decreases. (ie. increasing radius of curvature → decreasing RLS and vice versa).

An **increase** in the *actual liquid superheat* (ALS) around a bubble, produced either by an increase in the liquid temperature or by a decrease in the liquid pressure, will always induce liquid vaporization (bubble volume increases).

A **decrease** in the ALS around a bubble, produced either by a decrease in the liquid temperature or by an increase in the liquid pressure, will always induce condensation (bubble volume decreases).

Consequently, a bubble in which its radius of curvature increases as a result of an increase of its volume will continue to grow without limit (ie. increasing ALS → decreasing RLS), and a bubble in which its radius of curvature decreases as a result of a decrease of its volume will continue to shrink until it collapses (ie. decreasing ALS → increasing RLS). The only possible stable bubble is that in which its radius of curvature decreases with increasing volume, and vice versa (increasing ALS → increasing RLS and decreasing ALS → decreasing RLS).

The focus of this chapter is, therefore, to analyze the behaviour of the bubble radius of curvature as a result of the interaction between the bubble and a solid surface, for various cavity geometries and liquid contact angles, in order to determine what regions of a cavity are stable locations for a bubble, (ie. locations where the bubble could resist variations in the ALS of the surrounding liquid).

For simplicity in the numerical analysis, the geometry of the cavities to be analyzed are based on regular cones. This results in three classes of cavities:

- positive conical (positive values of the cavity angle).

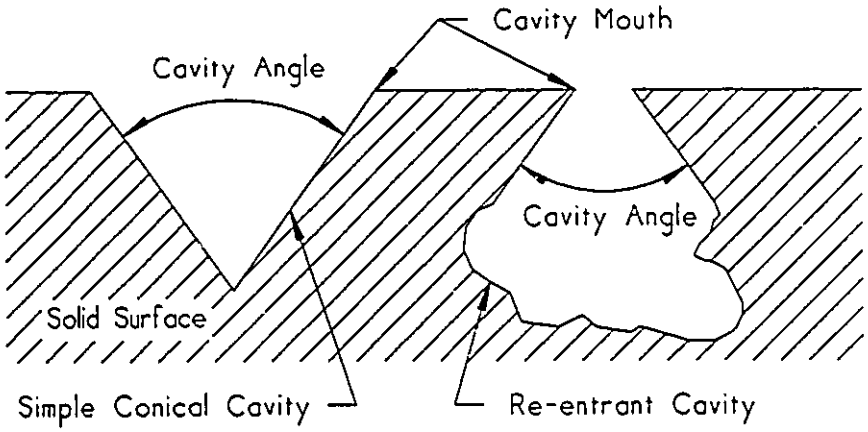

Figure VI.1. Characterization of the conical and re-entrant cavities.

- negative conical or re-entrant (negative values of the cavity angle).
- combined positive and negative conical or conical re-entrant (top angle positive and bottom angle negative).

These geometries are shown in Figures VI.1 and VI.2.

B. Bubble Geometry in an Isothermal Conical Cavity.

A bubble attached to a solid surface is no longer a perfect sphere, but only a spherical segment. For a given liquid-solid-gas combination, the angle formed by a bubble with respect to the solid surface, at the triple interface, is referred as the *contact*

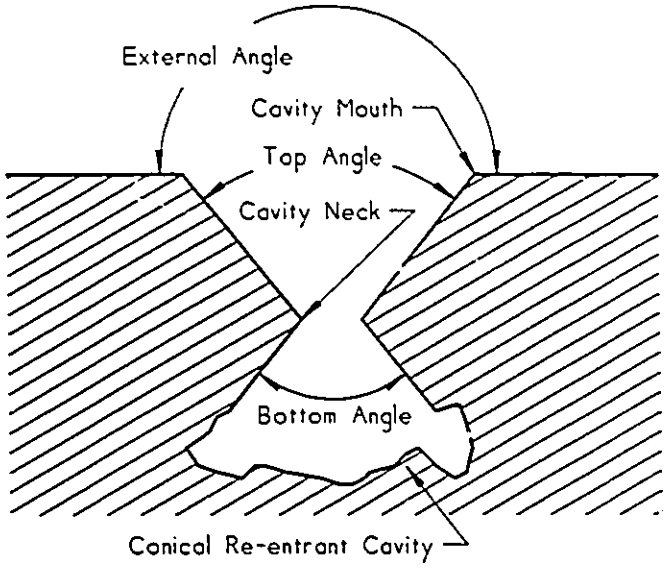

Figure VI.2. Characterization of the conical re-entrant cavity.

angle (ß). It should be noted that the contact angle of a given liquid-solid combination is a function only of temperature and hence the orientation of the bubble liquid-vapour boundary is a function only of the solid surface orientation **at the triple interface line.**

B.1. Bubbles Attached to the Walls of Isothermal Conical Cavities.

A bubble attached to the walls of a positive conical cavity is depicted in Figures VI.3 (A) and VI.4 (A). The radius of curvature of any bubble within a conical cavity forms an angle, with respect to the horizontal, that remains constant until the bubble reaches the mouth (bubbles A and B in Figures VI.3 and VI.4. During the bubble growth process within the cavity (increasing trapped vapour volume), the bubble radius

of curvature therefore increases continuously. Thus, the cavity walls are an unstable location for any bubble. The same argument applies for a shrinking bubble.

B.2. The Bubble at the Cavity Lip.

At the cavity lip the cavity angle may be considered to change abruptly to 180°. A growing bubble attached to the cavity lip will increase in volume until its contact angle

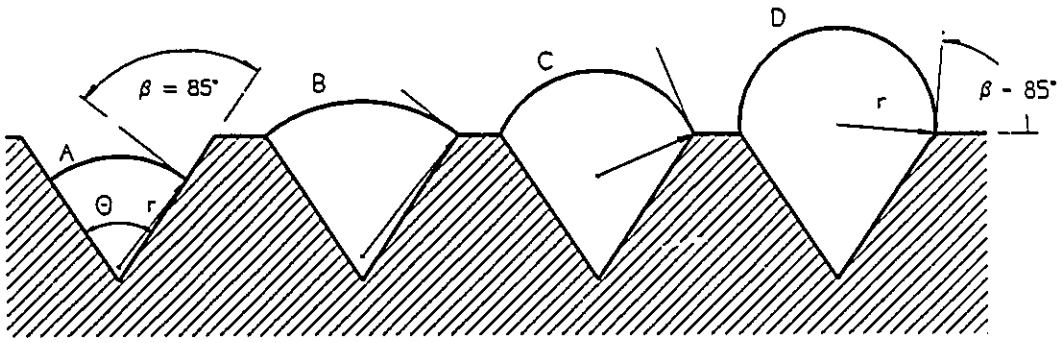

Figure VI.3. The growth of a 85° contact angle bubble.

with respect to the external surface becomes equal to its normal contact angle. During this process the bubble radius of curvature will change by rotating over the cavity lip, as can be observed with bubbles B, C and D in Figure VI.3. Once this is achieved the bubble can spread outside of the cavity mouth.

When the angle formed by the bubble radius of curvature with respect to the horizontal is positive (below the horizontal), as the bubble first reaches the cavity lip during the growing process as shown in Figure VI.3 (B) for a bubble of 85°, the bubble radius of curvature will undergo a reduction during the bubble growth from B to D at

the mouth of a cavity. Thus such a bubble can attach at the cavity mouth.

When the angle is negative (above the horizontal) as the bubble first reaches the cavity mouth (Figure VI.4 B for a 10° contact angle bubble), the radius of curvature will

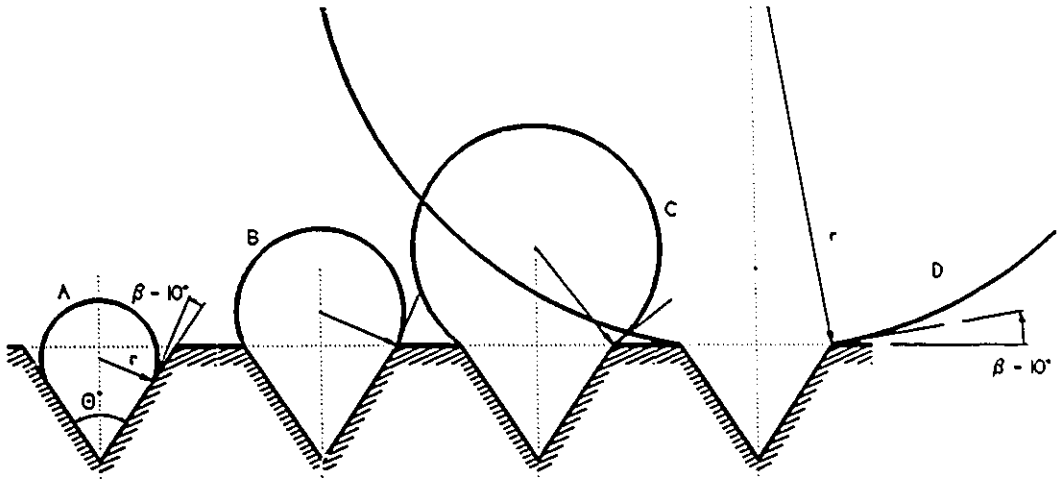

Figure VI.4. The growth of a bubble at the cavity mouth for a 10° contact angle.

increase as the bubble expands out of the mouth of the cavity. This situation occurs when the liquid contact angle is small. Such a fluid bubble cannot attach to the cavity lip.

C. Bubble Radius of Curvature.

Based on Figures VI.5 or VI.6, an analytical expression can be derived to calculate the bubble radius of curvature (r) as a function of the cavity angle (Θ), contact angle (ß) and the horizontal radius between the cavity axis and the contact point between the bubble and the cavity wall (R). The radius of curvature of the bubble, r, can be written as:

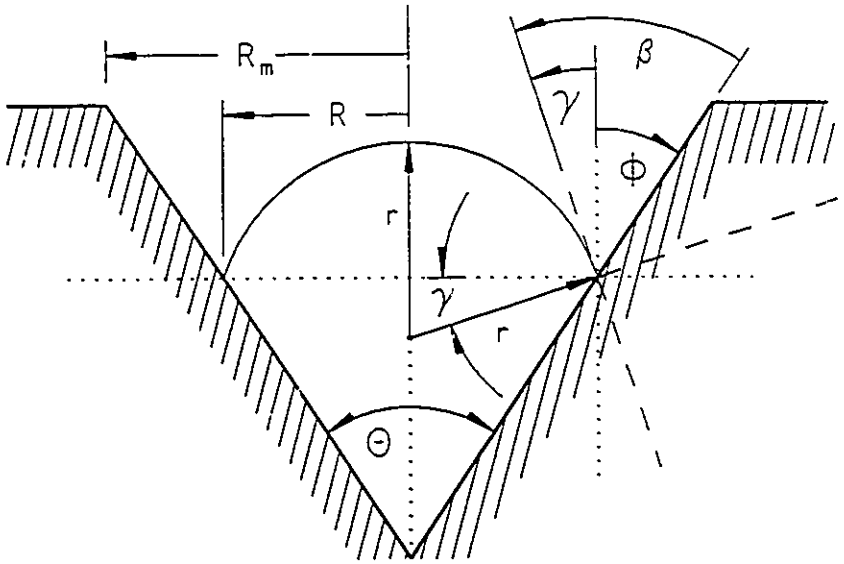

Figure VI.5. Geometry of a bubble in a conical cavity.

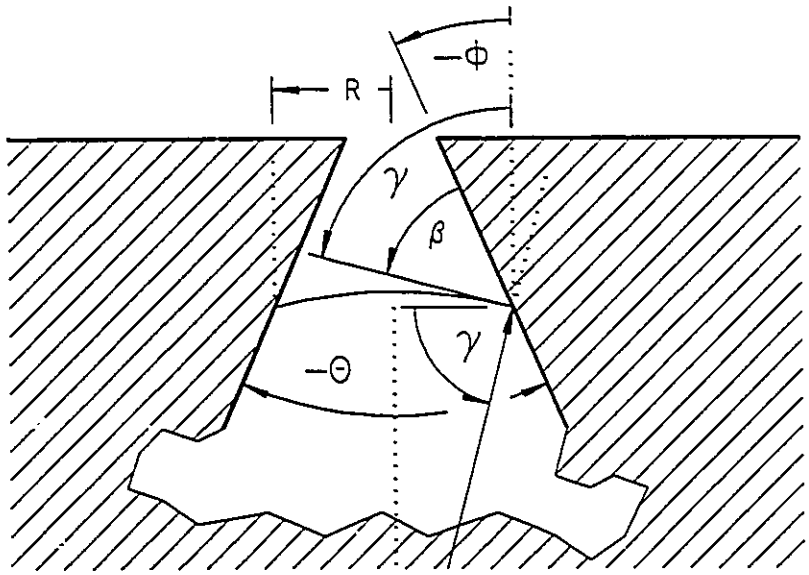

Figure VI.6. Geometry of a bubble in a re-entrant cavity.

$$r = \frac{R}{\cos(\gamma)} \qquad \text{(VI.1)}$$

Where the angle γ is the difference:

$$\gamma = \beta - \phi \qquad \text{(VI.2)}$$

And the angle ϕ is:

$$\phi = \frac{\theta}{2} \qquad \text{(VI.3)}$$

The relationship between the bubble radius of curvature and the contact angle, the cavity angle and the distance R, given in equations (VI.1), (VI.2) and (VI.3), seems straightforward, but a closer analysis reveals important details about the behaviour of the radius of curvature inside a cavity and at the cavity lip.

The angle gamma (γ) is a constant for a bubble inside a conical cavity. Gamma increases as the bubble grows while attached to the cavity lip, and then remains constant as the bubble spreads outside of the cavity mouth.

The angle ϕ is the orientation of the solid surface with respect to the axis of the cavity at the point where the bubble liquid-vapour surface contacts the wall of the cavity. Inside a conical cavity, ϕ equals one half of the cavity angle Θ, and at the external surface equals 90°.

Common cavities would have angles ranging from $\Theta \approx 0°$ to $\Theta \approx 60°$, but from the bubble's perspective, the change in the solid surface orientation at the cavity lip appears as an increase in cavity angle to 180°. In the following analysis the term "Cavity Angle" will refer to two times the solid surface orientation with respect to the vertical (2ϕ).

C.1. Small Contact Angles. (Poor Wetting Fluids, eg Water)

From equation (VI.1) we know that the ratio:

$$\frac{r}{R} = \frac{1}{\cos(\gamma)} \geq 1 \qquad \text{(VI.4)}$$

Figure VI.7 shows a graph of gamma (γ) and r / R as a function of cavity angle, for a substance with a contact angle of 10°. It can be readily observed that, for this contact angle:

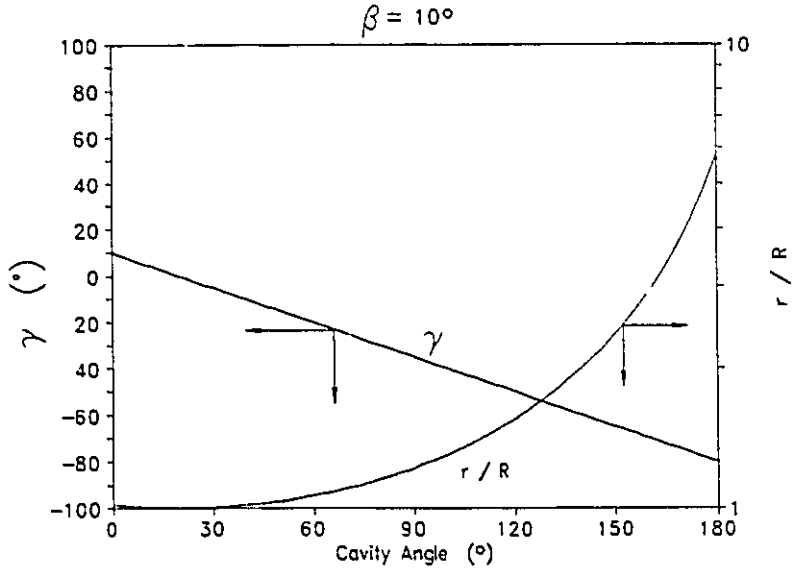

Figure VI.7. Behaviour of the angle gamma (γ) for a contact angle (β) of 10°.

- the ratio r / R is always larger than 1.0, except for $\gamma = 0$ ($\Theta = 2\ \beta$), therefore the radius of curvature of a bubble *growing*

inside a conical cavity will always increase.

- the angle γ has positive values at cavity angles smaller than 2 ß. For a bubble growing at the cavity lip with a cavity angle smaller than 2 ß, the radius of curvature must first shrink, down to the same radius as the cavity mouth and then increase as the bubble grows out of the cavity. For cavities with cavity angle larger than 2 ß the bubble radius of curvature only increases.
- for cavities with angles in the range from 0° to about 60°, which probably covers all the actual cavities in a surface, the magnitude of the bubble radius of curvature will be almost the same as the radial distance (R), since the ratio r / R acquires values very close to 1.0 in that range.
- for the case shown, the bubble radius of curvature would grow to almost six times the size of the cavity mouth radius before starting to spread over the adjacent surface.

Figure VI.8 shows how the bubble radius of curvature within the cavity is insensitive to the cavity angle up to 50° and continues to increase as the bubble grows. Note the large increase in radius of curvature experienced at the cavity lip.

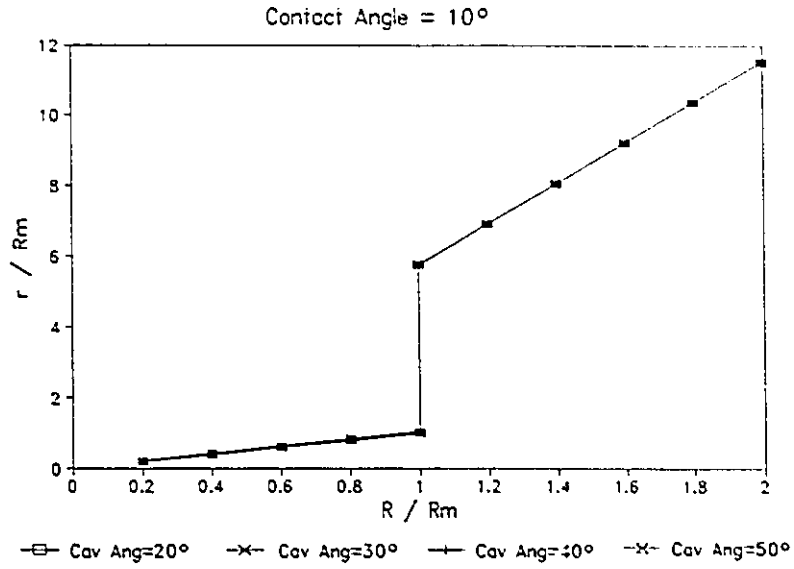

Figure VI.8. Effect of the cavity angle on the radius of curvature for a substance with β = 10°.

C.2. Large Contact Angles.

Figure VI.9 shows the graph of gamma (γ) and r / R, as a function of cavity

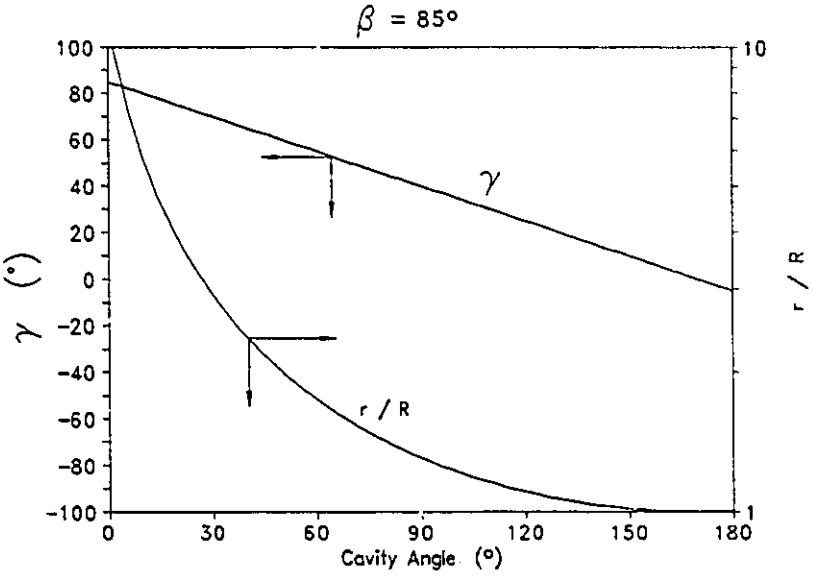

Figure VI.9. Behaviour of the angle γ and r / R for a contact angle (β) of 85°.

angle, for a substance with a contact angle of 85°. It can be readily observed that, for this contact angle:

- the ratio r / R has always values larger than 1.0, therefore the radius of curvature of a bubble *growing inside* a cavity will always increase.
- the angle γ has positive values for cavity angles smaller than 170° (2 ß), therefore, for bubbles growing at the lip of any cavity on a flat surface, the radius of curvature must first shrink down to the same radius as the cavity mouth before it again increases as the bubble spreads out of the cavity.
- for nucleation sites with cavity angles in the range from 0° to about 60°, the magnitude of the bubble radius of curvature could vary from more than 10 to 1.5 times the size the radial distance (R).
- the magnitude of the bubble radius of curvature is very sensitive to the value of the cavity angle, for cavities in the range 0° to about 120°.
- the bubble radius of curvature must shrink down to the same radius as the cavity mouth before it can leave the cavity lip. This fact is very important because the *bubble radius of curvature* at the onset of nucleate boiling can be characterized by the *cavity mouth*

radius.

Figure VI.10 shows how the radius of curvature of a fluid-solid interface with a contact angle of 85° varies with position as it grows with a cavity for various cavity

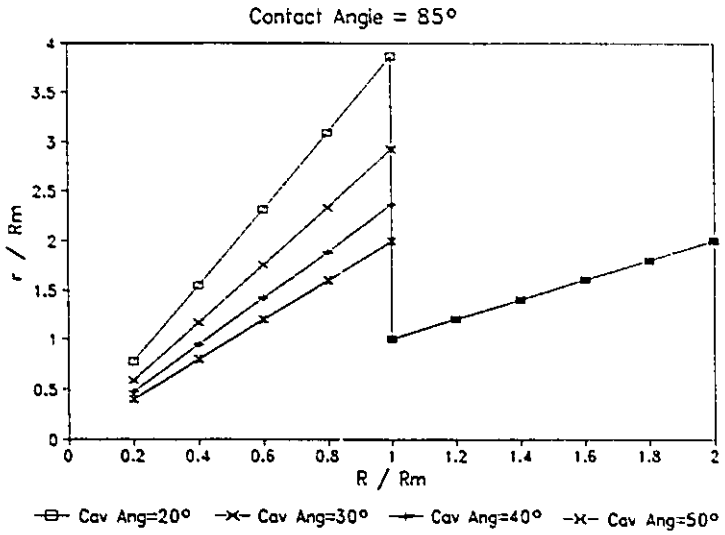

Figure VI.10. Effect of the cavity angle on the radius of curvature for a substance with β = 85°.

angles, and how it always shrinks at the cavity lip.

C.3. Three Cases Compared.

Figure VI.11 shows graphs for substances with contact angles of 10°, 45° and 85° to better observe the strong effect of the contact angle over the bubble radius of curvature at every possible cavity angle, and also the almost opposite behaviour between substances with small contact angles when compared to those with large contact angles.

Real cavities could be expected to have cavity angles varying between 0° and 60°,

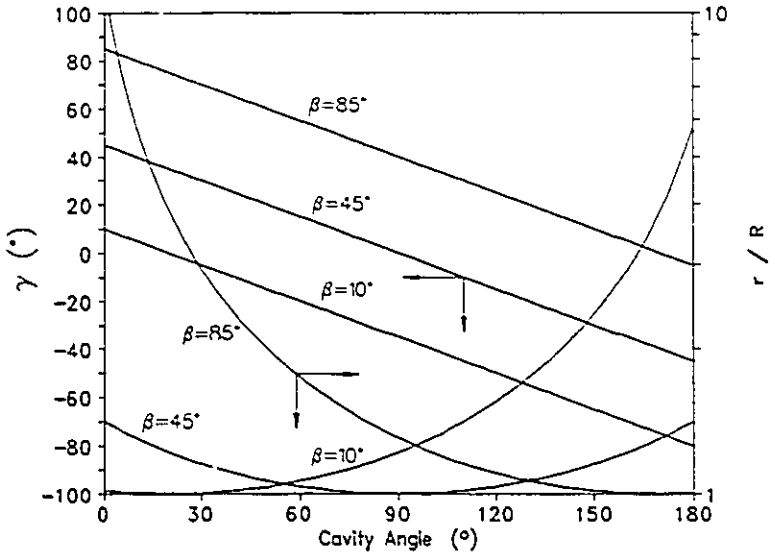

Figure VI.11. Behaviour of γ and r / R for contact angles of 10°, 45° and 85°.

Figure VI.12 shows, for this range, the strong differences in the size of the bubble radius of curvature that are to be encountered between substances of small, medium and large contact angles.

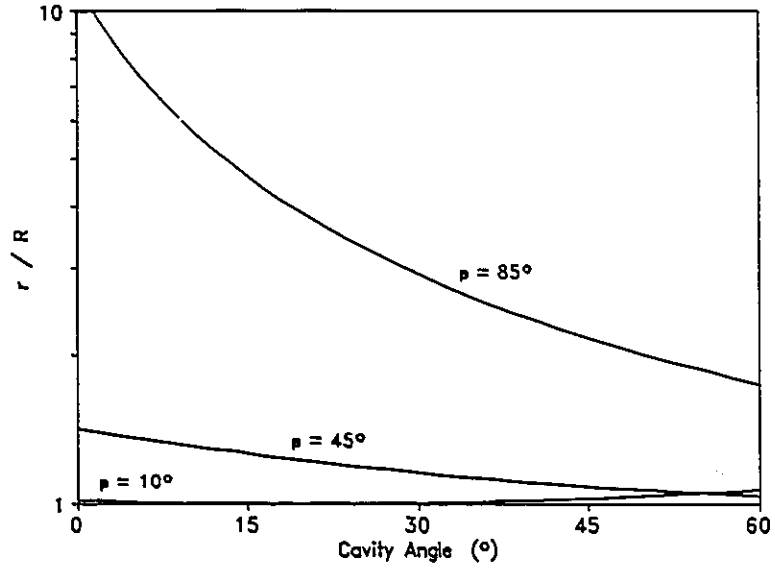

Figure VI.12. Behaviour of r / R for contact angles of 10°, 45° and 85° in common cavities.

D. The Evolution of the Radius of Curvature During the Growth Process.

The evolution of the radius of curvature of a bubble that starts growing deep inside of a conical cavity of a given cavity angle, expands to reach the cavity mouth and

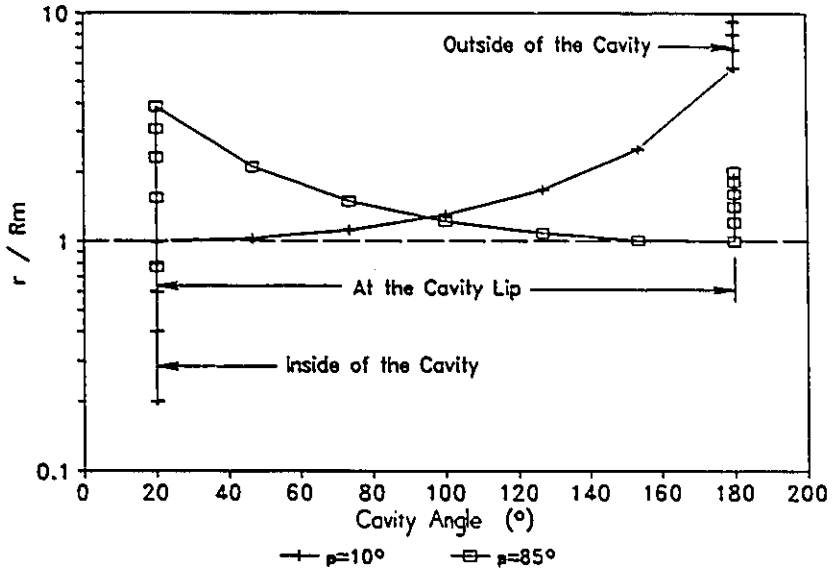

Figure VI.13. Bubble curvature radius evolution over a 20° cavity.

finally outgrows it and spreads over the outside flat surface will be now compared for substances with contact angles of 10° and 85°. These two contact angles are typical of commercial refrigerants and of water respectively. Figure VI.13 shows the special case where the cavity angle is 20°. For this case, at the cavity mouth, the cavity angle effectively changes from 20° to 180°. Note that:

- the initial radius of curvature, deep inside of the cavity, is much

smaller for the small contact angle substance than that of the large contact angle.

- when the bubbles first reach the cavity mouth the 10° substance radius of curvature is the same size as the cavity mouth radius, while the 85° substance radius of curvature is about four times larger.
- during the growing process at the cavity lip, the radius of curvature of the small contact angle substance increases to six times the cavity mouth radius, while the radius of curvature of the large contact angle substance first reduces to the same size as the cavity mouth radius then resumes growth.
- both substances experience an increase in their radius of curvature as the bubble grows beyond the cavity mouth.

Figure VI.14 shows a similar process for a cavity with an angle of 80°.

Comparing Figures VI.13 and VI.14 the following observations should be noted:

- the evolution of the radius of curvature of both substances at and beyond the cavity lip is independent of the cavity angle, and hence a single graph of r / R_m as a function of angle from 0° to 180° can be used to represent the behaviour for bubble growth at the mouth of all cavities with angles from 0° to 180°.
- the radius of curvature when the bubble first reaches the mouth of

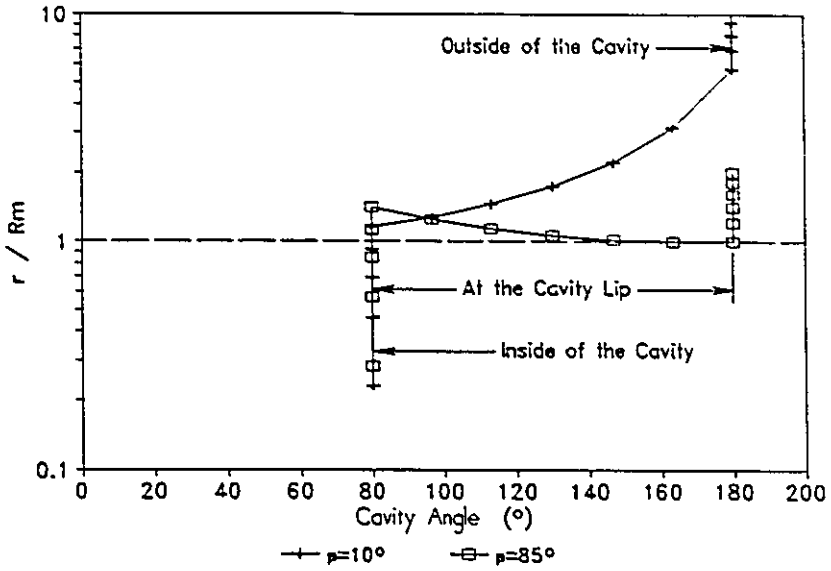

Figure VI.14. Bubble curvature radius evolution over a 80° cavity.

the cavity is the same for both substances when the cavity angle Θ is equal to $(10° + 85°) = 95°$.

E. The Re-entrant Cavity.

From the previous sections we can observe that in a positively angled conical cavity the bubble radius of curvature reduces as the bubble slides into the cavity. Bubbles of smaller radius of curvature require larger liquid superheats (higher temperatures) to maintain their equilibrium, therefore a bubble that shrinks into a positive isothermal conical cavity will collapse and disappear. The only thing that could prevent such a complete collapse would be a change in the orientation of the cavity walls, which causes an increase in the bubble radius of curvature.

In order to avoid a discontinuity in the description of the surface angle at a sharp edge, the surface at that point will be assumed to have an infinitesimal radius.

When the cavity wall surface orientation with respect to the vertical "ϕ" becomes negative, the cavity is described as *re-entrant*. Figure VI.15 shows examples of such

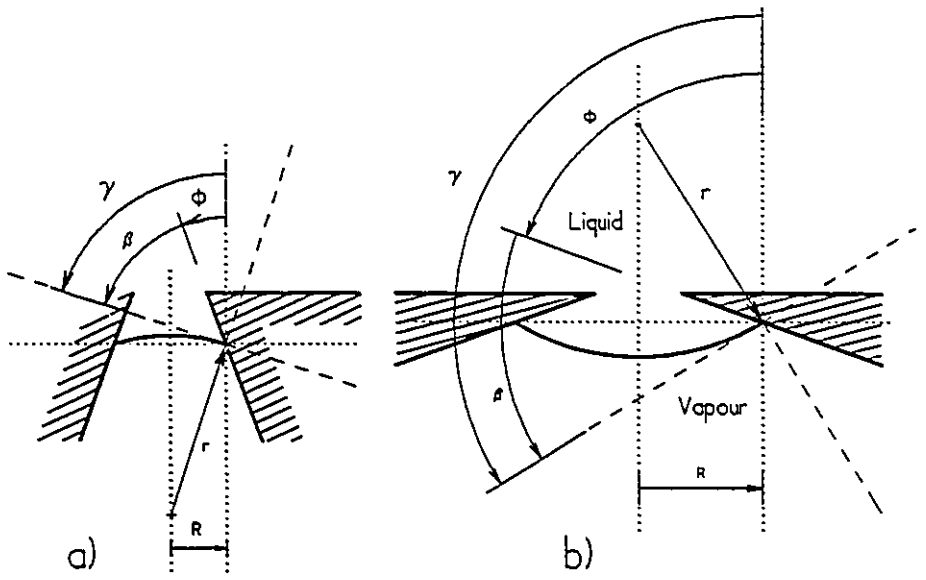

Figure VI.15. *Re-entrant cavity shapes.*

cavities. Case (a) shows a bubble with a positive radius of curvature and case (b) shows a cavity of larger negative ϕ, for which the bubble radius of curvature becomes *negative*. A negative radius of curvature means that the bubble is now convex with respect to the vapour phase and the surface tension forces act against the liquid phase. In both these cases the radius of curvature increases as the bubble recedes into the cavity.

From Figure VI.15 it is readily obvious that for some combinations of surface orientation ϕ and liquid contact angle ß the bubble becomes flat and its radius of

curvature infinite (for $\gamma = \beta - \phi = 90°$). When this condition occurs, the pressures on both sides of the bubble interface are the same and the thermodynamic states are those of saturation for both phases. If the bubble radius of curvature becomes negative the surface tension forces compress the liquid phase. Such a cavity will permit the vapour to remain saturated and in equilibrium with *subcooled* liquid.

It should be noted that the minimum possible positive value for the bubble radius of curvature occurs at the edge of the re-entrant mouth. For a given fluid, if the bottom cavity angle (negative) is large enough to create a convex bubble (negative bubble radius of curvature), then the bubble radius of curvature will also attain a maximum positive value at the re-entrant mouth as the bubble surface becomes flat when the radius of curvature pivots at the re-entrant mouth, and then will turn negative as the bubble surface changes to convex. After this point, the bubble radius of curvature will keep reducing its negative magnitude until the contact angle acquires its normal value with respect to the inner cavity walls. As the bubble size continues to shrink the radius of curvature increases in magnitude. Note that:

- the *minimum* bubble radius of curvature occurs when the bubble is at the re-entrant mouth. The minimum concave radius of curvature is equal to the mouth radius. The minimum convex radius of curvature occurs when the bubble is about to recede into the cavity below the mouth and will always be greater than the mouth radius.
- the *minimum concave* value of the radius of curvature will

determine the superheat required for a bubble to depart from the mouth, (ie. the minimum required superheat to activate such a cavity).

- the *minimum convex* radius of curvature will dictate the maximum subcooling that the bubble embryo could resist before the liquid floods (quenches) the cavity.

For a given re-entrant cavity mouth radius, the angles of the surfaces above and below the mouth will determine the shape and radius of curvature of a bubble at the point

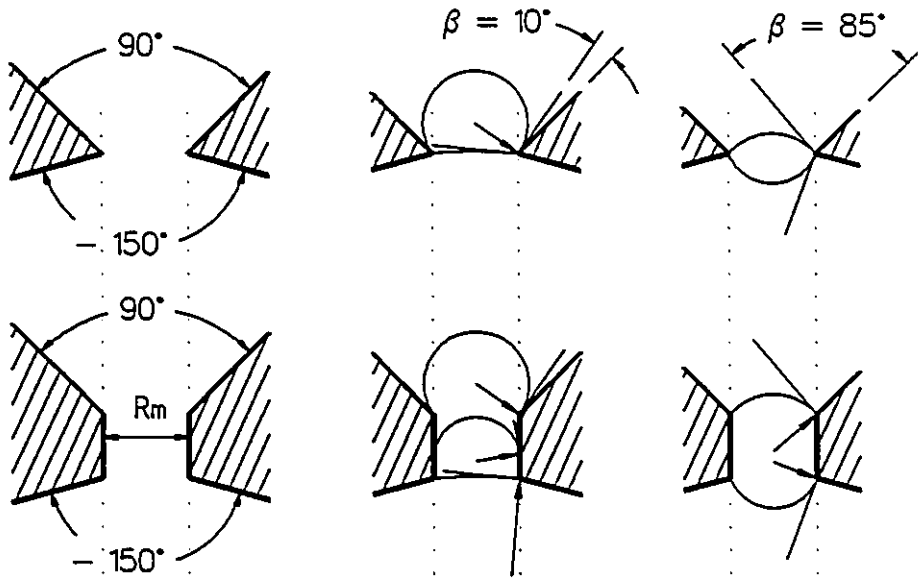

Figure VI.16. The generalized re-entrant cavity.

where the bubble grows outside of the cavity mouth. These conditions are shown in Figure VI.16, where in the top row of figures, bubbles of 10 and 85 degrees of contact angle are shown with the limiting shapes they acquire just before leaving the cavity neck.

At this point it is very useful to recognize that the evolution of the bubble radius of curvature at the re-entrant neck is NOT affected at all if the sharp mouth edge is modified as shown in the lower row of figures in Figure VI.16, where the neck now has a finite thickness. During bubble growth, the addition of the vertical section stops the bubble radius of curvature evolution at a certain stage on the lower edge. The bubble then moves to the top edge *with no change in the shape of the interface*. Once the bubble reaches the top edge it completes its evolution exactly as would have happened with the sharp edge cavity neck.

F. The Generalized Conical Re-entrant Cavity.

After the previous analysis we can now generalize the shape of the re-entrant cavity by allowing the angles of the walls above and below the neck to have a value from 0 to 360 degrees and from 0 to -360 degrees respectively. The complete picture of the

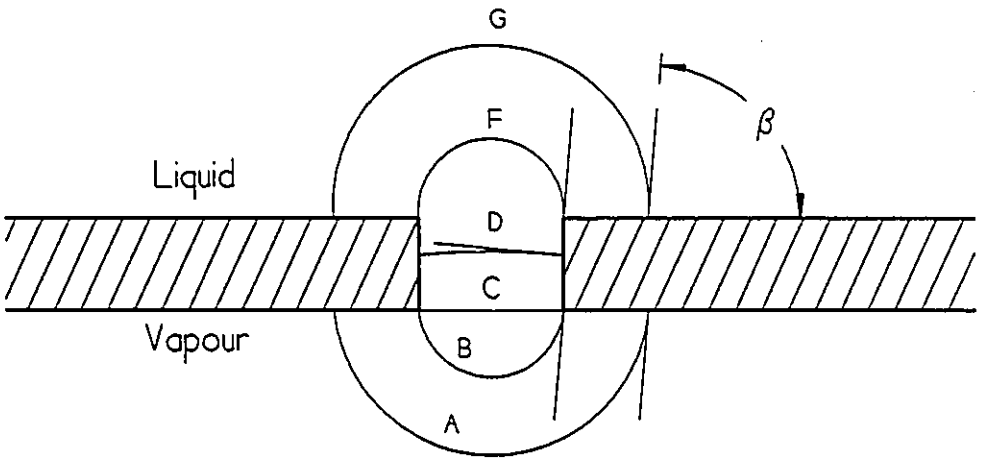

Figure VI.17. Evolution of a 85° contact angle bubble on a flat cavity.

evolution of the bubble radius of curvature is obtained for the case of a re-entrant *cavity* with a top surface of 180 degrees and a bottom surface of -180 degrees, as shown in Figures VI.17 (a) and (b), where bubbles of substances of 85 and 10 degrees of contact

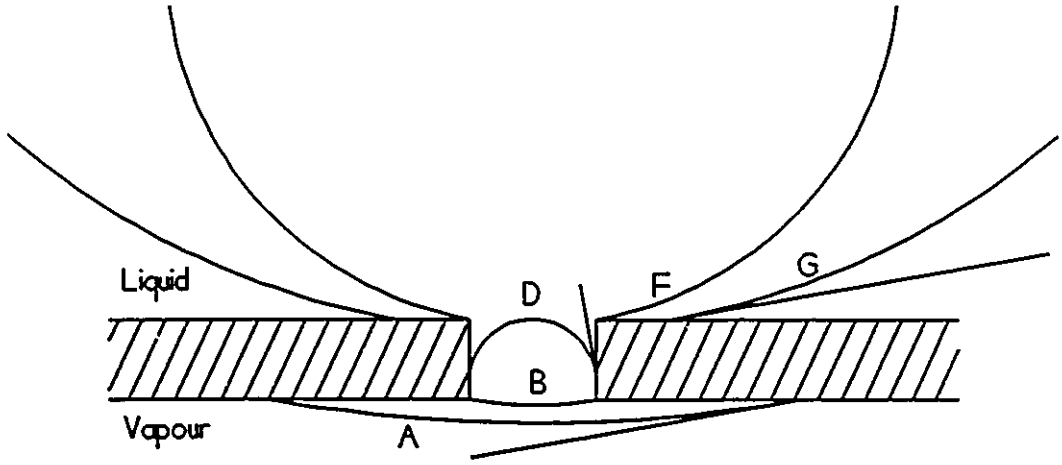

Figure VI.18. Evolution of a 10° contact angle bubble on a flat cavity.

angle respectively are depicted at several stages of evolution.

The evolution of the bubble radius of curvature at the mouth of a completely re-entrant cavity (flat above and below) is shown in Figure VI.19 for a substance with a contact angle of 85° (eg. water), and in Figure VI.20 for a substance with a contact angle of 10°. In both figures the vertical axis is the log of the ratio of the bubble radius of curvature to the radius of the mouth of the cavity. The horizontal axis is the cavity angle Θ and equals two times the surface orientation angle ϕ ($\Theta = 2\ \phi$).

A description of the processes shown in the figures is:

- processes B → A occurs when the convex bubble leaves the mouth

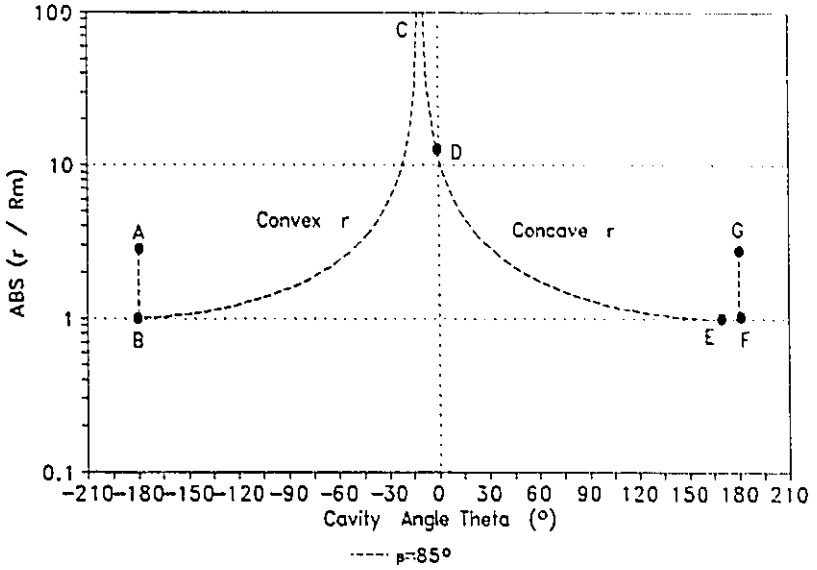

Figure VI.19. The evolution of r in a generalized (flat) re-entrant cavity, for β = 85°.

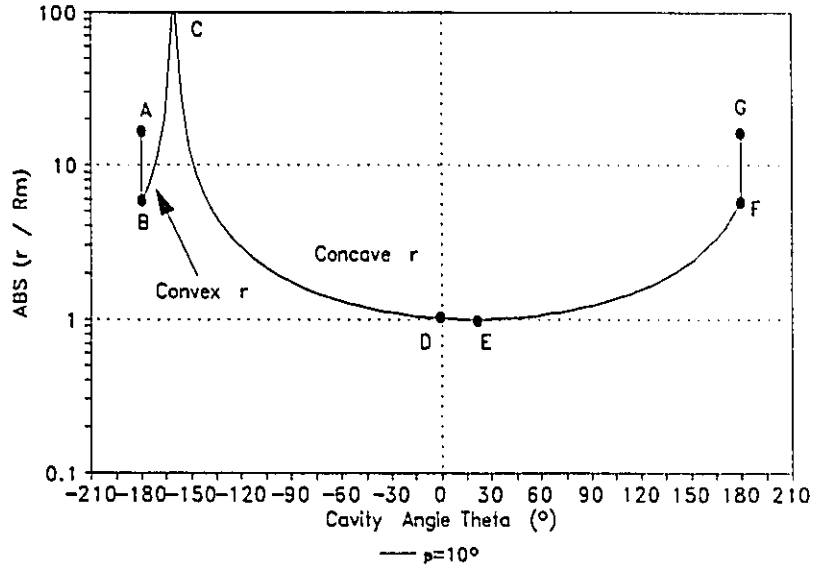

Figure VI.20. The evolution of r in a generalized (flat) re-entrant cavity, for β = 10°.

and contracts in volume further *into* the cavity.

- processes E → F occurs when the concave bubble leaves the mouth

and expands in volume further *out* of the cavity.

- condition C exists when the bubble becomes flat and its radius of curvature becomes infinite.
- condition E is when the bubble radius of curvature ratio reaches its minimum value of 1. In both cases this occurs only for concave shaped surfaces.
- the minimum radius of curvature for convex bubble surfaces occurs at -180° for both substances for this geometric configuration.

The *absolute minimum* radius of curvature for convex bubble surfaces would occur at larger negative cavity angles, where $\gamma = 180°$, and be equal to the mouth radius, but it could be reached only if the re-entrant surface would have had values beyond the -180° used in this example, as $\Theta = 2 (\beta - 180°)$. ($\Theta = -340°$ for the case of $\beta = 10°$ and $\Theta = 190°$ for the case of $\beta = 85°$).

Chapter VII

REQUIRED LIQUID SUPERHEAT IN CONICAL RE-ENTRANT CAVITIES

A. Introduction.

The concepts discussed in previous chapters will be applied here to analyze the behaviour of the liquid superheat required for the equilibrium of bubbles in cavities.

Refrigerant R-11 and water will be utilized in conical re-entrant cavities to illustrate the required liquid superheat behaviour of bubbles.

The cavity size is normalized to the *cavity mouth radius* in order to generalize the results.

The postulation given in Chapter III will be numerically demonstrated in this chapter, showing that:

- a simple conical cavity with cross sectional area increasing toward the surface ($\Theta > 0$) cannot contain a pure vapour bubble nucleus after a non-boiling period.
- no stable bubble can exist along the length of the smooth walls of a conical cavity of constant $\Theta > 0$.
- a re-entrant conical cavity in which the cross sectional area decreases toward the surface ($\Theta < 0$) is a necessary requirement

for a pure vapour bubble nucleus to survive during a non-boiling period.

- a stable vapour bubble can exist at the re-entrant cavity neck, for a certain temperature range at a given pressure, for substances of any contact angle.
- a stable vapour bubble can exist at the conical cavity mouth *only* for poor wetting substances and under certain conditions.

The concepts developed in previous chapters are of general validity but in this chapter we will use a conical re-entrant cavity geometry to study the thermal state of stable cavity bubbles. Cavities with this geometry provide an explanation of the observed independence of the incipient wall superheat with respect to flow conditions, that is characteristic of well wetting fluids, and an explanation of how sites are quenched and conditions for dormancy.

Actual cavities in commercial heat transfer surfaces would have different geometries, but those able to resist non-boiling periods and subcooling must have some cavity shapes that are re-entrant. For this type of cavities the following will be shown in this chapter:

- models for predicting the ONB, developed assuming that a bubble exists attached to the cavity mouth and is exposed to the flow conditions outside of the cavity, are not applicable for well wetting fluids.

- for well wetting substances, the maximum required liquid superheat *always* occurs at the re-entrant neck (for all cavity and re-entrant neck sizes, cavity angles and pressures).
- for poor wetting substances, the maximum RLS can occur either at the re-entrant neck or at the cavity mouth, depending on the cavity angle and on the size of the re-entrant neck, relative to the cavity radius. Therefore water can have a behaviour similar to that of the well wetting substances for certain types of cavities, when its maximum RLS occurs at the re-entrant neck of the cavity.
- at a given re-entrant cavity (and pressure), water bubble nucleii can survive much larger subcooling than those of R-11.

B. Re-entrant Cavities.

From Chapter VI it is know that the radius of curvature of a bubble inside of a conical cavity will continuously shrink when the bubble slides deeper, towards the cavity apex. The reduction of the radius of curvature means an increase in the RLS and consequently the bubble will keep on shrinking until a total collapse occurs at the cavity apex, or until the RLS is reduced by some mechanism. In this work it is proposed that a change in the cavity wall orientation, a re-entrant region, can provide such a mechanism.

The shape of the cavity to be analyzed in this work is shown in Figure VII.1. The

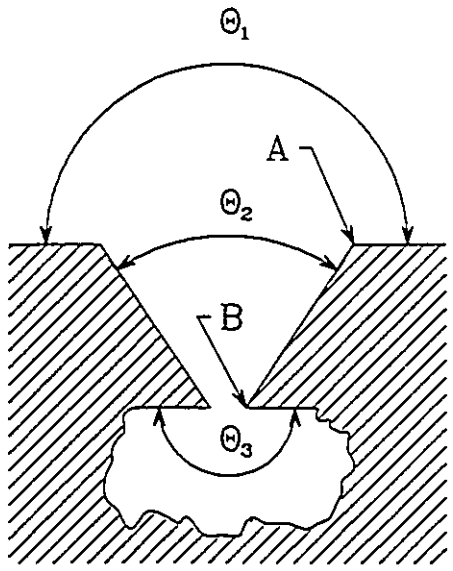

Figure VII.1. The profile of a re-entrant cavity.

cavity is axi-symmetrical and "A" is the lip of the cavity mouth and "B" is the re-entrant neck. The solid surface orientation changes from $\Theta_1 = 180°$ (the external surface), to Θ_2 inside the conical region of the cavity to $\Theta_3 = -180°$ inside the re-entrant region of the cavity.

In this chapter the top angle of the re-entrant cavity will be used as a variable, and Θ_1 and Θ_3 will have the constant values mentioned above. The top angle will be referred as the *cavity angle*.

Several cavity angles, mouth radii (the radial distance from the vertical axis to the cavity lip) and re-entrant neck radii are analyzed.

The basic assumption made in this analysis is that the value of the static contact angle is a constant for a given solid-liquid-gas combination, and therefore the bubble shape and radius of curvature are determined by the surface orientation and the vapour

volume trapped inside the bubble.

As shown in Figure VII.2, the re-entrant portion of the cavity forces the bubble radius of curvature to change from the small positive value it has when it reaches the

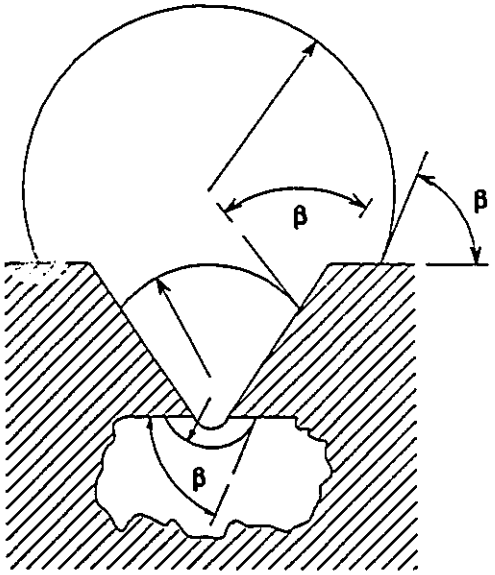

Figure VII.2. Bubble shapes in a re-entrant cavity.

re-entrant neck to a negative value. When the radius of curvature acquires a negative value it means that the bubble is *inverted*, with the liquid phase inside the spherical segment, and therefore the surface tension is no longer compressing the vapour phase. The net effect is that at this point the vapour phase will now benefit from the action of the surface tension over the liquid phase, in the sense that the RLS now becomes *negative*, a required *subcooling*, (and no longer a thermodynamic metastable state), and the saturated vapour phase can coexist with the subcooled liquid without collapsing.

The re-entrant cavity provides a means for explaining how a bubble nuclei can

survive a subcooled time period without collapsing.

C. Computer Simulation for a Bubble Inside a Cavity.

A simulation procedure was written, using an electronic spreadsheet, to calculate the RLS of bubbles in a re-entrant cavity. The parameters to be varied were:

- substance. Refrigerant R-11 and water.
- cavity angle. Positive values.
- cavity size. Defined by the cavity mouth radius.
- pressure.
- re-entrant neck size.

The contact angle and the surface tension parameters are defined once the fluid is selected (R-11 or water), since they are thermodynamic properties of the substance.

The RLS estimation was done using the saturation temperature $T_s(P)$ and the surface tension $\sigma(T_s)$ curve fitted correlations described in Appendix B, with the surface tension evaluated at the bubble temperature. It was shown in Chapter IV that, by using curve fitted correlations, the error introduced by evaluating the surface tension at the liquid saturation temperature, rather than at the bubble temperature, is not very important. Nevertheless, for the following calculations and since the bubble temperature is an unknown, its value was approximated by using the temperature of the *previous* larger bubble in the calculation series.

The calculation series started with a large bubble, well out of the cavity, and its

surface tension was calculated at the liquid saturation temperature, the series then progressed towards smaller bubbles approaching the cavity mouth, using decrements of 0.1 R_m, and the surface tension being calculated at the temperature of the previous bubble.

In all the following the RLS is plotted vs. the dimensionless radius with the cavity profile superimposed, for illustrative purposes.

The datum used for each of the parameters was as follows:

- cavity angle, $\Theta = 20°$
- cavity mouth radius, $R_m = 1\ \mu m$
- pressure, $P = 101.3$ kPa
- re-entrant neck radius, $R_n = 0.1\ R_m$

The effect of varying each of these parameters was studied about these values.

D. Presentation and Interpretation of the Results.

It is very important to clearly differentiate between *Required* Liquid Superheat (RLS) and the *Actual* Liquid Superheat (ALS), when looking at the results. RLS is the superheat that a bubble of a certain radius of curvature requires to maintain the thermo-mechanical equilibrium, it changes with the radius of curvature and therefore with the location of the bubble over the cavity. The ALS is the liquid superheat that actually exists around the bubble.

In this study the following assumptions were made:

- the temperature field around the bubble is constant everywhere inside the cavity.
- the temperature field outside the cavity in the thermal boundary layer is also considered as constant.

A more detailed analysis is required to take into account the possible effects of a temperature gradient in the boundary layer for very large bubbles that protrude into the

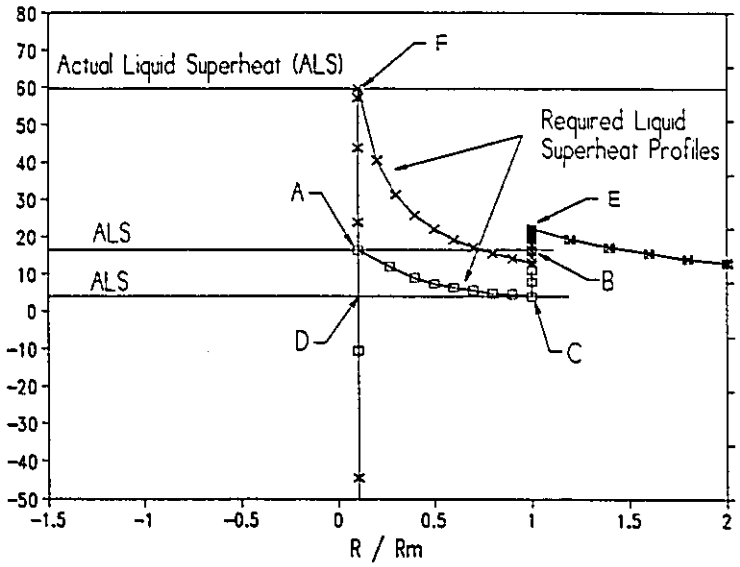

Figure VII.3. Typical results graphs for a poor wetting fluid.

boundary layer. In this study this effect is not really important, as will be shown later.

Figures VII.3 and VII.4 provide two typical graphs that can be used to illustrate the relationship between the wall superheat (and subcooling) required for a stable bubble and the bubble radius of curvature or bubbles at various stages of growth within the modelled conical re-entrant cavity. The cavity profile is superimposed in Figure VII.4

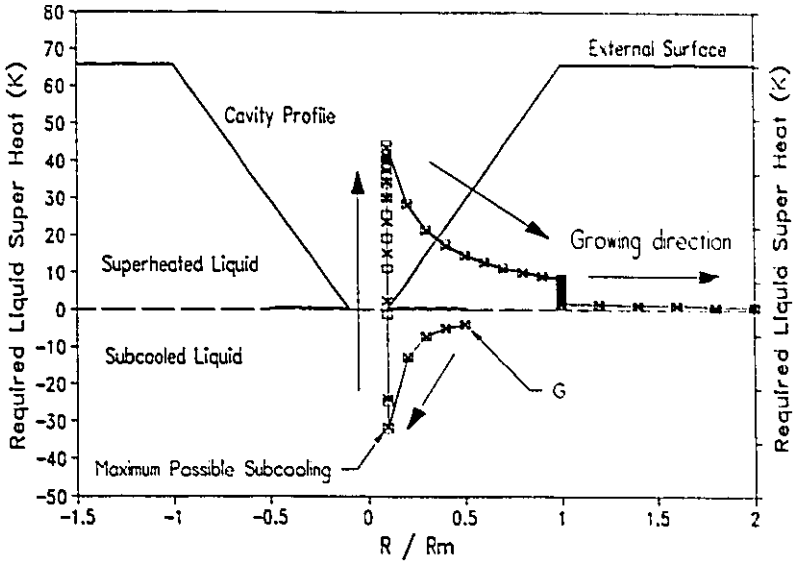

Figure VII.4. Typical results graphs for a well wetting fluid.

in order to illustrate the location of the RLS profile relative to the cavity more clearly and only the horizontal scale has a meaning. Three different ALS lines are shown in Figure VII.3. The intersection between each ALS line and the RLS profile represents a thermo-mechanical equilibrium point, where the ALS, around the bubble, equals the RLS. The bubble growth (increasing volume) direction is shown by the arrows in Figure VII.4. It should be noted that the RLS always increases with bubble growth at the re-entrant neck. The RLS can also increase at the cavity mouth as the bubble grows for poor wetting fluids.

D.1. Bubble Equilibrium Conditions.

A bubble will be in a *stable equilibrium* condition if, while at an equilibrium state, the following is true:

- a small change in the ALS (heating or cooling), which produces a volume change on the bubble (growth or shrinkage), will produce a new RLS (along the RLS profile) that is again equal to the (new) ALS.

These states exist only along the parts of the RLS profile where the vertical component of the *growing* direction goes upwards. It will be shown that such stable regions, along the RLS profile, exist at the re-entrant neck for both R-11 and water, but only for water at the cavity lip.

Consequently the regions of the RLS profile where the vertical component of the bubble *growing* direction goes downwards are unstable, and the bubble will:

- keep growing until it finally detaches from the solid surface.
- keep shrinking until it finally collapses inside the cavity.
- grow or shrink until the RLS reaches a point where the ALS line *again* intersects the RLS profile.

These processes can be observed in Figure VII.3 where:

- for the RLS profile shown by the "X" symbols, a bubble located at the re-entrant neck at state "F" (ALS $\approx$ 60 K) will grow without limit (until detachment) if the ALS further increases.

- for the RLS profile delimited with squares, a bubble located at the re-entrant neck with the state "A" (ALS ≈ 17 K) will also lose its equilibrium and grow if the ALS increases, but it will reach the cavity lip and stop growing at the state "B". This bubble will require that the ALS increases enough as to exceed point "E" in order to lose its stable equilibrium again and grow without limit until it detaches from the surface.
- for the RLS profile delimited by squares, a bubble located at the cavity lip at state "C" (ALS ≈ 3 K) will lose its equilibrium and shrink if the ALS slightly diminishes, and will reach the re-entrant neck and stop at the state "D", where a new stable equilibrium is attained.

E. The Behaviour of R-11 and Water in the Same Cavity.

The change in the trapped vapour volume, relative to the cavity volume, that R-11 and water will suffer when growing in a similar cavity, at the same pressure, is shown in Figure VII.5. The refrigerant undergoes an enormous change in volume at the cavity lip, and the buoyant forces are expected to cause departure from the surface before it can spread beyond the cavity mouth.

The RLS profile of both substances, over the re-entrant cavity, are shown in

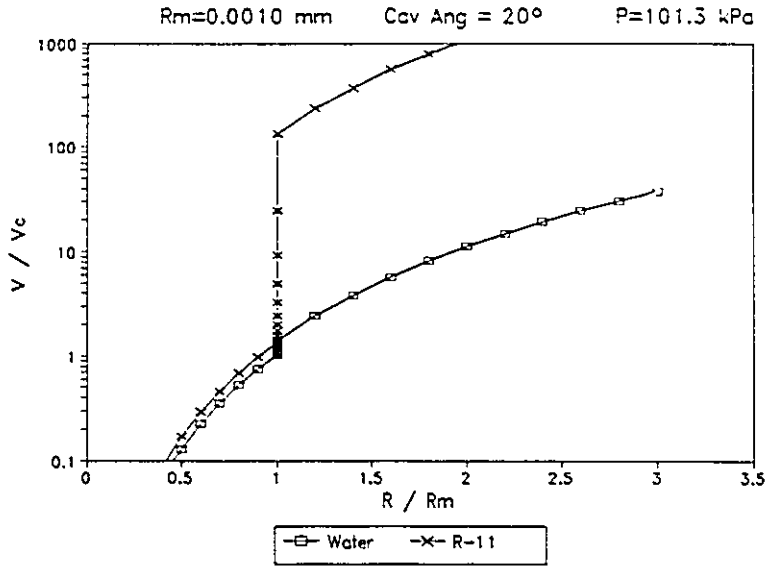

Figure VII.5. Dimensionless trapped volume for R-11 and water.

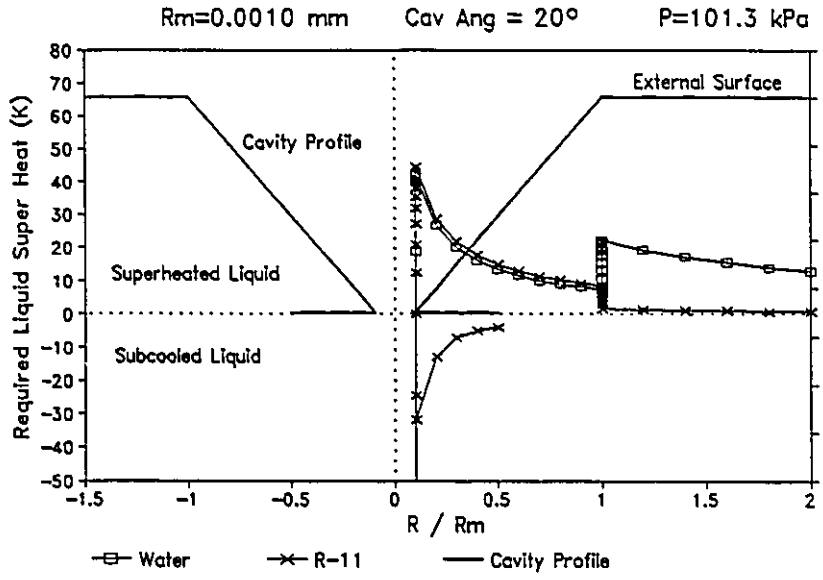

Figure VII.6. Liquid superheat profiles, R-11 and water vs radius.

Figure VII.6.

This figure illustrates the following:

- when growing at the cavity lip, the RLS for water increases (presents a stable region), while for R-11 the RLS decreases (and is therefore unstable).
- for the chosen cavity angle and size, the RLS profiles of both substances, inside the cavity, are very similar in magnitude.
- the refrigerant bubble nuclei will be able to survive a subcooling of up to about 30 K (or a *negative* superheat?) before collapsing and the site is quenched. The water bubble nucleus cannot be quenched as the liquid will freeze first.
- for this example, the maximum RLS for both substances occurs at the re-entrant neck, therefore, when the ALS exceeds this maximum the bubbles lose their equilibrium and keep on growing out of the cavity and over the surrounding external surface until detach.

Figure VII.7 shows the RLS profiles for the same substances, using a simple conical cavity geometry, as a function of the trapped volume normalized to the cavity volume. The use of the trapped volume, as independent variable to represent the RLS behaviour in cavities, is the most common in the literature, therefore is included here. However, the use of the trapped volume, as an independent variable, seams to provide less information about the phenomenon as compared to the use of R/R_m.

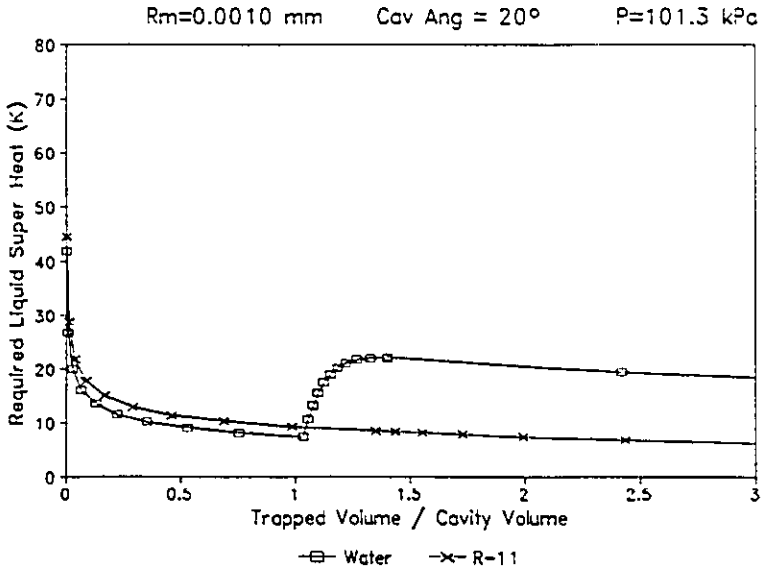

Figure VII.7. RLS profiles, R-11 and water vs trapped volume.

F. The Effect of the Cavity Angle.

As concluded in Chapter IV, based on a study of the radius of curvature, the cavity angle has no appreciable effect on the behaviour of the RLS for refrigerant R-11. Figure VII.8 illustrates that R-11 in such a cavity can survive subcooling up to 30 K (-30 K superheat), before being quenched. A surviving nucleus would require an ALS in excess of $\approx$ 45 K in order to grow beyond the re-entrant neck and reactivate the site. Once this is reached the bubbles will burst non-stop out of the cavity to detach from the surface.

The simulation found that a water nucleus in a similar sized cavity cannot be quenched. However, Figure VII.9 shows that the cavity angle has an appreciable effect on the RLS. The ALS necessary to push the bubble out of the re-entrant neck, varies

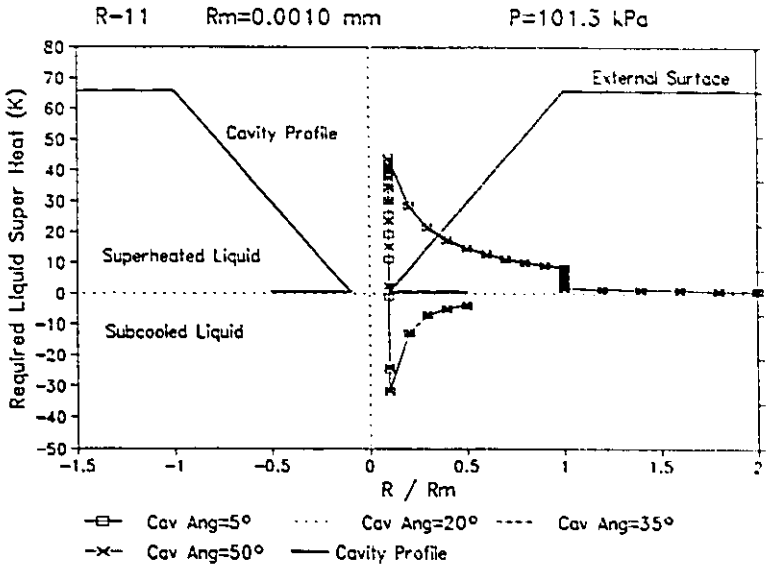

Figure VII.8. Effect of the cavity angle for R-11. (for R_n = 0.1 R_m)

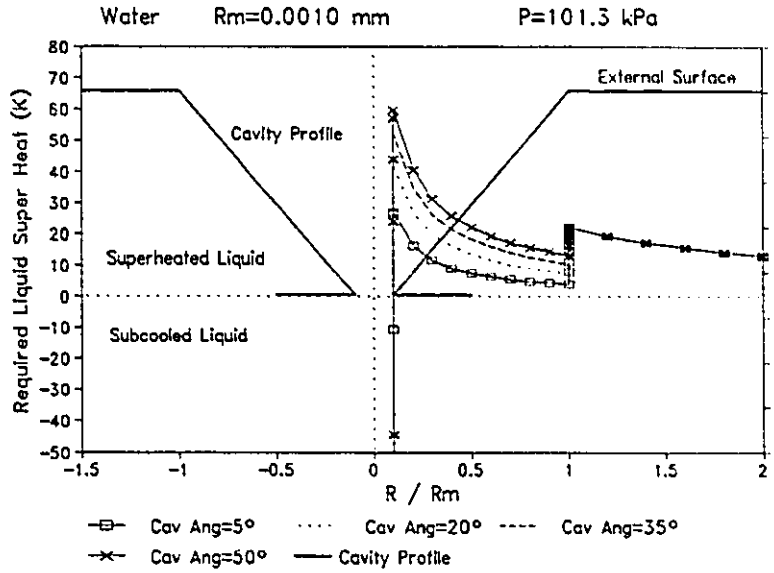

Figure VII.9. Effect of the cavity angle for water. (for R_n = 0.1 R_m)

from ≈ 25 K for a cavity angle of 5° up to ≈ 60 K for a cavity of 50°. Note that the *local* maximum RLS at the *cavity lip* ($R / R_m = 1$) is independent of the cavity angle.

G. The Effect of the Cavity Size.

Cavity size has a significant effect on the RLS for incipient boiling and for the subcooling required to quench the site. Figure VII.10 shows that, for R-11, a decrease in cavity radius from 0.001 mm to 0.0005 mm produces an increase in the maximum

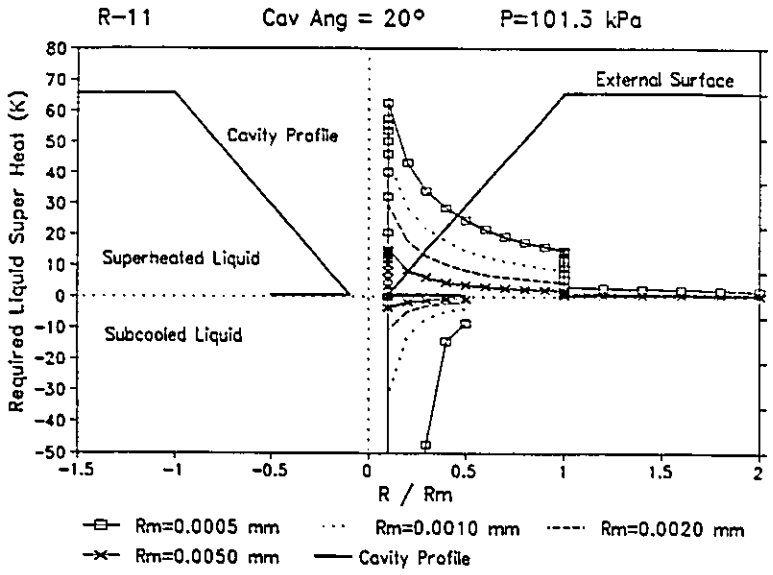

Figure VII.10. Effect of the cavity size for R-11.

RLS at the re-entrant neck of ≈ 20 K. The results shown in Figure VII.10 allows the following conclusions to be drawn for well wetting substances when boiling takes place from commercial surfaces:

- small re-entrant cavities can survive large subcoolings without collapsing. In the figure the 0.5 μm cavity radius goes well below -50 K, but also requires a very large superheat in order to reactivate the site.

- large cavities are quenched very easily even at modest subcoolings, but also require small superheats to be activated. In Figure VII.10 the 5 μm radius cavity resists only $\approx$ 5 K of subcooling and nucleates at ALS $\approx$ 15 K.
- in a heat transfer surface that undergoes subcooled temperatures, the larger cavities are the first to become quenched. The model predicts that, for a given fluid, there is a re-entrant neck radius below which it is impossible to quench an existing bubble embryo. During the reheating process the surface temperature has to be raised high enough so as to activate the largest of the surviving nucleii. They, in turn become active and serve to seed the surrounding larger cavities.

For q^* = constant, as the larger cavities become active, after the ONB, the heat transfer coefficient increases and the surface temperature decreases. This model predicts that, for a previously subcooled surface, very small re-entrant cavities act as the *triggering mechanism* of the ONB. Once vigorous nucleate boiling is established, on a q^* = constant surface, the subsequent decrease in surface temperature makes them dormant again, leaving active only larger cavities seeded by the initial sites. Any study of the subsequent boiling sites does not provide any information about the sites which initiated the ONB.

A similar simulation is shown in Figure VII.11. Note that the behaviour of the

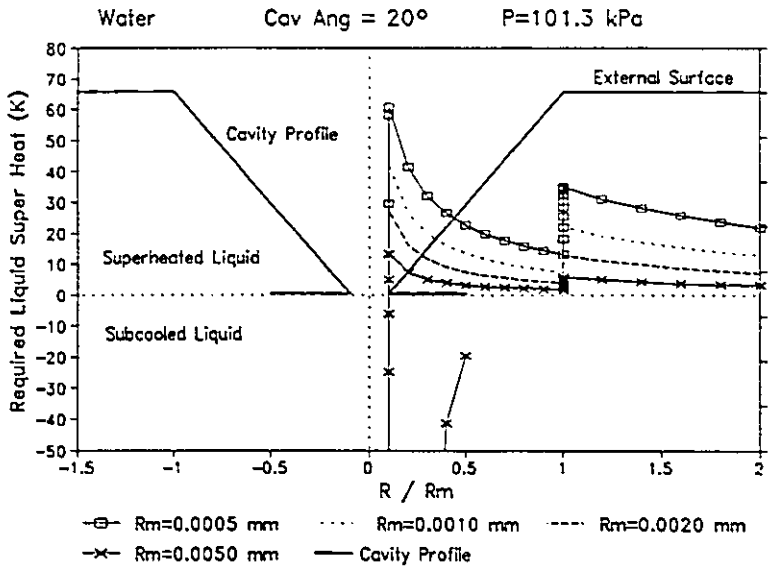

Figure VII.11. Effect of the cavity size for water.

RLS is similar to that of R-11 for activation at the re-entrant neck, but water resists quenching much better.

For cavity radii less than 0.005 mm it was found that the nucleus would not collapse regardless of the amount of subcooling. When compared to R-11, much larger nuclei will survive with water when subcooled and hence the re-activation of the surface will occur at lower superheats.

H. The Effect of Pressure.

The effect of pressure is similar to that of the cavity size, in the sense that a higher pressure imposes a higher saturation temperature and the surface tension decreases almost linearly with the temperature, therefore the RLS profiles for increasing pressures

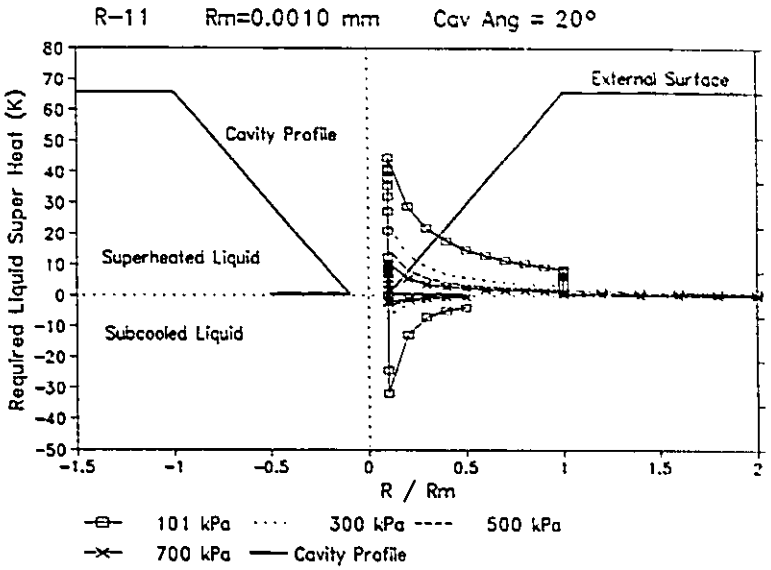

Figure VII.12. Effect of pressure for R-11.

behave like those for decreasing cavity sizes. This can be seen in Figure VII.12 for R-11 and in Figure VII.13 for water.

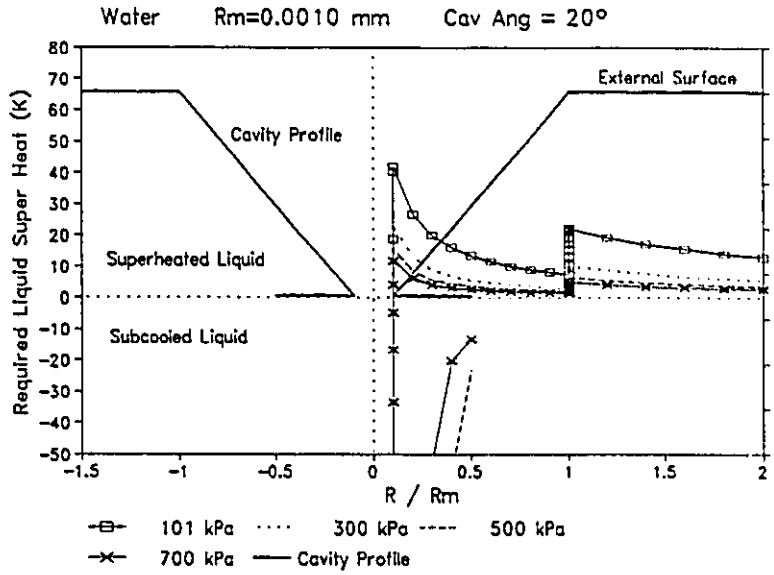

Figure VII.13. Effect of pressure for water.

I. The Effect of the Re-entrant Neck Size.

In all the previous cases the re-entrant neck was considered fixed at 0.1 R_m, regardless of cavity angle or size. In this section we analyze the effects of having larger re-entrant neck sizes, relative to the cavity mouth size.

The size of the re-entrant neck, relative to the cavity mouth size, becomes

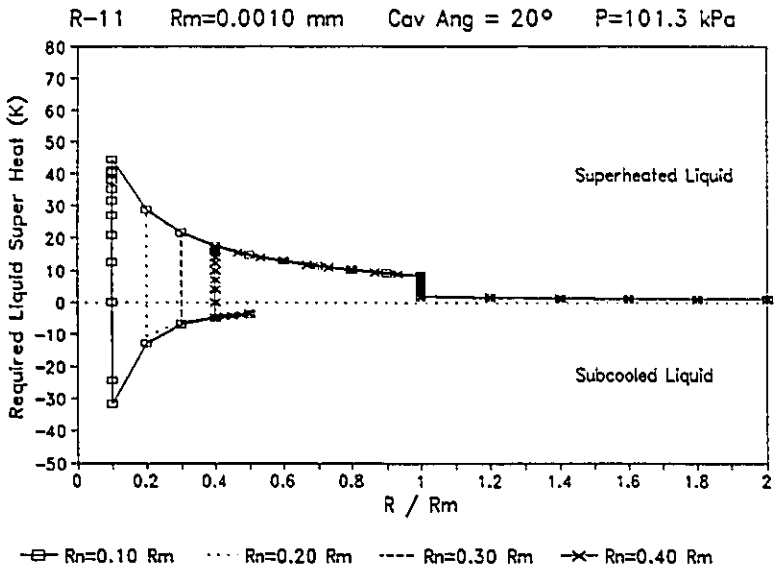

Figure VII.14. Effect of the re-entrant neck size for R-11.

specially important for the case of poor wetting fluids since increasingly large re-entrant necks impose lower RLS to the bubble nucleii at that point, and the locus of the maximum RLS (over the RLS profile) may then shift from the neck to the cavity mouth.

Figure VII.14 shows that for R-11 the re-entrant neck size reduces the RLS for activation, but also severely reduces the ability of the cavity to resist subcooling.

Figure VII.15 shows that for water the RLS at the re-entrant neck is also reduced

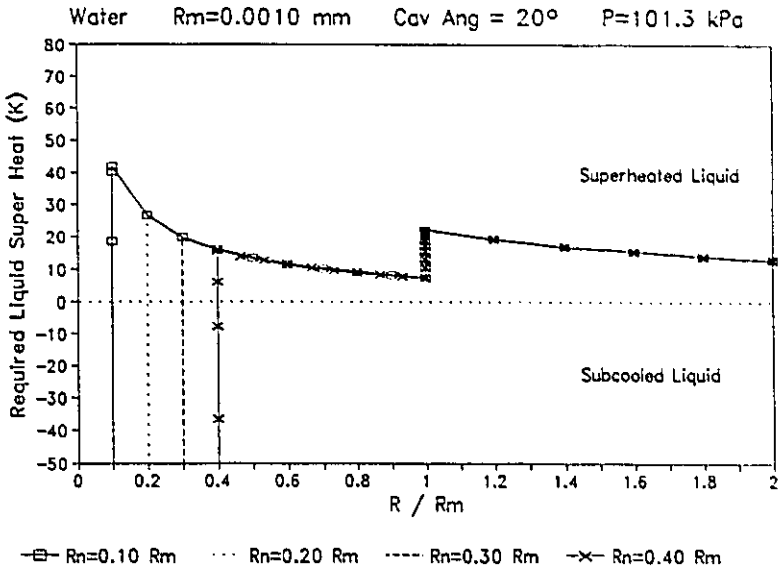

Figure VII.15. Effect of the re-entrant neck size for water.

for relatively larger neck sizes, and for the conditions shown, the RLS at the neck is larger that at the lip for neck sizes of 0.1 and 0.2 R_m, but for 0.3 and 0.4 R_m the RLS at the cavity mouth becomes larger than that at the neck, and the bubble should now become stable at the cavity mouth after having outgrown the re-entrant neck and slid down the cavity walls. It is also shown that for water the ability to resist subcooling is not affected noticeably.

These predictions show that, for water, both cavity angle and re-entrant neck size can shift the location where the incipient wall superheat occurs from the neck to the cavity mouth, or vice versa. As a result, some cavities will nucleate water bubbles directly from the re-entrant neck (cavities with large angles or small re-entrant necks). Such sites are highly unlikely to be affected by the external flow. Other cavities will have the bubble attached to its mouth, where the bubbles are exposed to the external flow

(cavities with small angles or large re-entrant necks).

Well wetting substances, on the other hand, are neither affected by the cavity angle nor by the re-entrant neck size. They will always nucleate directly from the cavity re-entrant neck and hence be unaffected by flow conditions.

Chapter VIII

BUBBLE EMBRYO DORMANCY LIMITS IN A RE-ENTRANT CAVITY

A. Introduction.

When a nucleation site is active, bubbles continuously grow and depart from its mouth. When a bubble departs, the cavity is left with a small amount of vapour, a bubble embryo, that acts as a *seed* for the next bubble formation. When an active nucleation site is cooled, bubbles will stop leaving the cavity at certain wall superheat that is termed the *incipient boiling* wall superheat. If the bubble embryo left inside the cavity is *able* to maintain an equilibrium state at that moment, the site has become *dormant*. If the bubble embryo left inside the cavity is *unable* to maintain an equilibrium state at that moment, the bubble will collapse and the site has been *quenched*. Bubble embryos of poor wetting substances, such as water, can reach dormancy conditions attached to a cavity mouth and also at a re-entrant cavity neck. Bubble embryos of well wetting substances can only be dormant at a re-entrant cavity neck. A dormant embryo can survive a further decrease in the wall superheat without losing its equilibrium and collapsing. Depending upon the cavity geometry, a wall superheat (or wall subcooling) may be reached where the cavity will be quenched. The wall superheat or wall subcooling when this occurs is referred to as the *incipient quench* condition.

A dormant cavity will become active when the wall superheat exceeds the incipient boiling wall superheat for that cavity. The only way a quenched cavity will become active again is when the wall superheat exceeds the incipient boiling wall superheat for that cavity and vapour from another already active cavity displaces the liquid within, thus seeding it, or until the wall superheat grows to the very large value required for spontaneous (homogeneous) nucleation.

This chapter discusses the factors (cavity geometry and pressure) that affect the incipient boiling and the incipient quenching wall superheats (bubble embryo upper and lower dormancy limits).

From the previous chapter it is known that the cavity mouth can affect the incipient wall superheat (the largest RLS in the bubble's life) only for poor wetting fluids like water, and then only when the mouth and neck radii sizes are close in magnitude. Only those cavity geometries in which the neck controls the activation of the site will be considered in the remainder of this chapter.

To investigate the effect of re-entrant neck geometry on the bubble embryo dormancy limits, the incipient boiling and incipient quenching wall superheats were studied as a function of the re-entrant neck radius for water and R-11, using the top and bottom cavity angles as parameters. The effect of pressure on the bubble embryo dormancy limits were also studied for the case where the top cavity angle is 180°. A comparative analysis of the effect of the reduced pressure ratio on the boiling incipience wall superheat was also investigated for water and R-11.

B. The Re-entrant Neck.

Figure VIII.1 shows the generalized re-entrant cavity neck region. The addition of thickness to the re-entrant neck, a straight passage of zero cavity angle, does not

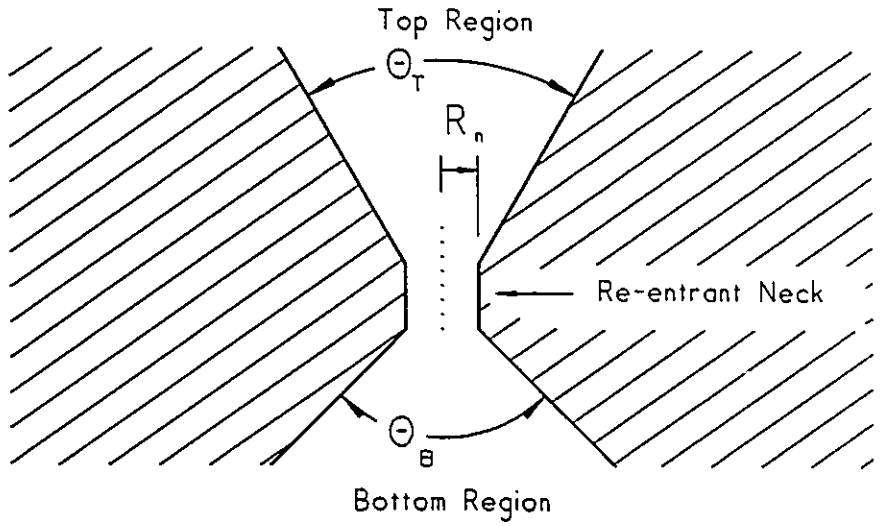

Figure VIII.1. The re-entrant cavity neck.

change the characteristics of the bubble behaviour at the neck. In the following analysis some configurations will have top and bottom cavity angles that when added together could sum up to more than 360°. This is possible for a re-entrant neck with a straight neck passage.

B.1. Incipient Boiling Wall Superheat.

The maximum liquid superheat that a bubble embryo can attain at the re-entrant neck without breaking free (the incipient boiling wall superheat) corresponds either to a hemispherical bubble ($r / R_n = 1$) or to the radius of curvature of the bubble when it starts sliding out the top cone, whichever occurs first.

A bubble becomes hemispherical at a re-entrant neck when the top cavity angle is equal to or greater than twice the contact angle ($\Theta_T \geq 2$ ß). This is usually the case for well wetting substances since their contact angles are small, ß $\approx 10°$. Poor wetting substances, such as water (ß $\approx 85°$), posses much larger contact angles therefore the hemispherical condition is reached only when the top cavity angle reaches or exceeds 170°. If the top cavity angle is smaller than 2 ß, then the maximum required liquid superheat is a function of both neck size and top cavity angle.

B.2. Incipient Quenching Wall Superheat.

The least liquid superheat (or maximum subcooling) that a bubble embryo can sustain without collapsing determines the incipient quenching wall superheat for the cavity. It occurs while the bubble is attached to the re-entrant neck and corresponds either to a hemispherical bubble (convex with respect to the vapour), or to the radius of curvature of the bubble when it starts sliding out the bottom cone into the re-entrant region of the cavity, whichever occurs first. The incipient quenching wall superheat can be negative (subcooling) if the bubble embryo can reach convex shapes. The embryo

saturation temperature is reached when its shape becomes flat. At this point the radius of curvature becomes infinite. To reach this condition the bottom cavity angle, Θ_B, has to be greater than 10° for water and greater than 160° for R-11. This means that water can resist subcooling in cavities with very small bottom angles while R-11 requires 160° just to survive at saturation.

A bubble becomes hemispherical and convex when the bottom cavity angle is 2(180° - ß), 190° for water and 340° for R-11. Because of the large bottom cavity angles required, the minimum required liquid superheat would most frequently be a function of both the cavity neck size and the bottom cavity angle for both poor and well wetting substances.

C. Bubble Embryo Dormancy Limits.

In the previous chapter the figures showed the liquid superheat required to maintain a bubble at every possible location within the cavity. In this chapter we are interested only on the maximum and minimum values of liquid superheat which a bubble can sustain in equilibrium. These values correspond to the *incipient boiling* and to the *incipient quenching* wall superheats respectively for a given cavity.

C.1. Dormancy Limits for Water.

Figure VIII.2 shows the incipient boiling and quenching wall superheats limits between which a water bubble embryo can exist in the generalized re-entrant cavity. The

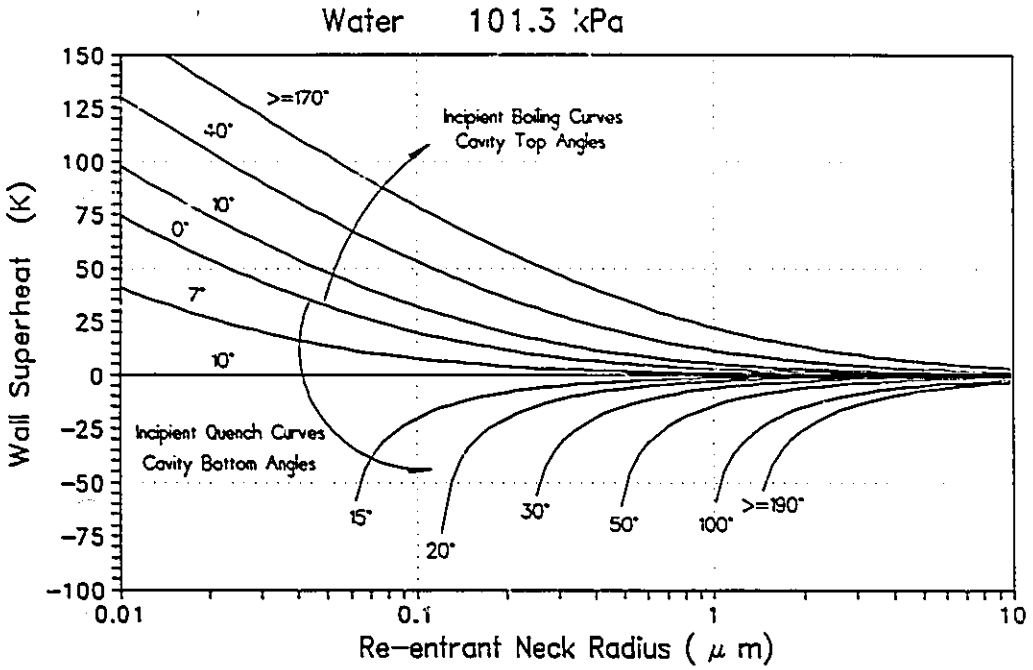

Figure VIII.2. Incipient boiling and incipient quenching curves of water in a re-entrant cavity.

three top-most curves correspond to incipient boiling for top cavity angles of 10°, 40° and ≥ 170°. As can be observed, the incipient boiling wall superheat for water is very sensitive to variations in the top cavity angle for small angles and gradually becomes less sensitive for larger values. The incipient quenching wall superheat is very sensitive to the bottom cavity angle. It should be noted that bubble embryos in cavities with a bottom cavity angle Θ_B between 0° and 10° are quenched even before saturation is reached and when $\Theta_B > 10°$, there exists a re-entrant neck size below which a bubble cannot be

quenched (for a given pressure). For $\Theta_B = 20°$ and $\Theta_B \geq 190°$, these limiting re-entrant neck sizes are approximately 0.1 μm and 1 μm respectively. Since the water bubble embryo becomes hemispherical at $\Theta_B = 190°$ (convex), it also means that *every* cavity larger than ï μm *can* be quenched, regardless of the Θ_B value.

C.2. Dormancy Limits for R-11.

Although the required liquid superheat for R-11 is a function of the top cavity angle only when less than 20°, (2 ß), the incipient boiling wall superheat varies little

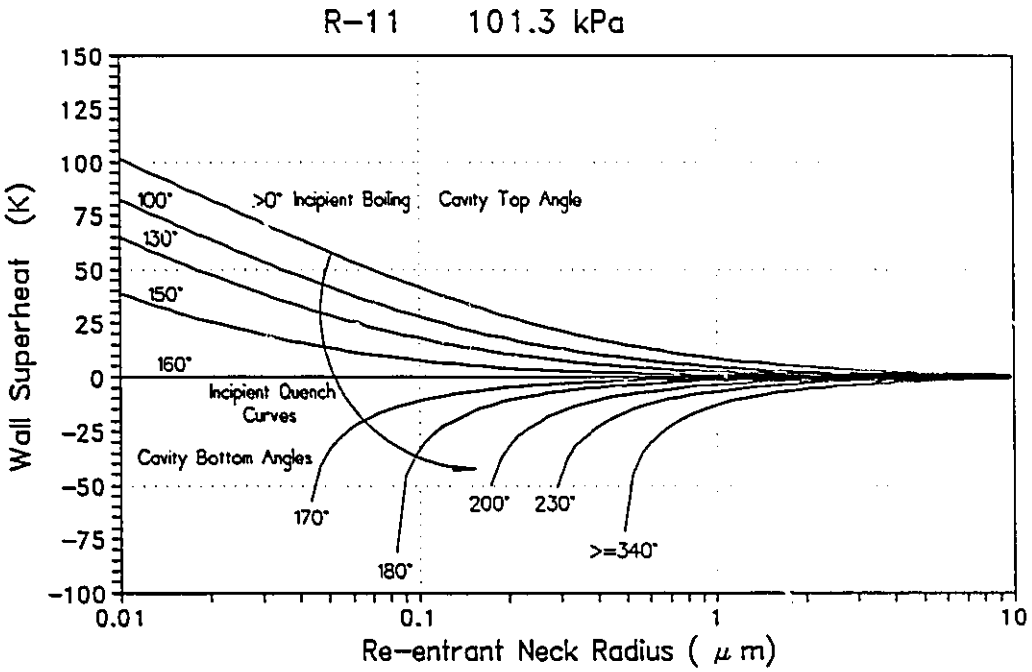

Figure VIII.3. Incipient boiling and incipient quenching curves for R-11 in a re-entrant cavity.

between 0 and 20°. Figure VIII.3 shows how all incipient boiling wall superheat curves for $\Theta_T > 0$ are superimposed one upon the other. The incipient quench wall superheat

is also insensitive to variations in the bottom cavity angles for small Θ_B. However, as Θ_B increases, its effect on the incipient quenching becomes very significant. At $\Theta_B = 160°$ the incipient quench curve corresponds to the saturation line. An R-11 bubble embryo in a cavity with a bottom cavity angle in the range $0° < \Theta_B < 160°$ cannot resist any subcooling. For cavities with bottom angles larger than 160° there exists a neck size below which the bubble embryo cannot be quenched (for a given pressure). For $\Theta_B = 180°$ and $\Theta_B = 340°$ these limiting neck sizes are approximately 0.08 μm and 0.4 μm, respectively. Since the R-11 bubble embryo becomes hemispherical at $\Theta_B = 340°$ (convex), it also means that *every* cavity larger than 0.4 μm *can* be quenched, regardless of the Θ_B value.

For a given re-entrant cavity geometry, the incipient quenching by using R-11 is much smaller than that obtained by using water.

D. Effect of Pressure on Dormancy Limits.

Figures VIII.4 and VIII.5 show the effect of neck size and pressure on the incipient boiling and incipient quenching wall superheats, for water and R-11 respectively, for a flat re-entrant cavity where both the top and bottom angles are held at 180°.

Both the incipient boiling and quenching wall superheats decrease with increasing liquid pressure, as a result of two combined effects:

- at higher pressures the saturation temperature is also higher, and

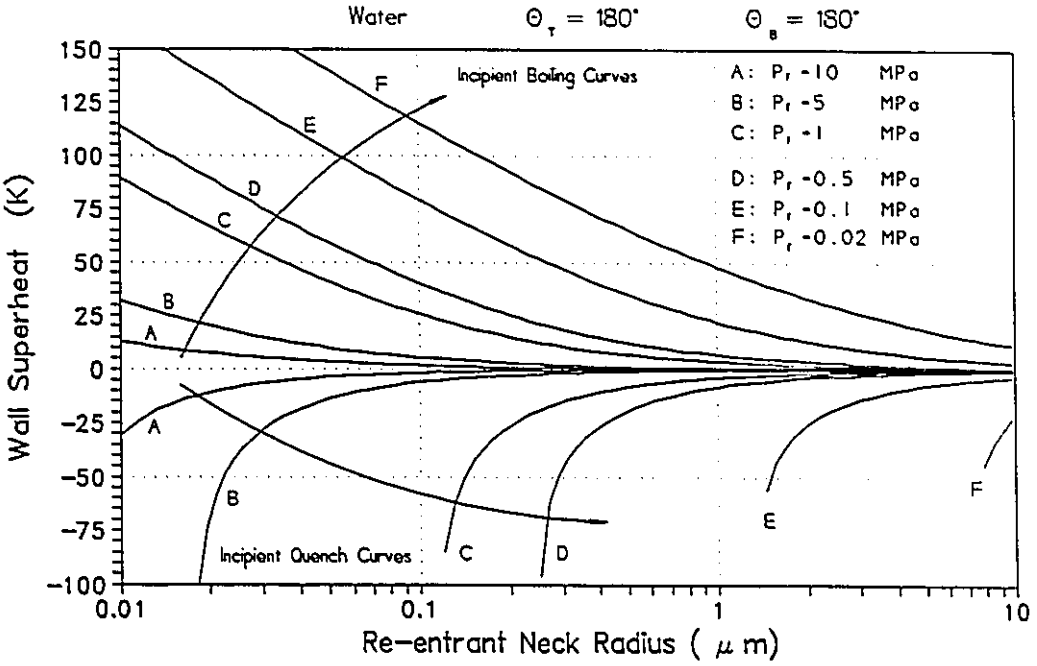

Figure VIII.4. The effect of pressure on the incipient boiling and incipient quenching for water.

the surface tension decreases with the temperature.

- the slope of the $T_s(P)$ curve gets smaller with increasing pressures, therefore, for the same pressure difference across the bubble interface, the resulting temperature difference (RLS) is smaller. These combined effects result in a large sensitivity to liquid pressure.

The net effect of pressure on the bubble embryo is that reduces its dormancy limits by bringing the upper and lower limits closer together. This means that the cavity becomes active at lower wall superheats with increasing liquid pressure, which is desirable, but also becomes quenched at lower subcoolings, which is undesirable for most

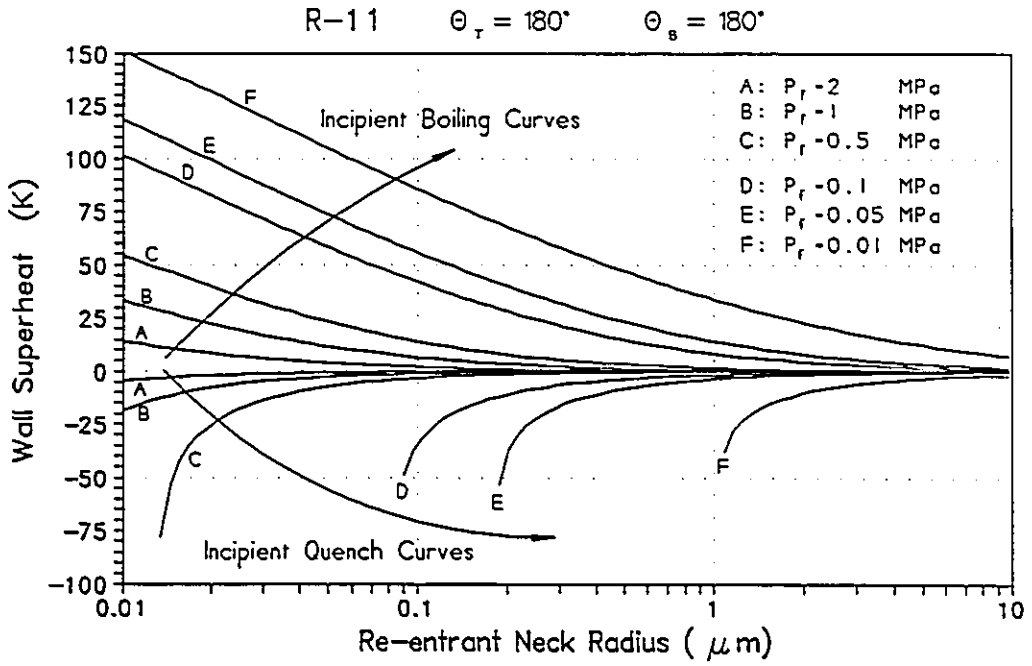

Figure VIII.5. Effect of pressure on the incipient boiling and incipient quenching for R-11.

heat transfer applications.

E. Incipient Boiling Behaviour Using Reduced Pressures.

In order to compare the behaviour of the incipient boiling curves of water and R-11, a series of computer simulations were made using equal reduced pressure values. The flat re-entrant cavity geometry used had a top cavity angle of 180°. Figure VIII.6 shows the remarkable similitude of the incipient boiling wall superheats obtained for both substances at high pressures. At low pressures the similitude starts to diverge for small neck sizes.

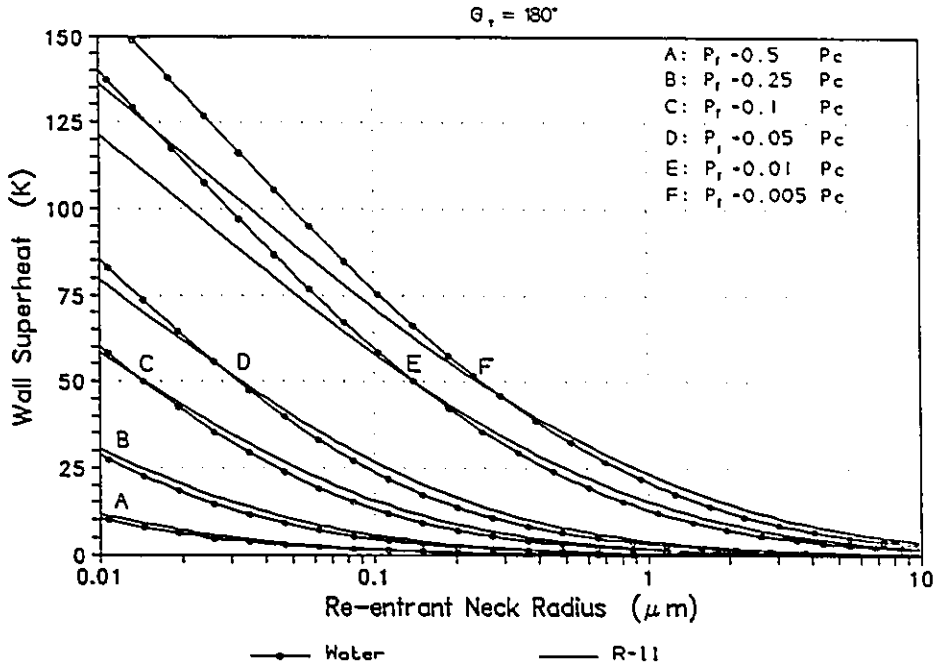

Figure VIII.6. Effect of reduced pressure on the incipient boiling for water and R-11.

The figure suggest that it may be possible to extrapolate the incipient boiling wall superheat results obtained in this study to other substances, particulary between refrigerants, by using reduced pressures since the agreement is very good even for such different substances as water and R-11.

Chapter IX

SUMMARY, CONCLUSIONS AND RECOMMENDATIONS

A. Summary.

An analysis of bubble stability in *conical* and *re-entrant* cavities was carried out.

The common approach observed in the literature when analyzing the phenomenon associated with the onset of nucleate boiling is based on the assumption that a bubble embryo somehow already exists, either trapped inside a cavity or attached to the cavity mouth, which protrudes into the fluid momentum and thermal boundary layers. Based on these assumptions, various methods are used to predict the required temperature gradients and flow conditions that would be required to make the bubble grow and detach from the cavity. The resulting wall superheat is considered to be the condition for incipient nucleate boiling.

From the literature it is known that boiling always occurs from cavities and that incipience occurs at temperatures lower than those required for homogeneous nucleation, even for the largest temperature overshoots reported. This indicates that small bubble embryos survive inside cavities and cause boiling incipience to be a heterogeneous nucleation process. It is also known that the radius of curvature of such bubble embryos must be of the order of one μm. In this work an attempt has been made to focus attention

on the behaviour of the bubble embryos and their interaction with the surrounding cavity. The fluid contact angle and the cavity geometry are the controlling variables, responsible for the survival of the bubble embryo through their effect on the bubble radius of curvature.

The required liquid superheat predictions obtained by using the integrated Clapeyron equation (II.31), in bubbles smaller than 1 μm, are shown to be unreliable. The use of saturation temperature versus pressure correlations were much better and hence were used in this study to relate the required liquid superheat surrounding a vapour bubble to the pressure rise within the bubble embryo. The pressure rise is proportional to the surface tension and inversely proportional to the bubble radius of curvature.

The radius of curvature of a spherical bubble in a fluid always increases as the bubble volume grows, and vice versa. In an isothermal fluid this is an unstable condition which results in unlimited growth or decay of the bubble. However, a bubble inside a re-entrant cavity can behave differently and can exist in stable equilibrium.

At the triple interface between a solid surface, a liquid and its vapour, three surface tension forces exist, one for each pair of phases, acting tangent to the interface surfaces. The relative magnitude of those forces determines the contact angle between the liquid and the solid. The contact angle is therefore a property of a given substance-solid combination and is assumed to depend only on the temperature in this work. In an isothermal environment the shape of a bubble surface at the interface with the solid surface is fixed by the contact angle magnitude. The radius of curvature of a

bubble in contact with a solid surface is a function of the contact angle and the solid surface orientation. The inclusion of the fluid properties (eg. saturation temperature, pressure and surface tension) permits the required liquid superheats at boiling incipience and at bubble quench for real fluids to be calculated. The resulting values compare favourably with observed magnitudes.

A conical cavity with a re-entrant region was chosen as the example cavity geometry for the model analysis. Two commonly used substances, water and refrigerant R-11, were selected as working fluids because of their very different reported behaviour at the onset of nucleate boiling. R-11 is representative of several other refrigerants having low contact angles. The required liquid superheat for bubble embryos in a cavity were obtained, using saturation temperature versus pressure curve fitted correlations, for various cavity sizes, cavity angles, pressures, and re-entrant neck sizes.

The analysis shows that:

- simple conical cavities cannot sustain bubble embryos of any wetting substance (contact angle $< 90°$) during a non-boiling period.
- a bubble embryo can survive in stable equilibrium at a re-entrant neck. Water embryos can resist much larger subcoolings than those of R-11 in the same cavity. The required liquid superheat at the point where the bubble embryo departs from the re-entrant neck is about the same for both substances in the same cavity. As

a consequence, the different wall superheats required by both substances at the onset of nucleate boiling arises from the fact that, after a non-boiling period and comparable subcoolings, the surviving water bubble embryos (dormant cavities) are much larger than those with R-11 and consequently the liquid superheat required to initiate nucleation will be smaller for water.

- the shape of the bubble surface may become convex at the re-entrant neck, permitting the bubble embryo to resist some degree of subcooling in the surrounding liquid without collapsing into the re-entrant region. This explains how bubble embryos may survive non-boiling periods trapped in cavities.
- increasing the wall superheat will cause bubble growth until eventually the bubble leaves the re-entrant neck, becomes unstable, and continues to grow toward the cavity mouth.
- a conical cavity with an internal re-entrant region may force a bubble of a wetting substance with a large contact angle (ß close to 90°) to become stable *also* at the cavity mouth. Bubbles with a small contact angle can not be stable at the cavity mouth.
- the large drop in wall superheat that occurs upon the onset of nucleate boiling with R-11, for a given heat flux, may be explained by the fact that larger cavities are seeded with vapour

from the initially active smaller ones. Once the larger cavities activate, less superheat is required to sustain the boiling.

Increasing the system pressure reduces the dormancy limits of the bubble embryos, by bringing the incipient boiling and quench curves closer to the saturation line.

An analysis of incipient boiling of water and R-11, at similar reduced pressures, as a function of the re-entrant neck radius, shows that at reduced pressures above $\approx 0.1\ P_r$ the incipient boiling superheats of both substances are remarkably similar. The observed similarity suggests that the results may be used to predict the behaviour of other refrigerants.

B. Conclusions.

Dormant vapour bubble embryos are required to initiate nucleate boiling once any initially present non-condensible gases are driven off by previous boiling periods.

The analysis carried out shows that the existence of a bubble embryo is dependant only on the fluid properties and the cavity geometry at the point of attachment. Thus the conclusions generated in this study for conical cavities may be applied to cavities in general since the intermediate shape of the cavities is irrelevant.

These bubble embryos can exist only at sites where the radius of curvature of the bubble embryo decreases with increasing bubble volume. For all substances this may occur at any location in a cavity where the bubble attachment cross sectional area

increases with depth from the surface (referred to as the re-entrant portion of the cavity).

The greater the amount of subcooling a surface is exposed to the smaller will be the surviving dormant embryo cavities and hence the larger superheat required to reactivate nucleate boiling. The largest of the surviving bubble embryos in a surface will activate first and could serve to seed other surrounding larger (quenched) cavities, serving as a triggering mechanism. This is the missing variable, responsible for the reported *randomness* or *non-repeatability* of the incipient wall superheat, the degree of subcooling or *thermal history* of the heat transfer surface between boiling cycles.

Only poor-wetting substances can have stable bubble embryos at a cavity mouth, therefore models for predicting the onset of nucleate boiling based on a bubble attached to a cavity mouth are not likely applicable for well-wetting substances.

C. Recommendations.

It is not possible to know the size, shape and number of cavities on a heat transfer surface. However, the model presented in this work for the conical re-entrant cavity could serve as a basis to develop a *surface calibration* technique, based on the response of the surface to cycles of controlled cooling and re-heating processes. Such a calibration technique might determine the *equivalent size and geometry* of cavities present on the surface and their *relative sensitivity* to quenching and reactivation at the given conditions.

For those heat transfer surfaces that must use well wetting substances in cyclic boiling duties, and in which the subcooling conditions cannot be avoided and/or the

occurrence of temperature overshoots must also be controlled and reduced to a minimum, the model presented in this work permits one to *design* the best possible artificial cavity for a particular application (the one with the minimum required liquid superheat at the boiling incipience and with the highest resistance to become quenched). The fabrication of such artificial cavities into the actual heat transfer surfaces looks impossible, given the required sizes, but small attachments containing a number of artificial cavities can be fabricated and located on the heat transfer surface to serve as promoters of the nucleate boiling process, capable of seeding the surface with vapour, making it active before temperature overshoots build up. The author is currently working on an easy-to-fabricate design of such a *boiling promoter*.

REFERENCES

Abdelmessih, A.H.; Fakhri, A. and Yin, S.T. *Hysteresis effects in incipient boiling superheat of Freon-11.* Heat Transfer 1974. JSME 5th Int. Heat Transfer Conf. v.4 pp.165-169 1974

Anderson, T.M. and Mudawwar, I. *Microelectronics cooling by enhanced pool boiling of a dielectric fluorocarbon liquid.* ASME HTD v.96 pp.551-560 1988

ASHRAE Handbook-Fundamentals SI. American Society of Refrigerating Heating and Air-Conditioning Engineers Inc. Atlanta 1989

Ayub, Z.H. and Bergles, A.E. *Nucleate pool boiling curve hysteresis for GEWA-T surfaces in saturated R-113.* ASME HTD v.96 pp.515-521 1988

Bankoff, S.G. *Entrapment of gas in the spreading of a liquid over a rough surface.* AIChE J. v.4 n.1 pp.24-26 1958

Bankoff, S.G. *The prediction of surface temperatures at incipient boiling.* Chem. Engr. Progress Symposium Series. v.55 n.29 pp.87-94 1959

Bankoff, S.G. *Ebullition from solid surfaces in the absence of a pre-existing gaseous phase.* ASME Trans. v.79 May pp.735-740 1957

Bar-Cohen, A. Simon, T.W. *Wall superheat excursions in the boiling incipience of dielectric fluids.* Heat Trans. Eng. v.9 n.3 pp.19-31 1988

Belhadj, M.; Aldemir, T. and Christiansen, R.N. *Onset of nucleate boiling in research reactors with thin rectangular channels under low-velocity upward-flow conditions.* Nucl. Techn. v.82 Sep pp.330-340 1988

Bergles, A.E. and Rohsenow, W.M. *The determination of forced convection surface-boiling heat transfer.* J. Heat Transfer ASME Ser. C v.86 Aug pp.365-372 1964

Bergles, A.E. and Chyu, M.C. *Characteristics of nucleate pool boiling from porous metallic coatings.* J. Heat Trans. ASME v.104 May pp.279-285 1982

Bräuer, H. and Mayinger, F. *Subcooled boiling heat transfer to R-12 in annular vertical channel.* Chem. Eng. Technol. v.11 pp.320-327 1988

Bräuer, H. *Wärmeübergang und Siedebeginn beim unterkülten Sieden unter Zwangskonvektion.* Dr. Ing. Dissertation Tech. Univ. München. Germany. (Adv. F. Mayinger). 1988

Bucher, B. *Beitrag zum Siedebeginn beim unterkülten Sieden mit Zwangskonvektion.* Dr. Ing. Dissertation Univ. Hannover, Germany. (Adv. F. Mayinger) 1979

Chen, J.C. *Incipient boiling superheats in liquid metals.* J. Heat Transfer ASME v.90 Aug pp.303-312 1968

Clark, H.B.; Strenge, P.S. and Westwater, J.W. *Active sites for nucleate boiling.* Chem. Eng. Prog. Symp. Series (Heat Transfer Chicago) v.55 n.29 pp.103-110 1959

Clarke, R.H. and Robertson, J.M. *Investigations into the onset of convective boiling with liquid nitrogen in plate-fin heat exchanger passages under constant wall temperature boundary conditions.* AIChE Symposium Series v.80 n.23 pp.98-103 1984

Coeling, K.J. and Merte, H. *Incipient and nucleate boiling of liquid hydrogen.* J. Engineering for Industry May pp.513-520 1969

Cornwell, K. *On boiling incipience due to contact angle hysteresis.* Int. J. Heat Mass Transfer v.25 n.2 pp.205-211 1982

Corty, C. and Foust, A.S. *Surface variables in nucleate boiling.* Chem. Eng. Progr. Symp. v.51 n.17 Sep pp.1-12 1955

Davies, E.J. and **Anderson, G.H.** *The incipience of nucleate boiling in forced convection flow.* AIChE Journal v.12 n.4 Jul pp.774-780 1966

Dittus, F.W. and Boelter, L.M.K. *Heat transfer in automobile radiators of tubular type.* University of California Publications on Engineering. v.2 p.443 Berkeley, CA 1930

Dougall, R.S. and Panian, D.J. *Subcooled forced convection boiling of trichlorotrifluoroethane*. NASA Contractor Report, CR-2137, Washington, D.C. 1972

Dwyer, O.E.; Strickland, G. and Kalish, S. *Incipient-Boiling superheat for sodium in turbulent, channel flow: Effects of heat flux and flow rate.* Int. J. Heat Mass Transfer v.16 pp.971-984 1973

Eddington, R.I. and Kenning, D.B.R. *The effect of contact angle on bubble nucleation*. Int. J. Heat Mass Transfer v.22 pp.1231-1236 1979

Frost, W. and Dzakowic, G.S. *An extension of the method for predicting incipient boiling on commercially finished surfaces*. ASME Paper 67-HT-61 1967

Hahne, E.; Spindler, K. and **Shen, N.** *Incipience of flow boiling in subcooled well wetting fluids*. Heat Transfer 1990. 9th Intl. Heat Transfer Conf. Jerusalem. v.2 pp.69-74 1990

Han, C.-Y. and Griffith, P. *The mechanism of heat transfer in nucleate pool boiling Part I: Bubble initiation, growth and departure*. Int. J. Heat Mass Transfer v.8 pp.887-904 1965

Hein, D. and Köler, W. *Messungen zum Siedebeginn in hochbelasteten Kanälen*. Bericht-Nr.:43.02.05, MAN. Germany. 1969

Hino, R. and **Ueda, T.** *Studies on heat transfer and flow characteristics in subcooled flow boiling. Part 1: Boiling characteristics*. Intl. J. Multiphase Flow v.11 n.3 pp.269-281 1985

Hodgson, A.S. *Forced convection, sub-cooled boiling heat transfer with water in an electrically heated tube at 100-550 lb/in²*. Trans. Instn. Chem. Engrs. v.46 pp.T25-T31 1968

Howell, J.R. and Siegel, R. *Incipience, growth and detachment of boiling bubbles in saturated water from artificial nucleation sites of known geometry and size*. Procc. 3rd Int. Conf. Heat Transfer, Chicago, v.4 pp.12-21 1966

Hsu, Y.Y. *On the size range of active nucleation cavities on a heating surface*. J. Heat Transfer. Aug p.207-216 1962

Jemison, T.R.; Rivers, R.J. and Cole, R. *Incipient vapor nucleation of methanol from an artificial site - Uniform superheat.* J. Heat Transfer v.104 Aug pp.567-569 1982

Joudi, K.A. and James, D.D. *Incipient boiling characteristics at atmospheric and subatmospheric pressures.* Trans. ASME J. Heat Transfer v.99 Aug pp.398-403 1977

Kim, C.J. and Bergles, A.E. *Incipient boiling behaviour of porous boiling surfaces used for cooling of microelectronic chips.* Particulate Phenomena and Multiphase Transport v.2 Veziroglu, T.N. Editor, Hemisphere 1988

Lee, C.H.; Chang, C.J.; Yin, S.T. and Huang, Y.D. *Prediction of incipient boiling with forced convective flow at 0.1 to 20.7 MPa.* ASME HTD v.96 (Procc. 1988 Heat Transfer Conf.) pp.469-474 1988

Lee, T.Y. and Simon, T.W. *High-heat-flux forced convection boiling from small regions. Heat Transfer in electronics 1989.* ASME HTD v.111 pp.7-16 1989

Lienhard, J.H. *Corresponding states correlations of the Spinodal and homogeneous nucleation limits.* J. Heat Transfer ASME v.104 May pp.379-381 1982

Lorenz, J.J. Mikic, B.B. and Rohsenow, W.M. *The effect of surface conditions on boiling characteristics.* Heat Transfer 1974, 5th Int. Heat Transfer Conf. v.4 pp.35-39 1974

Maddox, D.E. and Mudawwar, I. *Single and two-phase convective heat transfer from smooth and enhanced microelectronic heat sources in a rectangular channel.* Proc. 1988 Natl. Heat Transfer Conf. ASME HTD v.1 pp.533-541 1988

Marsh, W.J. and **Mudawwar, I.** *Effects of surface tension and contact angle on sensible heating and boiling incipience in dielectric falling films.* Proc. 1988 Natl. Heat Transfer Conf. ASME HTD-96 v.1 pp.543-550 1988

Marsh, W.J. and Mudawwar, I. *Predicting the onset of nucleate boiling in wavy free-falling turbulent liquid films.* Int. J. Heat Mass Transfer v.32 n.2 pp.361-378 1989

Martín-Domínguez, I.R. and **McDonald, T.W.** *Correlations for some saturated thermodynamic and transport properties of refrigerant R-22.* ASHRAE Transactions: Research. 1993 v.99 Pt.1 pp.344-348 1993

Martín-Domínguez, I.R. and McDonald, T.W. *Correlations for some saturated thermodynamic and transport properties of refrigerant R-113.* Memorias (Procc.) XVI Reunión Nacional de Energía Solar. 7-9 Oct 1992, Oaxaca, Oax. ANES (Asociación Nacional de Energía Solar). pp.237-241 México. 1992a

Martín-Domínguez, I.R. and **McDonald, T.W.** *Correlations for some saturated thermodynamic and transport properties of refrigerant R-11.* Memorias (Procc.) XVI Reunión Nacional de Energía Solar. 7-9 Oct 1992, Oaxaca, Oax. ANES (Asociación Nacional de Energía Solar). pp.232-236 México. 1992b

Marto, P.J. and Lepere, V.J. *Pool boiling heat transfer from enhanced surfaces to dielectric fluids.* J. Heat Transfer v.104 May pp.292-299 1982

Marto, P.J. and Rohsenow, W.M. *Effects of surface conditions on nucleate pool boiling of sodium.* J. Heat Transfer May p.196-204 1966

Marto, P.J. and Anderson, C.L. *Nucleate boiling characteristics of R-113 in a small tube bundle.* J. Heat Transfer v.114 May pp.425-443 1992

Marto, P.J.; Moulson, J.A. and Maynard, M.D. *Nucleate pool boiling of nitrogen with different surface conditions.* J. Heat Transfer Nov p.437-444 1968

McDonald, T.W. and **Shivprasad, D.** *Incipient nucleate boiling and quench study.* Procc. 2nd World Congress on Heating Ventilating and Air Conditioning - CLIMA 2000. Aug-27 Sep-1 Sarajevo, Yugoeslavia. v.1 pp.347-352 1989

Mizukami, K. *The effect of gases on the stability and nucleation of vapor bubble nuclei.* Letters in Heat and Mass Transfer. v.4 n.1 pp.17-24 1977

Mizukami, K.; Abe, F. and **Futagami, K.** *A mechanical model for prediction of boiling inception condition.* Heat Transfer 1990. 9th Intl. Heat Transfer Conf. Jerusalem. v.2 pp.117-122 1990

Murphy, R.W. and Bergles, A.E. *Subcooled flow boiling of fluorocarbons - Hysteresis and dissolved gas effects on heat transfer.* Proc. 1972 Heat Transfer and Fluid Mechanics Inst. pp.400-416 Stanford Univ. Press 1972

Nukiyama, S. *The maximum and minimum values of heat transmitted from metal to boiling water under atmospheric pressure.* J. Japan Soc. Mech. Eng. v.37 p.367 (Translation: Int. J. Heat Mass Transfer v.9 p.1419 1966) 1934

Park, K.A. and Bergles, A.E. *Effects of size of simulated microelectronics chips on boiling and critical heat flux.* J. Heat Transfer. v.110 Aug pp.728-734 1988

Park, K.A. and Bergles, A.E. *Boiling heat transfer characteristics of simulated microelectronics chips with detachable heat sinks.* Heat Transfer 1986. 8th Int. Heat Transfer Conf. San Francisco v.4 p.2099-2104 1986

Ricque, R. and **Siboul, R.** *Ebullition locale de l'eau en convection forcée.* CEA R-3894, Commissariat à l'Energie Atomique. 1970

Robertson, J.M. and Clarke, R.H. *The onset of boiling of liquid nitrogen in plate-fin heat exchangers.* AIChE Symposium Series Heat Transfer v.77 n.20 pp.86-95 1981

Rohsenow, W.M. *A method of correlating heat transfer data for surface boiling liquids.* Trans. ASME v.74 p.969 1952

Rohsenow, W.M. *General Boiling.* Chap.6 in *Handbook of Multiphase Systems.* **Hetsroni, G. Editor.** Hemisphere Publ. 1982

Sabersky, R.H. and Gates, C.W. *On the start of nucleation in boiling heat transfer.* Jet Propulsion v.25 Feb pp.67-70 1955

Sato, T. and Matsumura, H. *On the conditions of incipient subcooled-boiling with forced convection.* Bul. JSME v.7 n.26 pp.392-398 1964

Shah, M.M. *A general correlation for heat transfer during subcooled boiling in pipes and annuli.* ASHRAE Transactions v.83 Part 1 n.2443 pp.202-217 1977

Shakir, S. and Thome, J.R. *Boiling nucleation of mixtures on smooth and enhanced surfaces*. Heat Transfer 1986. 8th Int. Heat Transfer Conf. San Francisco v.4 pp.2081-2086 1986

Spindler, K. and Hahne, E. *Beitrag zum Siedebeginn beim unterkülten Sieden mit Zwangskonvektion*. Chem. Ing. Techn. v.60 n.1 pp.54-55 (Synopsis), and full manuscript from the authors: Institut für Thermodynamik und Wärmetechnik, Univ. Stuttgart, Germany. 1988

Stephan, K. *Wärmeübergang beim Kondensieren und beim Sieden.* Springer Verlag 1988

Sudo, Y.; Miyata, K.; Ikawa, H. and **Kaminaga, M.** *Experimental study of incipient nucleate boiling in narrow vertical rectangular channel simulating subchannel of upgraded JRR-3*. J. Nucl. Science and Technology v.23 n.1 Jan pp.73-82 1986

Thome, J.R.; Shakir, S. and Mercier, C. *Effect of composition on boiling incipient superheats in binary liquid mixtures*. Heat Transfer 82, 7th Int. Heat Transfer Conf. München v.4 pp.95-100 1982

Thormälen, I. *Superheating of liquids at the onset of boiling*. Heat Transfer 1986 Procc. 8th Int. Conf. San Francisco v.4 pp.2001-2006 1986

Tong, W.; Bar-Cohen, A.; Simon, T.W. and **You, S.M.** *Contact angle effects on boiling incipience of highly-wetting liquids*. Int. J. Heat Mass Transfer v.33 n.1 pp.91-103 1990

Tong, W.; Simon, T.W. and Bar-Cohen, A. *Effect of dissolved gas on boiling incipience in highly-wetting liquids*. Procc. 5th Miami Int. Symp. on Multi-phase Transport and Particulate Phenomena 1989

Torikai, K.; Shimamune, H. and Fujishiro, T. *The effect of the dissolved gas content upon incipient boiling superheats*. Heat Transfer 1970. 4th Int. Heat Transfer Conf. Paris. v.5 pap.B2.11 1970

Turton, J.S. *The effects of pressure and acceleration on the pool boiling of water and Arcton 11*. Int. J. Heat Mass Transfer v.11 May pp.1295-1310 1968

Van Vleet, R.J. *A study of the initiation of subcooled boiling during power transients*. Ph.D. Dissertation. Kansas State University 1981

Wark, K. *Thermodynamics*. McGraw-Hill. 1988

Yin, S.T. *Incipient boiling of Freon 11 in forced convection vertical flow.* Ph. D. Dissertation Univ. of Toronto. Canada. 1974

Yin, S.T. and Abdelmessih, A.H. *Prediction of incipient flow boiling from a uniformly heated surface*. AIChE Symposium Series v.73 n.16 pp.236-243 1974

You, S.M.; Simon, T.W.; Bar-Cohen, A. and **Tong, W.** *Experimental investigation of nucleate boiling incipience with a highly-wetting dielectric fluid (R-113)*. Int. J. Heat Mass Transfer v.33 n.1 pp.105-117 1990a

You, S.M.; Simon, T.W. and **Bar-Cohen, A.** *Experiments on boiling incipience with a highly-wetting dielectric fluid; effects of pressure, subcooling and dissolved gas content*. Heat Transfer 1990. 9th Intl. Heat Transfer Conf. Jerusalem. v.2 pp.337-342 1990b

You, S.M.; Simon, T.W. and **Bar-Cohen, A.** *Reduced incipient superheats in boiling of fluids which hold dissolved gas*. Phase Change Heat Transfer 1991. ASME HTD v.159 pp.109-117 1991

Appendix A

CHRONOLOGICAL LITERATURE REVIEW

Sabersky, R.H. and **Gates, C.W.** (1955) investigated the effects of water pre-pressurization on the onset of nucleate boiling in nichrome wires. The pre-pressurization consisted in rising the water pressure up to 15,000 psia for a period of 15 min and then allowing the sample to return to atmospheric conditions, then the wire was electrically heated and they found that the surface could reach values of up to 325°F before the ONB, and temperature overshoots of up to 85°F were observed. They attributed this behaviour to a possible elimination of vapour or gas trapped in the larger cavities of the solid surface. They observed also that once the surface had been exposed to vapour masses, further ONB would occur at normal temperatures.

Corty, C. and **Foust, A.S.** (1955) conducted experimental work with ether, pentane and R-113 on copper and nickel surfaces. They analyzed the effects of surface roughness on the ONB and on the heat transfer coefficients in nucleate boiling. The effect of boiling history on the deactivation of boiling sites and boiling hysteresis was also investigated.

They found that their smoothest surface required the highest wall superheat (WS) during nucleate boiling whereas the largest temperature overshoot (TOS) occurred with

the roughest surface. Their explanation was that the larger cavities of the rough surface were flooded easily and as a result higher wall superheats were required to initiate the nucleation in the small remaining cavities. Once nucleation started the larger cavities were seeded. The resulting bubble nucleii were of larger curvature radius and hence required a lower WS.

The different hysteretic paths that the boiling curve describes when the heat flux is partially decreased after vigorous boiling and then increased again, were also analyzed:

- when all the active sites were allowed to die and the surface kept free of bubbles for at least 10 min, TOS up to 25°C were observed.
- when the last remaining active sites were just permitted to die and the power input then immediately increased, the sites last active reactivated first, and upon further power increase, they became the centre of violent boiling patches, while the rest of the surface remained bare.
- when the power was increased when there still were a number of active sites, the patchwise pattern of boiling emerged again, but the patches merged together.

From this they concluded that the initial bubble forms at the spot most resistant to loss of residual vapour, and this re-activates other sites in its neighbourhood by pressure surges or by seeding them with vapour during their growth, beyond the cavity

mouth.

Bankoff, S.G. (1957) analyzed the necessary conditions to initiate the nucleation of bubbles from a flat surface, a curved surface and from cavities. He demonstrated that the possibility of nucleation within a homogeneous liquid, at a flat or at a projecting solid surface can be dismissed from consideration, since the required pressure (temperature) differences are very high. Well wetted cavities were also rejected for the same reasons. The only possible option was nucleation in a non well-wetted cavity, where vapour or other gas remained trapped.

Bankoff, S.G. (1958) analyzed the conditions for gas and liquid entrapment in cavities, during advancing and receding liquid fronts, based in geometric considerations. He assumed conical cavities and concluded that, depending on the combination of cavity angle and liquid contact angle, cavities could be classified in four categories:

- always filled with liquid.
- always filled with gas.
- those in which complete displacement of gas by liquid is possible, but not vice versa.
- those in which complete displacement of liquid by gas is possible, but not vice versa.

Clark, H.B.; Strenge, P.S. and **Westwater, J.W.** (1959) conducted a photographic study during and after nucleate boiling, to identify active bubble-producing sites. All the sites identified were pits, scratches or boundaries between the test metal and the packing plastic material used to seal gaps.

Hsu, Y.Y. (1962) assumed that a bubble nucleus already existed over the mouth of a cavity, from a preceding one, and performed a transient heat conduction analysis over the limiting thermal boundary layer thickness, to find the temperature distribution as a function of the layer thickness, thermal diffusivity and time. He found an expression for the minimum and maximum radius of cavities that have a finite waiting period, and calls them "effective" cavities. An equation was presented to estimate the point of boiling incipience.

Bergles, A.E. and **Rohsenow, W.M.** (1964) derived an expression for the onset of nucleate boiling in forced flow conditions by using the Clausius-Clapeyron equation (perfect gas assumption) to express the bubble thermo-mechanic equilibrium. They assumed that the temperature profile in the boundary layer is linear and that the condition for the bubble to start growing is when the curve of the required liquid superheat and the boundary layer temperature profile become tangents.

Since it was not possible to solve for the heat flux from their equations they presented a graphical solution and fitted a curve as a function of pressure and wall

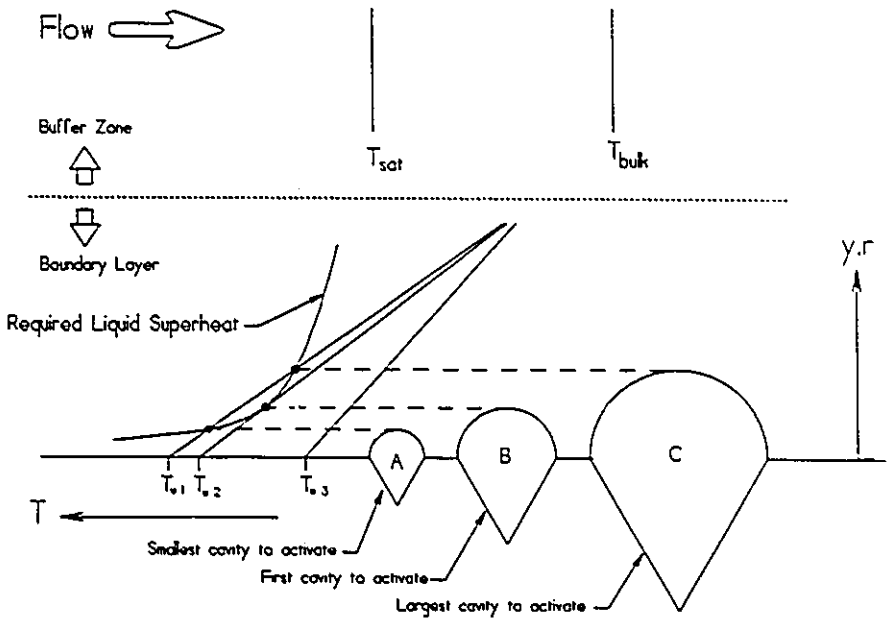

Figure A.1. Bergles & Rohsenow bubble activation model.

superheat. Equation (A.1) is the equation they determined.

$$q^{*} = 1.76\times10^{-3}\, P^{1.156}\left[\frac{9}{5}\left(T_w - T_s\right)\right]^{\frac{2.83}{P^{0.0234}}} \qquad (A.1)$$

They mention that, since a wide range of cavity sizes could be expected to exist in commercial surfaces, the ONB should then be independent of surface conditions. This model is shown in Figure A.2.

Sato, T. and **Matsumura, H.** (1964) assumed a spherical bubble already existed at the heating surface, with no mention of cavities. The temperature-pressure relationship at saturation was obtained by integrating the Clausius equation by assuming the term $h_{fg} / (T\, v_{fg})$ a constant. Taking the temperature distribution in the boundary layer as

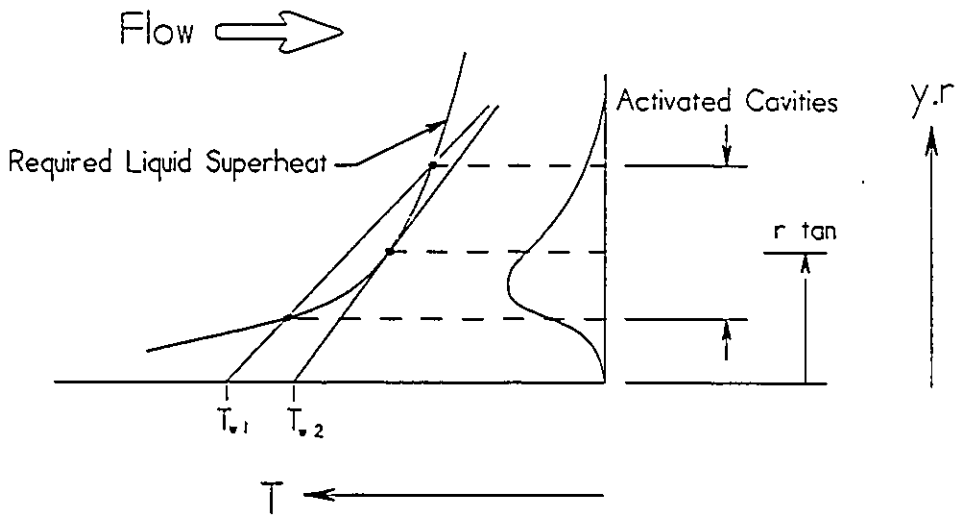

Figure A.2. Bergles & Rohsenow r_{can} criteria.

linear led to the conclusion that the *critical* bubble radius (bubble radius at the boiling inception condition) should be one half of the boundary layer thickness. An equation for the heat flux in nucleate boiling, in terms of the wall superheat, liquid thermal conductivity, h_{fg}, surface tension, v_{fg} and saturation temperature was presented.

$$q^{"} = \frac{\kappa_f h_{fg}}{8 \sigma T_s v_{fg}} (T_w - T_s)^2 \qquad (A.2)$$

They defined the ONB as the intersection between their equation and that for single-phase forced convection based on the McAdams correlation.

$$Nu = 0.023 Re^{0.8} Pr^{0.4} \qquad (A.3)$$

which yields the expression

$$q^{"} = 0.023\ Re^{0.8}\ Pr^{0.4}\ \frac{\kappa}{D_h}\left[\left(T_w - T_s\right) + \left(T_s - T_b\right)\right] \qquad (A.4)$$

The intersection of equations (A.2) and (A.4) is shown in Figure A.3.

By equating equations (A.2) and (A.4) the expression shown in equation (A.5)

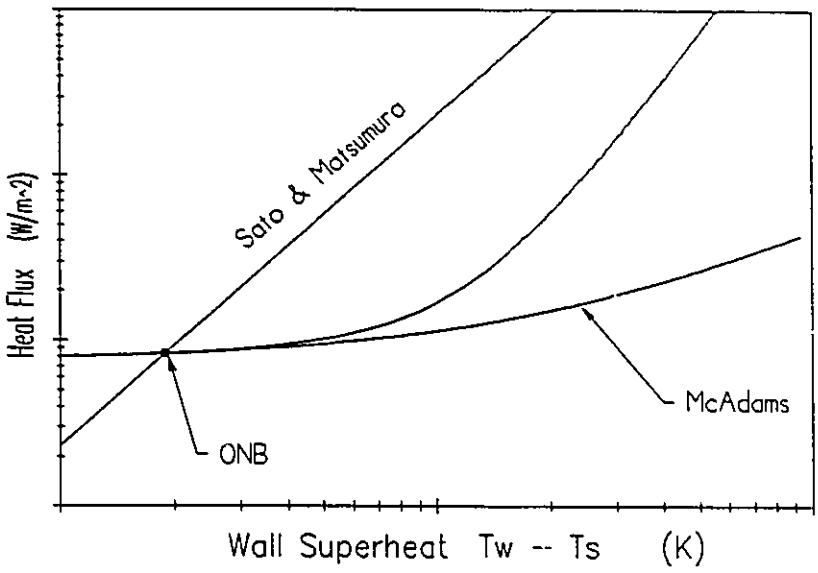

Figure A.3. Onset of nucleate boiling after Sato & Matsumura.

was obtained relating the wall heat flux at the ONB with flow conditions and liquid subcooling.

$$q^{"} = \frac{\kappa\ h_{fg}}{8\ \sigma\ T_s\ v_{fg}}\left[\frac{q^{"}\ D_h}{0.023\ Re^{0.8}\ Pr^{0.4}\ \kappa} - \left(T_s - T_b\right)\right]^2 \qquad (A.5)$$

Han, C.-Y. and **Griffith, P.** (1965) presented an analysis similar to that of **Hsu,**

Y.Y. (1962), but they assumed that the temperature profile in the boundary layer was distorted by the presence of the bubble nucleus. They derived a different expression for the bubble critical radius.

Davies, E.J. and **Anderson, G.H.** (1966) conducted experiments with water and found large discrepancies with the predictions from **Bergles and Rohsenow** (1964) for the ONB. They proposed a new analysis, based on the Bergles and Rohsenow model, by assuming that the bubble nucleus at the cavity mouth has a truncated sphere shape rather than the original hemispherical and by including the contact angle into the analysis. The resulting equation is similar to that of **Sato and Matsumura**, but includes the effect of the contact angle.

$$q^{*} = \frac{\kappa_f \; h_{fg}}{8 \; C_1 \; \sigma \; T_s \; v_{fg}} \; (T_w - T_s)^2 \qquad (A.6)$$

where the constant C_1 is defined as:

$$C_1 = 1 + \cos(\beta) \qquad (A.7)$$

The effect of the inclusion of the contact angle is shown Figure A.4.

Frost, W. and **Dzakowic, G.S.** (1967) introduced two modifications to the **Bergles and Rohsenow** model: a). The *Clapeyron* equation was used assuming that the term $h_{fg} / (T \; v_{fg})$ to be constant over the range of integration. b). The distance from the

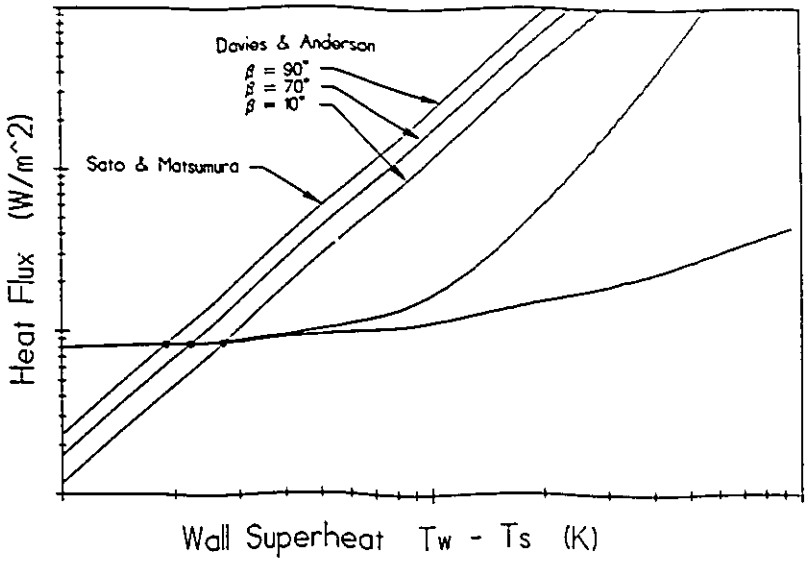

Figure A.4. Onset of nucleate boiling after Davies & Anderson.

wall, at which the boundary layer temperature profile and the thermo-mechanic equilibrium temperature curve become tangents, was allowed to be a function of the Prandtl number.

$$q^{*} = \frac{\kappa_f \, h_{fg}}{8 \, \sigma \, T_s \, v_{fg}} \left(T_w - T_s\right)^2 \frac{1}{Pr^2} \qquad (A.8)$$

The graph resulting from this modification is shown on Figure A.5, where the **Sato and Matsumura** equation (A.2) is also shown for comparison.

They explained that it was not possible to give a theoretical derivation for such criteria, but since in any boundary layer the Prandtl number dictates the shape of the temperature profile, therefore one could expect the wall superheat to be proportional not just to the bubble radius but also to the Prandtl number.

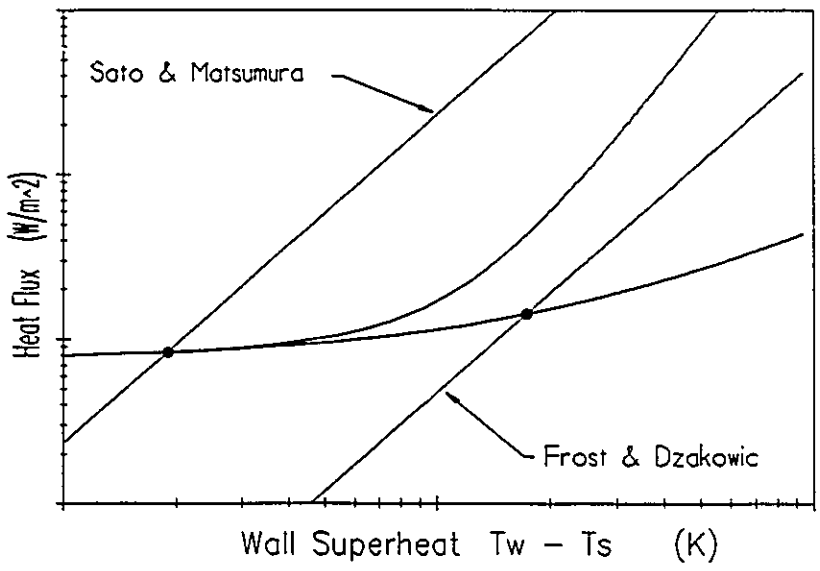

Figure A.5. Frost & Dzakowic model.

Turton, J.S. (1968) conducted experiments in pool boiling on stainless steel tubes with water and Arcton 11. He measured only one case of temperature overshoot in water, but all his experiments with Arcton 11 showed large temperature overshoots and hysteresis. On the first run after filling his system with Arcton 11, the ONB occurred after a very small TOS of about 5 K. The heat flux was then decreased to a value smaller than the previous incipience value and increased again, giving a TOS of 16.7 K this time. After an undisclosed time interval, the heat flux was increased from zero and the obtained TOS was approximately 40 K. He explained these results in terms of the purging of air trapped in the surface's cavities and replaced by vapour, thus causing the next ONB to occur at higher temperatures.

Hodgson, A.S. (1968) conducted experiments with subcooled water flowing in

stainless steel tubes. His graphs show hysteretic behaviour between the heating and cooling processes. He stated that an analytical approach to develop a theory to cover the whole range of boiling was unrealistic, and chose to follow an empirical approach.

Using dimensional analysis and introducing two parameters X and Z, where:

$$X = \frac{dT_{sat}}{dP} \tag{A.9}$$

and

$$Z = -\frac{d\left(\frac{\rho_f}{\rho_g}\right)}{dP} \tag{A.10}$$

he developed a general equation for forced convection and nucleate boiling, in terms of dimensionless parameters. As an incipient boiling criterion, he set the ratio between the Stanton (St) number for boiling and the St for forced convection equal to one (unity) in his equation. The resulting expression, given by equation (A.11), is a function of his two parameters, subcooling, specific heat, vaporization enthalpy, heat and mass flux, but does not include surface tension, contact angle or surface characteristics.

$$Bo = 8.5 \times 10^{-4} \; Ja^{0.785} \left(\frac{Z\, h_{fg}}{X\, Cp_f}\right)^{0.114} \tag{A.11}$$

where:

$$Bo = \frac{q''}{\dot{m}'' h_{fg}} \qquad and \qquad Ja = \frac{Cp_f (T_s - T_i)}{h_{fg}} \qquad (A.12)$$

Chen, J.C. (1968). Since experimental evidence showed that incipient superheats with liquid metals were much higher than those predicted by Hsu's model, then concluded that a further criteria was needed to predict the dimension of the largest unflooded cavity (largest potential site) which will set a real limit on the required wall superheat at the ONB. He proposed an equation in terms of the cavity angle, surface tension and deactivation pressure and temperature (history). Since the amount of gas initially trapped in a cavity is unknown it is regarded as an empirical constant, with some average value for a given surface an filling operation, and included into the equation.

Coeling, K.J. and Merte Jr, H. (1969) studied the incipience of nucleate boiling in liquid hydrogen. They tested stainless steel, copper and Teflon at different orientations in a liquid pool. Hysteresis was detected in most of the runs.

Murphy, R.W. and **Bergles, A.E.** (1972) conducted experiments in a vertical flow using subcooled R-113. Large temperature overshoots at the ONB were observed. They found that large concentrations of dissolved gas caused a reduction of about 15°F in the wall superheat at the ONB when compared with the low gas concentration case. They modified the **Bergles and Rohsenow** (1964) equation to include an "adjusted" or

"gassy" saturation temperature that depends on the pressure and the content of dissolved gas. By comparing their equation vs. experimental data they concluded that the model appears to adequately predict the point where nucleation dies, rather than the ONB.

Yin, S.T. (1974) conducted experiments with R-11 flowing inside a Stainless Steel tube to observe the incipient boiling superheat and hysteresis effects. After analyzing the existing models he concludes that they were inadequate to predict the ONB.

Yin, S.T. and **Abdelmessih, A.H.** (1974). They pointed out that since the then existing models for the prediction of the ONB were only useful in determining the point where nucleation ceases during cooling, a better analysis was necessary. They assumed conical cavities with bubbles of a truncated sphere shape attached to the cavity mouth, which detached when the superheated liquid boundary layer was thick enough so that a net heat flux into the bubble existed. The resulting equation was given in terms of the contact angle, height of the bubble and boundary layer thickness.

Lorenz, J.J.; **Mikic, B.B.** and **Rohsenow, W.M.** (1974). An analysis of the effects of the contact and cavity angles on the bubble curvature radius was presented. A graph of the reciprocal of the curvature radius vs. trapped volume was presented to explain why the superheat required to activate a cavity depends upon the cavity radius or on the bubble curvature radius, whichever was smaller. By analyzing the vapour

trapping mechanism, they found that the ratio between bubble curvature and the cavity radius was a function only of the contact and cavity angles.

Joudi, K.A. and **James, D.D.** (1977) conducted an experimental work in saturated pool boiling with R-113, water and methanol, over a flat Stainless Steel surface of artificial roughness. They reported that temperature overshoots occurred only with R-113 and methanol, but not with water, for all the pressures investigated.

Thome, J.R.; Shakir, S. and **Mercier, C.** (1982). Two sets of experiments were conducted, one with cryogenic fluids (nitrogen-argon), and other with water-ethanol mixtures in pool boiling over polished copper surfaces at atmospheric pressure. Series of tests following identical procedures were conducted to produce identical prior history on the heated surfaces. Trial tests show that even small pre-pressurizations cause a substantial increase in the ONB superheats. The size of the heat flux increments, from one steady state to the next, as well as the time interval between subsequent tests, also affected the incipient wall superheats. The wall superheat at the ONB was unaffected by mixture composition for the cryogenic fluids, which both have very small contact angles. The water-ethanol mixture, on the other hand, showed a large dependence on the composition. In this case the contact angle varied from 80° for pure water to almost zero for pure ethanol.

Cornwell, K. (1982). No engineering surface is truly smooth, the contact angle at the liquid-solid interface at the microscopic scale will have variations according to the surface roughness. By using this argument he explained how a conical cavity could trap and retain bubble nucleii within the cavity-wall micro-roughness deep inside the cavity, by postulating an inversion of the radius of curvature of the bubble nucleii meniscus. He noted that contact angles measured for water-copper range from 0° for pure copper in vacuum, to 87° when fully oxidized in air. Contact angles also vary with temperature, and contact angle measurements are normally made at lower temperatures than those encountered during boiling experiments. Contact angle is also affected by surface contamination. He concluded that re-entrant cavities were physically unlikely to exist in large numbers. Examination of machined surfaces under the microscope indicated the existence of many positive angled cavities with rough internal surfaces. Therefore it is the internal roughness of cavities that explains how vapour can be trapped and retained inside cavities, and that the nucleii critical radius is generally smaller than the cavity mouth radius.

Bergles, A.E. and **Chyu, M.C.** (1982) conducted experiments in pool boiling of water and R-113 on plain and commercial porous metallic matrix surfaces. On the plain surface no temperature overshoots with water were found, only modest values with R-113 (fraction of a degree). On the porous surface water showed TOS of up to 3 K and R-113 of up to 8 K.

Clarke, R.H. and Robertson, J.M. (1984). Experimental work with vertical flow boiling of nitrogen was performed, using condensing steam as a heat source in plate-fin heat exchangers. The controlled variable on their experiments was the pressure. They reported temperature overshoots at the ONB.

Hino, R. and **Ueda, T.** (1985) conducted experiments in vertical subcooled annular flow with R-113. They compared their results at the ONB vs. **Sato and Matsumura** (1964) and **Bergles and Rohsenow** (1964) predictions, and since the agreement was poor, they proposed a new equation, without derivation:

$$q^{*} = \frac{\kappa}{r_{max}} \left(T_w - T_s \right) - \frac{2\,\sigma\,\kappa\,T_s}{h_{fg}\,\rho_g\,r_{max}^2} \qquad (A.13)$$

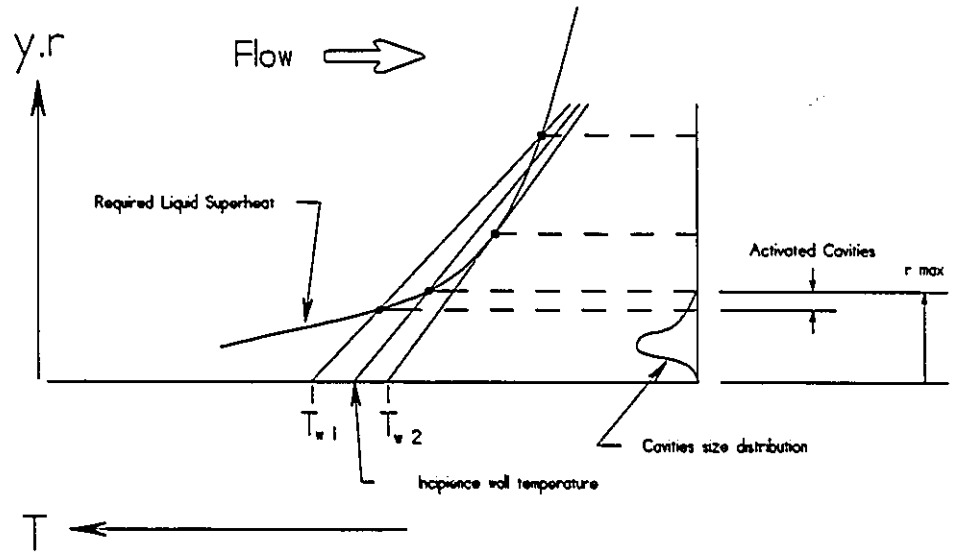

Figure A.6. Hino & Ueda r_{max} criteria for cavity activation.

They concluded that this equation should be valid when there exists an upper limit on the sizes of available cavities.

They proposed that the intersection of their equation with the single-phase forced convection equation from Dittus-Boelter would correspond to the ONB.

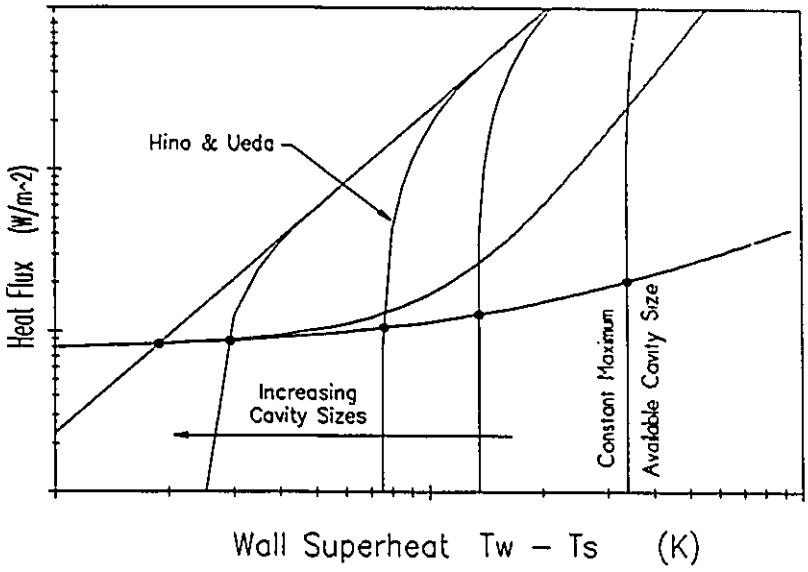

Figure A.7. Maximum available cavity size equation by Hino & Ueda.

Kim, C.J. and **Bergles, A.E.** (1986). Experimental work was performed in saturated pool boiling with R-113 over artificially porous surfaces (sintered copper powders) and a plain surface. Wall superheats at the ONB in the plain surface occurred within 30-40 K, while in the porous surfaces this occurred within 20-30 K. The plain surface exhibited a typical hysteretic behaviour while in the porous surface, during the cooling process, nucleate boiling was sustained down to very low wall superheats,

following a path substantially different than during the heating process.

Sudo, Y.; Miyata, K.; Ikawa, H. and **Kaminaga, M.** (1986). Performed experimental work with a subcooled vertical flow of water in narrow channels to observe the accuracy of the **Bergles and Rohsenow** equation in predicting the ONB. They compared their experimental results with the equations from **Bergles and Rohsenow** and **Sato and Matsumura**, and found that the measured wall superheats at the ONB were higher than the predicted, although the data showed the same tendency as the predictive equations both for different mass fluxes and subcoolings. They reported the occurrence of only one case of temperature overshoot (2 K) and hysteresis. The comparison of their data vs. **Hino and Ueda**'s model resulted in a range of maximum available cavity sizes spreading over one order of magnitude.

Spindler, K. and **Hahne, E.** (1988) conducted experiments in subcooled flow of R-11 inside copper tubes. Their results showed no dependence between the wall superheat, at the ONB, and flow velocity or subcooling. By comparing their results with the models from **Davies and Anderson** (1966), **Frost and Dzakowic** (1967), **Hsu** (1962) and others, they found very poor agreement and only the model from Hino and Ueda (1985) correctly predicted the ONB **if** the cavity mouth radius size was properly ***selected***. They also compared their results with the dimensionless models from **Hodgson** (1968) and **Bucher** (1979) and found that the one from Hodgson reproduced theirs, and others',

results better but neither equation seemed to be of general validity since they did not include important parameters as the surface roughness.

Marsh, W.J. and **Mudawwar, I.** (1988) performed experimental work with falling films of FC-72. They found **no** temperature overshoot or hysteresis effects. Their results showed that the wall superheat at the ONB is independent from subcooling, flow rate or heat flux. They mentioned that these trends are different with less wetting fluids, like water, where other authors have found clear relationships. The model from **Hino and Ueda** predicted a cavity size range from 0.35 to 0.45 μm, however, microscopic analysis of the actual surface revealed sizes from 0.5 to 10.0 μm. Therefore they concluded that neither **Sato and Matsumura** or **Hino and Ueda** equation types were valid for their data, and postulated that the ONB for highly wetting fluids was solely the function of the initial radius of the trapped vapour embryo, or in turn, of the contact angle, depth and cone angle of the cavities. This meant that the surface acted as though it had cavity sizes much smaller than the actual ones.

Maddox, D.E. and **Mudawwar, I.** (1988) performed experimental work in forced flow with FC-72 over simulated microelectronics heat sources. Test surfaces included smooth case and microstuds, all prepared with a vapour blast treatment to provide uniform surface microstructure. They reported that an important factor affecting the boiling hysteresis was the period of time during which the heating surface remained in

the non-boiling state, both before and during the heating process. The presence of dissolved air, and the microstuds, reduced the temperature overshoot at the ONB. The worst case they measured (7.5 K of TOS) was with the smooth surface at low velocity (0.75 m/s) and almost zero subcooling.

Lee, C.H.; Chang, C.J.; Yin, S.T. and **Huang, Y.D.** (1988) proposed to modify **Hsu**'s model, which was difficult to use since it requires knowledge of the boundary layer thickness, by assuming that such thickness could be calculated as the ratio of the liquid thermal conductivity to the subcooled heat transfer coefficient. With that assumption they tested four different subcooled heat transfer correlations, as well as the one from **Shah, M.M.**, in order to get the best results by predicting the ONB vs. their own experimental forced convective water data, (within 30%). They compared their data and model with those from **Bergles and Rohsenow** (1964) and **Davies and Anderson** (1966) and only the first (B and R) showed good agreement, but only at low pressures.

Bräuer, H. (1988), **Bräuer, H.** and **Mayinger, F.** (1988) undertook theoretic and experimental work with vertical forced convective flow of R-12. The experimental part showed that:

- heat flux at the ONB varied strongly with mass flow rate, moderately with subcooling and was almost independent of pressure.

- wall superheat at the ONB decreased with increasing pressure but was almost independent from mass flow rate and moderately dependent from subcooling.

They performed a detailed heat transfer analysis, following the **Bergles and Rohsenow** model, dividing in several zones a spherical bubble, sitting at the cavity mouth. The resulting equation was almost identical to that from **Sato and Matsumura**, and for R-12 was given as:

$$q^{"} = \frac{\kappa_f \, h_{fg}}{194.83 \; \sigma \; T_s \; v_{fg}} \left(T_w - T_s\right)^2 \qquad \text{(A.14)}$$

A graphic comparison of their equation vs. **Bergles and Rohsenow**, **Davies and Anderson** and **Frost and Dzakowic** showed that all follow the same trend, but their equation predicted higher heat fluxes at the same wall superheat. Comparison against their own experimental data showed a very good agreement at different subcoolings, mass flow rates and pressures. They argued that even when the proposed model gave very good results, a simpler easy-to-use equation was desirable for the field engineer, and another equation was then proposed. This second equation was in terms of dimensionless numbers and no explanation about its derivation was given.

$$Bo = 0.0015 \;\; Re^{-0.112} \left(\frac{P}{P_c}\right) \left(Ja_{\text{mod}}\right)^{0.773} \qquad \text{(A.15)}$$

Where the boiling number and the modified Jakob number are:

$$Bo = \frac{q''}{\dot{m}'' h_{fg}} \qquad and \qquad Ja_{mod} = \frac{h_s - h_i}{h_{fg}} \cdot \frac{\rho_f - \rho_g}{\rho_g} \qquad (A.16)$$

The required exponents and coefficients are obtained by a regression process, and a comparison of measured vs. calculated boiling number showed a very good agreement. They also performed an analogy between R-12 and water, to compare the temperature profiles that could exist in an annular flow section for both substances, by using similitude concepts to obtain an equivalent water mass flow rate after equating the reduced pressure, Jakob and Reynolds numbers. They concluded that the temperature gradient in the vicinity of the heated wall should be smaller when using water, therefore the wall superheat at the ONB should be also smaller. A comparison between predicted ONB and experimental water data from **Hein and Köler** (1969) showed fairly good agreement. Finally, the dimensionless equation was used to predict the results from other nine authors, with R-11, R-12, R-113 and water flowing in different geometries. The agreement was very good with the data of **Hino and Ueda** (1985), **Dougall and Panian** (1973) and **Hein and Köler** (1969); the agreement was not as good but still close for the data of **Spindler and Hahne** (1988), **Bucher** (1979) and **Abdelmessih, Fakhri and Yin** (1974).

Belhadj, M.; Aldemir, T. and **Christiansen, R.N.** (1988) performed experimental work with demineralizated water flowing in simulated nuclear reactor core channels. They found no temperature overshoots at the ONB. The equations

recommended by the International Atomic Energy Agency were found to overpredict the data of **Bergles and Rohsenow** (1964) and underpredict the data of **Ricque and Siboul** (1970) for the ONB. They proposed a new correlation in terms of the Reynolds number and the channel gap, which they obtained by a regression analysis. The correlation predicted their data within 13%, but they warn that it was only valid for upward flow of water where , Re < 700, channel gap size range from 2 to 4 mm, and pressures between 1.4 and 1.46 atm.

Bar-Cohen, A. and **Simon, T.W.** (1988). A detailed historic perspective of thermal control of microelectronics by immersion cooling in liquids was given, and the main problem encountered to implement this technic was the uncertainty associated with nucleation and boiling incipience. The homogeneous and heterogeneous nucleation mechanisms were discussed and they observed that the incipience superheat was bounded from above by homogeneous nucleation. Published results of incipience superheats were given and discussed, for bare and enhanced surfaces.

Ayub, Z.H. and **Bergles, A.E.** (1988) undertook an experimental study in pool boiling of R-113 over four different GEWA-T surfaces and a smooth tube at atmospheric pressure. They measured temperature overshoots of the order of 2 to 4 K in all four enhanced surfaces.

Anderson, T.M. and **Mudawwar, I.** (1988) undertook a theoretic and experimental study with FC-72 in pool boiling over four categories of surfaces:

- smooth surfaces with different degrees of roughness: mirror finish, sanded and vapour blasted.
- vapour blasted surfaces with arrays of artificial (drilled) cavities, 0.356 mm diameter, normal and inclined respect to the surfaces.
- low-profile enhancement structures: microfins, microstuds and inclined microgroove.
- low-aspect ratio square studs.

The artificial cavities are drilled as linear arrays of 17, running horizontally in one case and vertically in other, along the centre line of a square surface, for the normally drilled case. For the case of inclined drilled cavities they attempted to use gravity to aid retention of stable vapour embryos by drilling upwards, this array ran along the bottom edge of the square surface.

They found that the time, temperature and pressure history prior to boiling was a primary factor affecting the magnitude of incipient boiling hysteresis, and therefore a standardized test procedure was established. They reported only the length of the non-boiling periods, but not the temperature and/or pressure history on those periods. Their results showed that the same mirror finished surface requires ONB wall superheats of 15°C after 8 h, 23°C after 19 h and 30.6°C after 72 h of waiting time, which precluded the use of theories based only in the cavity radius to calculate the wall

superheat at the ONB in fluids with low contact angle.

In testing the effects of surface roughness they found that, subjected to equivalent initial conditions, increasing roughness promoted earlier incipience and reduced the probability of significant temperature overshoot.

The results with the artificial cavities showed that, after 8 h of waiting periods, nucleation started near the upper edge of the surfaces, not at the cavities. On the vertical array surface, after incipience of the first cavity, the large bubbles produced activated the next cavity immediately below and the boiling front rapidly advanced downwards. On the horizontal array surfaces cavities started to boil just when the boiling front patch passed over them. Cavities were the last to cease boiling as the flux was decreased, but after only 10 min of non-boiling period they became quenched.

Tong, W.; Simon, T.W. and **Bar-Cohen, A.** (1989), theoretical work. They pointed out that for the high wetting liquids used for cooling microelectronic components, air and other non-polar gases are easily dissolved. The solubility of air in FC-72 is 25 times higher than in water at standard conditions. Usually dissolved gas merely reduces the surface tension of the dissolving liquid, but in refrigerants the surface tension is much smaller than in other common liquids and therefore even a small reduction can be relatively large. They proposed a model for the wall superheat at the ONB by using an equation for the critical bubble radius (**Tong, Bar-Cohen, Simon and You** 1990), in terms of cavity radius, cavity angle, static equilibrium contact angle and dynamic contact

angle, including also the dissolved gas content. No comparisons with experimental data were given.

McDonald, T.W. and **Shivprasad, D.** (1989) performed an experimental study with a vertical subcooled flow of R-11. Different hysteretic boiling curves are produced by re-heating the system after having been in fully developed boiling and then driven into the partially developed nucleate boiling zone, by reducing the heat flux. Different curves were obtained depending on how close to the single-phase zone the system was allowed to cool down. They observed that a site will reactivate upon re-heating if the wall superheat did not drop below 50% of the value required to maintain the cavity active.

Marsh, W.J. and **Mudawwar, I.** (1989) undertook experimental work with wavy free-falling turbulent liquid films of water and FC-72. Their results did not show ANY temperature overshoot at the ONB.

For the test results with **water**, equations based on the point of tangency, between the boundary layer temperature profile and the required temperature for the thermo-mechanical equilibrium, criteria (r_{tan}) (**Sato and Matsumura**, 1964; **Bergles and Rohsenow**, 1964; **Han and Griffith**, 1965; **Davies and Anderson**, 1966; **Yin and Abdelmessih**, 1974) failed to predict the wall superheat at the ONB by up to 4 K (50%), while the equations based on the maximum cavity radius, available for nucleation on the heated surface, criteria (r_{max}) (**Hino and Ueda**, 1985; **Sudo, Miyata and Ikawa**, 1986)

provided good agreement **IF** the r_{max} was chosen as 5.0-8.0 μm. Since the results with water showed the same trend as those predicted by the r_{tan} criteria equations, they proceeded to reexamine the shape of the temperature profile in the boundary layer and introduced a multiplier in the **Davies and Anderson** (1966) equation:

$$q^{*} = \frac{\kappa_f h_{fg}}{8 \sigma T_s v_{fg}} \left(T_w - T_s\right)^2 \frac{1}{\psi} \qquad (A.17)$$

which shifts the curve to the right in the Heat Flux vs. Wall Superheat coordinates, and provided a good agreement compared to the water data, and also the equation proposed by **Frost and Dzakowic** (1967). The multiplier resulted from multiplying two coefficients, one that accounts for the turbulent boundary layer effect and for which an elaborated analytical derivation was given. The second coefficient accounted for the effects of waves, turbulent eddies and isotherm curvature in a falling film. No analytical derivation was attempted for this coefficient. The value of the multiplier was obtained by a least squares approximation, from the experimental water data, resulting in:

$$\psi = 3.5 \qquad (A.18)$$

The experimental results with **FC-72** showed that wall superheat at the ONB appeared to be independent of subcooling or flow rate. For this liquid the equations based on the r_{tan} criteria failed for about 14 K, out of 18 K, and the equation based on the r_{max} criteria predicted cavity sizes of 0.3-0.4 μm, for the same test surface where with water

predicted cavity sizes of 5.0-8.0 μm. They examined the surface with a microscope and find cavities as large as 50 μm and large population of cavities of 0.5 to 10.0 μm. From these observations they concluded that both equations were invalid to predict the ONB in FC-72 falling films.

They concluded that for highly wetting fluids the nucleation process started inside the cavity, and the ONB was independent of the temperature distribution outside of the cavity. The true important variable was the initial vapour embryo radius. From a numerical integration of the thermo-mechanical equilibrium equation, based on the Clapeyron equation, they observed that for a wall superheat of 15 K, the embryo curvature radius for FC-72 should be of 0.224 μm, one order of magnitude smaller than the typical cavity radius detected by microscopic photographs.

Lee, T.Y. and **Simon, T.W.** (1989) undertook experimental work with subcooled flow of FC-72 over small platinum heat sources, in a rectangular channel. They reported that the wall superheat at the ONB and the temperature overshoot depended on the mass flow rate and on the subcooling. Wall superheat diminished with increasing mass flow rate from $\approx$ 38°C @ 2.46 m/s to $\approx$ 22°C @ 8.62 m/s, and the TOS was reduced from 16 K to zero. They found that as the subcooling increased the temperature overshoot and the wall superheat at the ONB increased. At low subcooling ($<$ 24 K), the TOS disappeared. Only a weak relationship between wall superheat and pressure was found:

Pressure Kpa	Wall superheat °C	Temperature Overshoot K
274	29.1	9.4
205	27.4	6.1

Tong, W.; Bar-Cohen, A.; Simon, T.W. and **You, S.M.** (1990), carried out a theoretical analysis of the influence of the contact angle hysteresis on the bubble growth process. The contact angle was affected by both liquid and solid characteristics. Solids may experience adsorption and oxidation. Liquids may experience chemical reactions at the solid-liquid interface and possess and/or develop impurities, which tend to concentrate at the interfaces. The contact angle is also affected by the state of motion of the liquid-solid-gas boundary, static ($ß_s$) and dynamic ($ß_d$), and the dynamic contact angle has different values for advancing and receding liquid fronts when surfaces are even slightly rough. They tried to modify the **Lorenz, Mikic and Rohsenow** (1974) vapour/air trapping model by introducing the effects of the dynamic contact angle, which resulted in an almost similar equation. From this model they observed that for well wetting liquids, even with large dynamic contact angles, bubbles at critical radius always occurs inside the cavities. They derived an equation to predict the ONB, based in a typical thermo-mechanical equilibrium analysis, including the effects of the static and dynamic contact angles, and recommended using the wall temperature value, rather than the liquid temperature, to evaluate the vapour pressure and the surface tension:

$$\exp\left(a - \frac{b}{T_w}\right) - P_f = \frac{2\,\sigma\,T_w}{R_o\,f(\beta_s,\,\beta_d,\,\phi)} - \sum P_g^* \qquad (A.19)$$

where a and b are correlation coefficients, R_o is the cavity radius, ϕ is the cavity angle, P_g^* is the partial pressure of a different gas within the bubble and:

$$f(\beta_s,\,\beta_d,\,\phi) = \frac{\sqrt{1 - \frac{2\,\phi}{\beta_d}}}{\sqrt[3]{\left(1 + \phi\left[2 - 3\left(\beta_s - \phi\right) + \left(\beta_s - \phi\right)^3\right]\right)}} \qquad (A.20)$$

You, S.M.; Simon, T.W.; Bar-Cohen, A. and **Tong, W.** (1990) conducted experimental work on pool boiling with saturated R-113 at 1 atm using chromel wires and platinum surfaces. They questioned the validity of assuming the slope of the T-P curve to be constant, during the integration of the *Clapeyron* equation for the case of well wetting fluids since a significant error in the calculated liquid superheat occur with substances where large temperature overshoot occur. They concluded that the mechanism of incipience for highly-wetting fluids might be different than that of poor-wetting ones, since:

- on a given surface there will be larger number of active embryos with poor-wetting fluids than with highly-wetting.
- the residual bubble in highly-wetting liquids was small and

represents the configuration of minimum radius of curvature in its eventual growth. It required the maximum wall superheat of the bubble's life.

It was recommended that the surface tension is evaluated at the wall temperature rather than at the bulk temperature.

They ran a series of ostensively identical, computer-controlled tests, starting from zero heat flux and increasing power to a maximum value. Ten different results were obtained in ten runs for the wall superheat at the ONB, with no discernible tendency. Therefore they decided to display the results by statistical or probability means, and a graph of probability of boiling incipience vs. wall superheat at the ONB was presented, with ten measurements ranging from 23°C to 39°C. Timely variations in the wall superheat during convection but close to the point of incipience, showed that two standard deviations over a 50 s period amounted up to 2°C. They attributed the large unsteadiness and poor repeatability to the good wetting characteristics and variations of the fluid contact angle. They ran identical tests with a second cut of chromel wire, taken from the same manufactured run as the first, and the obtained boiling curve was different from the first.

Tests were run where the heat flux was decreased, after being in a fully nucleate boiling condition, down to a certain non-zero value, and after 1 min increased again to another, fixed, higher value. In the first run the lowest point still was in the partially developed boiling zone, and the reheating curve followed the same path than the cooling

curve. In the second run the lowest point was lower than in the first, but still in the partially developed boiling zone; the reheating curve shifted to the right slightly. In the third run, the lowest point reached was at the lowest end of the partially developed boiling zone, where no visible bubbles were left. For this case the reheating process shifted even more to the right and only two sites reactivated. In the fourth run, where the heat flux was decreased into the convective zone, the reheating process required a greater shift to the right than the original heating process since no sites reactivated.

They noted that this behaviour was consistent with the hypothesis that, for highly wetting fluids, the minimum radius of bubble embryos was attained within the cavity, and not at the cavity's mouth. Much larger wall superheats (50 to 72.5°C) and temperature overshoots (up to 53 K) are observed by using the platinum heater, which was much smoother than the chromel wires. Increases in the temperature overshoots (20%) were also observed by running tests where the heat flux was incremented in large steps between steady states.

You, S.M.; Simon, T.W. and **Bar-Cohen, A.** (1990), conducted experimental work using pool boiling with very low fluid circulations (less than 0.55 l/min) of FC-72, using a silicon surface. Parametric effects of pressure, subcooling and dissolved gas on the wall superheat at the ONB were investigated. The experiment was computer-controlled to step through precisely the same heat flux conditions from run to run. The reported values were averaged over 20 samples taken over 50 s periods. They

found again poor reproducibility between runs and adopted also the use of probabilistic representation to display their results.

They ran 56 runs as base case, in 5 different days spread over a 7-week period, using very similar conditions, to obtain five cases. The graph of probability (of ONB) vs. wall superheat from those cases showed wall superheat variations from 18°C up to 41°C, obtaining an area, or band, that enclosed all the 56 runs' data. This band was then used to compare the parametric effects of the variables of interest.

The tests for subcooling (10 runs and 28 K of subcooling), dissolved gas content (10 runs) and pressure (2 runs at a higher pressure), all gave results lying inside the base band. Only one test, which was run at a high dissolved gas content 0.005 moles/mol (compared with others at 0.001 to 0.004 moles/mol), produced results where the wall superheat was less than expected.

Hahne, E.; Spindler, K. and **Shen, N.** (1990). By equating the thermo-mechanical bubble equilibrium equation to an assumed linear temperature profile in the boundary layer, they derived **Sato and Matsumura**'s equation and then used the definition of convection heat transfer coefficient to eliminate the heat flux. Since well wetting fluids flood larger cavities, including those with radius of the critical size, the largest of the surviving was named as r^* and this term was inserted in their equation. This was equivalent to the criteria of the largest available cavity radius, from Hino and Ueda, only that here it was the largest of those which could survive being flooded by a

refrigerant. Since several other authors had reported very small experimental values for r^* (0.22 - 0.4, 0.01 - 0.1 μm), they inserted such values into their equation and then they noticed that the ratio h r^*/k was of the order of 1 x 10^{-3}, and it was simply neglected. The resulting effect was that the bubble temperature was then equal to the wall temperature and they concluded from this that the bubble should be located **within** the microstructure of the wall. In their equation the ratio 2 σ / r^* was the only unknown and they performed experiments and used the results, together with data from some other authors, to show that such ratio was a constant for a particular liquid. (They found one value for R-12 and other for R-11 and R-113.) They recommended using their two equations to predict the wall superheat at the ONB. (A close analysis of the equations revealed that if added together, they reduce to the definition of the forced convection coefficient).

Mizukami, K.; **Abe, F.** and **Futagami, K.** (1990) undertook theoretical work to investigate the effect of the contact angle and cavity shape on the boiling inception condition. Existing models to predict the ONB were classified as:

- *Mechanical*, when they depend on the most stringent suppression condition, and not in the heat flux. Such condition existed because the cavity was re-entrant and/or the contact angle was variable somewhere inside the cavity.
- *Thermal*, based on the loss of thermal equilibrium of a bubble

nucleus sitting on the cavity mouth. they depended on the heat flux.

Some nucleii inside cavities could collapse during liquid subcooling and some could survive. From the surviving nucleii, the most favourable cavity was the first that initiates boiling. Their *mechanical* model consisted of determining the shape of such cavity. Cylindrical and conical cavities could not trap vapour during liquid subcooling, therefore it was necessary to have a re-entrant shape. They analyzed shapes and angles of idealized re-entrant cavities (cylindrical, conical with sharp edges and conical with rounded mouth edges), and derived two equations for the bubble curvature radius in terms of the cavity angle, static contact angle, receding contact angle, advancing contact angle and cavity re-entrant-neck radius, which should predict the size of the most favourable cavity for boiling inception. Since their equation required knowledge of the maximum cavity characteristic angle and the value of 70° is assumed to be valid for naturally formed cavities on commercial surfaces.

You, S.M.; Simon, T.W. and **Bar-Cohen, A.** (1991), conducted an experimental study using pool boiling of FC-72. The behaviour of the bubble curvature radius as a result of the cavity geometry was analyzed and sketches of the inverse of the bubble curvature radius vs. bubble volume were presented. For well wetting fluids, they observe from the curves, the incipient bubble was probably far inside the cavity. They analyzed the boiling cessation process (in a conical cavity) in terms of the pressure inside the

bubble vs. the bubble curvature radius, and showed that a well wetting fluid bubble would either grow or collapse in such geometry. They mentioned that a similar scenario would proceed for a re-entrant cavity but no further analysis was given.

When the wall temperature dropped to lower values, after being in nucleate boiling, all the bubble nucleii would simply collapse and therefore boiling for the next heat-up cycle must be initiated by homogeneous nucleation. Nevertheless, experimental observations showed that initiation of boiling was a heterogeneous case, therefore a mechanism should exist such that prevents the bubble nucleii from collapsing. They attributed this to traces of residual non-condensable gases in the working fluid. An analysis of the mass transfer (diffusion) of gas through the liquid and the bubble nucleii interface was given, and it was argued that the wall superheat produced a temperature profile in the adjacent layer of liquid, therefore the layer could become *degassed*. Therefore is not just necessary to have high gas concentrations, but something has to be done to reduce the gas concentration gradient in the liquid layer, close to the wall.

Experiments were run to observe the effect of stirring the working fluid, and some others to observe the effect of bubbles, from a secondary heater in fully developed boiling, sliding over the test heater. A magnetic stirring bar, 2.5 cm long, was used at $\approx$ 7 cm from the test surface, and the results showed:

- unstirred, gassy and no-gas tests, high wall superheats and temperature overshoots were obtained, of almost the same magnitude for both liquids.

- stirred, no-gas, produced wall superheats and temperature overshoots only slightly smaller than those with the unstirred case.
- stirred, gassy, WS strongly reduced, to $\approx$ 4°C compared with $\approx$ 25°C for the unstirred case, and zero temperature overshoots.

For the case of bubbles sliding over the heater surface, compared to the secondary heater only in convective heat transfer, the wall superheat at the ONB reduced from 26°C to 14°C and the temperature overshoot from 11 K to zero.

Appendix B

CORRELATIONS FOR THERMODYNAMIC AND TRANSPORT PROPERTIES FOR R-11 AND WATER

A. Introduction.

In this appendix curve fitted correlations for saturation temperature $T_s(P)$, vaporization volume $v_{fg}(T_s)$, vaporization enthalpy $h_{fg}(T_s)$ and surface tension $\sigma(T_s)$, for refrigerant R-11 and water, are presented.

The thermodynamic properties of the refrigerant were previously published by **Martín-Domínguez and McDonald** (1992a).

The tabular property data for the refrigerant were obtained from **ASHRAE Fundamentals Handbook** (1989) and for water from **Wark** (1988).

Graphs are presented to show the accuracy of the correlations to reproduce the tabular data, the incurred error is shown as a temperature deviation in K for the saturation temperature and as a relative error for the other properties.

B. Saturation Temperature.

The correlation equation for the saturation temperature, as a function of pressure, for the refrigerant R-11 was of the form:

$$T_s = \exp\left[\left\{A + B\ln(P_r) + C\ln^2(P_r) + \cdots \atop \cdots + D\ln^3(P_r) + E\ln^4(P_r)\right\}^{-0.4}\right] \qquad \text{(B.1)}$$

And for water the equation was of the form:

$$T_s = \exp\left[A + B\ln(P_r) + C\ln^2(P_r) + D\ln^3(P_r)\right] \qquad \text{(B.2)}$$

The coefficients in equations (B.1) and (B.2) are given in Table B.1. Figure B.1 shows, over the complete range of the source, the data, the fitted curve and the absolute error between the fitted curve and the data. Figure B.2 shows the saturation temperature results for water.

The error graph in Figure B.2 shows that the source data has a print error for the data point at 13,730 kPa, 336.15°C (610 K), of about 2°C, which probably should read 334.15°C.

C. Vaporization Volume.

The equation utilized to correlate the vaporization volume for both R-11 and water was of the form:

$$v_{fg} = \exp\left[A + B\ln^{0.15}\left(T_r^{-1}\right) + C\,T_r^{-2} + D\,T_r^{-3} + E\,T_r^{-4}\right] \qquad \text{(B.3)}$$

The coefficients for equation (B.3) are given in Table B.2. Figure B.3 shows the data points, the fitted curve and the relative error for R-11 and Figure B.4 shows the

results for water. The data points for these correlations were obtained by subtracting v_f from v_g in the original source data. The two peaks in the error graph, shown in Figure B.4, are clearly print errors from the source data, but is hard to know which from v_f or v_g was wrong for those points.

D. Vaporization Enthalpy.

The equation form used to correlate the vaporization enthalpy, for both substances, was of the form:

$$h_{fg} = \exp\left[\sqrt{A + B \ln^{0.1}\left(T_r^{-1}\right) + C\, T_r^{-2} + D\, T_r^{-3} + E\, T_r^{-4}}\ \right] \qquad (B.4)$$

And the corresponding coefficients are listed in Table B.3. Figure B.5 shows the data points, fitted curve and relative error for R-11. Figure B.6 shows the results for water.

E. Surface Tension.

The equation for used to correlate the saturation surface tension, for both substances, was of the form:

$$\sigma = \exp\left[\, A + B\left(T_c - T_s\right) + C \ln\left(T_c - T_s\right) + D \ln^2\left(T_c - T_s\right)\,\right] \qquad (B.5)$$

And the correlation coefficients are given in Table B.4. Figure B.7 shows the data points, fitted curve and relative error for R-11. Figure B.8 shows the same results for

water.

Table B.1. Correlation coefficients for saturation temperature.

Substance:	R-11	Water
Pressure range:	2.6 to 3910 kPa	0.611 to 22120 kPa
A	1.063259194E-2	6.4736174489911
B	-6.6783043E-4	0.13648987578272
C	-1.07995994E-5	0.00752072071331
D	1.801004211E-6	0.000225354281899
E	1.482008243E-7	0.0
P_c	4410 kPa	22120 kPa
Error:	-0.037% to 0.028%	-0.32% to 0.08%

Table B.2. Coefficients for the vaporization volume.

Substance:	R-11	Water
Temperature range:	-70 to 190°C	0°C to 374.15°C
A	-11.0801463813	-10.808164111
B	5.420401818782	5.5308283665
C	2.05471177521	2.61649434736
D	-0.17077480986	-0.3380593481
E	-1.63205656E-3	0.01711204115
T_c	198.15°C	374.15°C

Table B.3. Coefficients for the vaporization enthalpy.

Substance:	R-11	Water
Temperature range:	-70 to 190°C	0°C to 374.15°C
A	-13.875226886	-4.4295797857
B	50.8040440667	77.6363990203
C	-8.5805955177	-9.2928341324
D	5.66096573451	5.00643795881
E	-1.1182456824	-0.8022342869
T_c	198.15°C	374.15°C

Table B.4. Coefficients for the saturation surface tension.

Substance:	R-11	Water
Temperature range:	-110 to 190°C	0°C to 374.15°C
A	-10.205005037154	-8.75854031224
B	-3.072918536511E-4	-2.20689503E-3
C	1.1111543433311	0.831212366136
D	1.8845549343159E-2	5.9213092279E-2
T_c	198.15°C	374.15°C

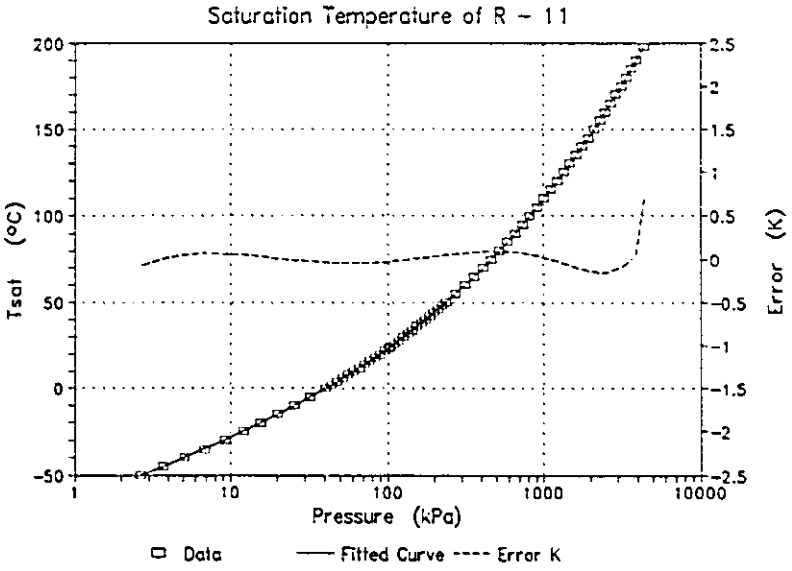

Figure B.1. Saturation temperature of R-11.

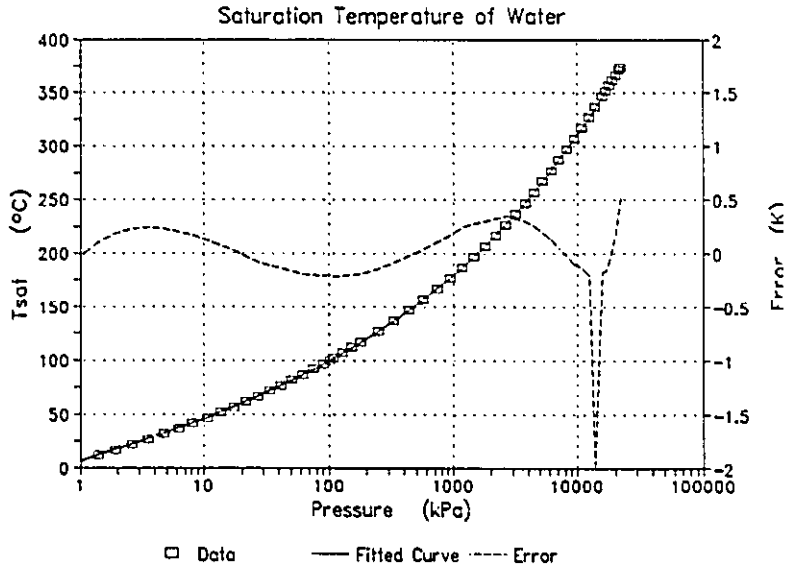

Figure B.2. Saturation temperature for water.

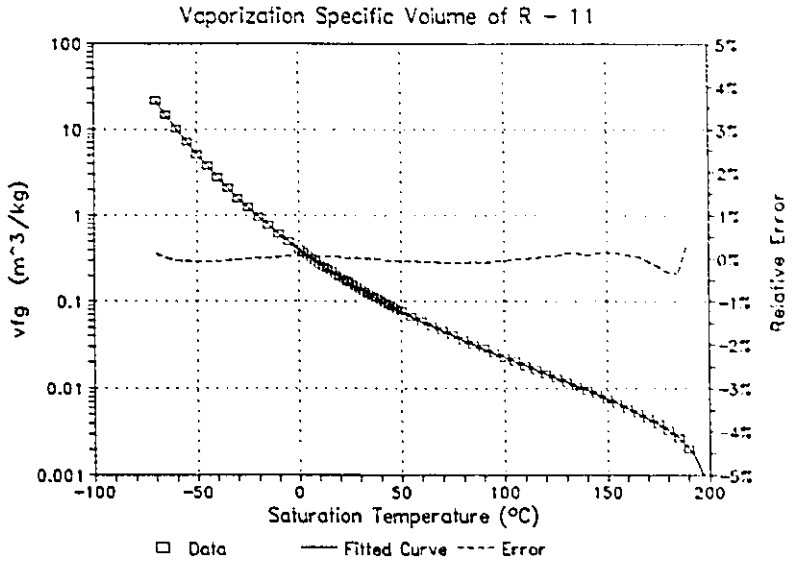

Figure B.3. Vaporization volume of R-11.

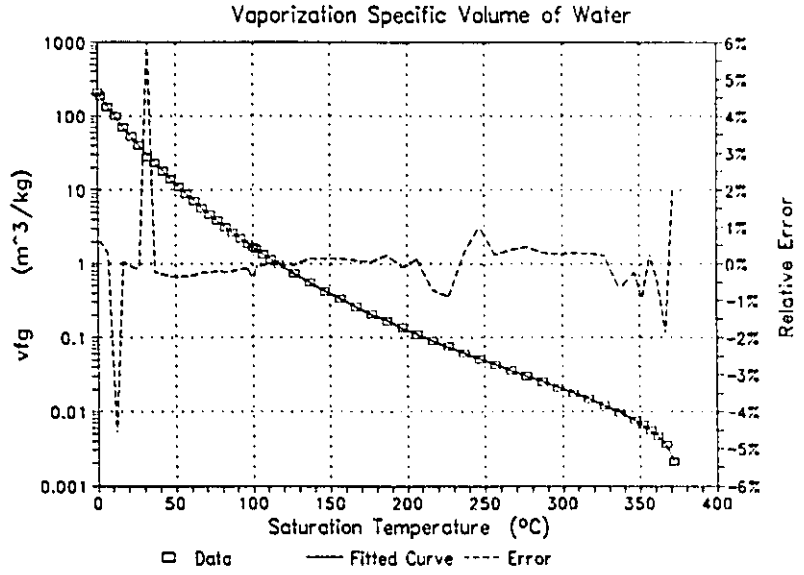

Figure B.4. Vaporization volume for water.

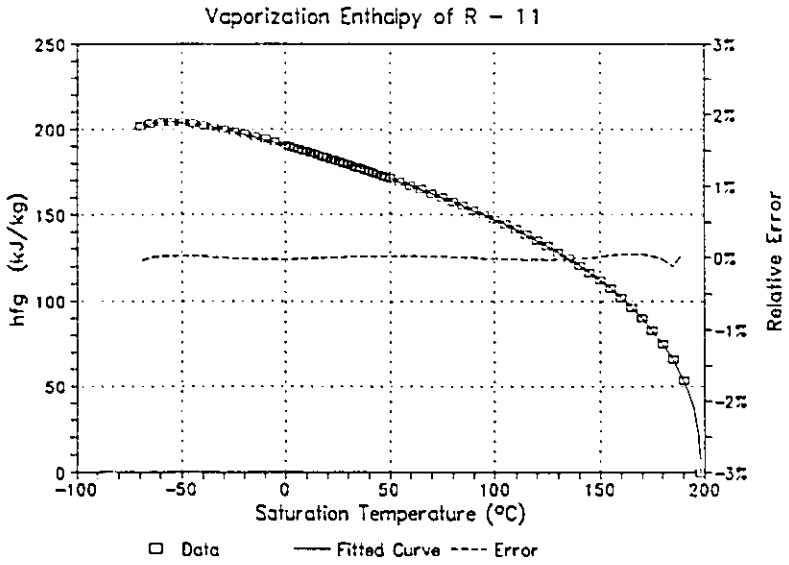

Figure B.5. Vaporization enthalpy of R-11.

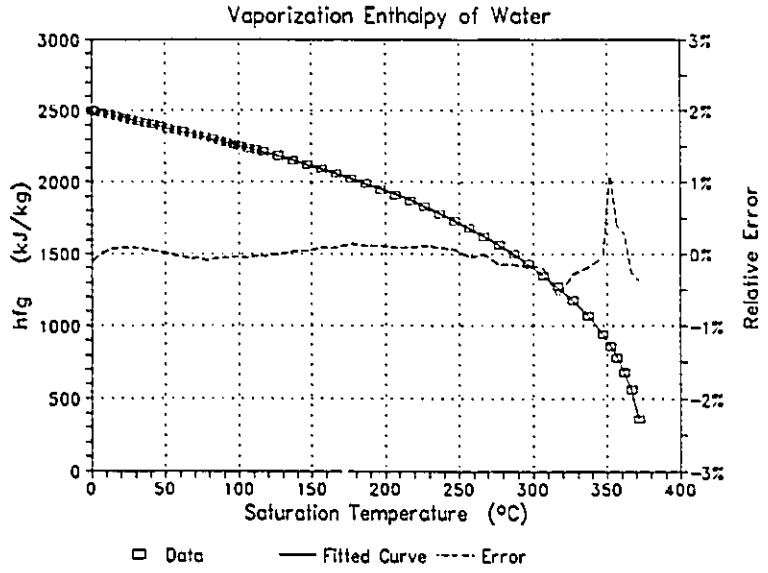

Figure B.6. Vaporization enthalpy of water.

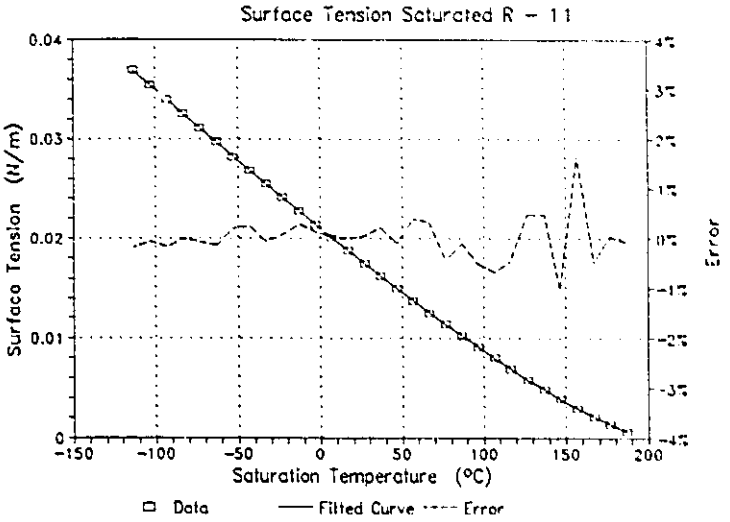

Figure B.7. Saturation surface tension of R-11.

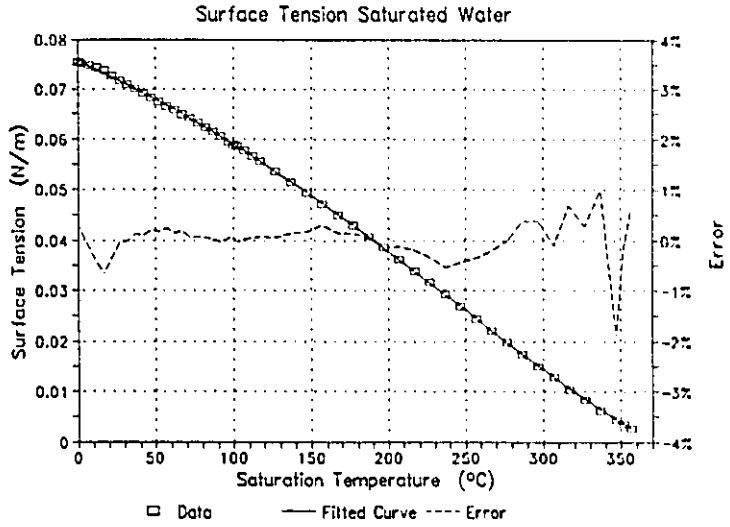

Figure B.8. Saturation surface tension of water.

INDEX OF AUTHORS

VITA AUCTORIS

Name:		Ignacio Ramiro Martín Domínguez
Place of birth:		Chilpancingo, Guerrero. México.
Date of birth:		July 29 of 1955
Education:	1974	**High School Certificate.** Durango Technological Institute. Durango City, Dgo. México.
	1978	**Bachelor of Sciences.** Industrial-Mechanical Engineering. Durango Technological Institute. Durango City, Dgo. México.
	1984	**Master of Science.** Mechanical Engineering. National Polytechnic Institute. México City, México.
	1985-1986	**Advanced Studies.** Institute of Turbomachinery. University of Hannover. Germany.
	1989-Date	**Ph. D. Candidate.** Mechanical Engineering. University of Windsor, Ontario. Canada.
Professional Experience:	1980	**Mexican Petroleum Institute.** Project Engineer. México City, México.
	1982	**Metropolitan Autonomous University-Azcapotzalco.** Lecturer. México City, México.
	1984	**Centre of Engineering and Industrial Development.** Project Engineer. México City, México.

1986 **Electrical Research Institute.** Research Engineer. Cuernavaca, Mor. México.

1989-Date **University of Windsor.** Research and Teaching Assistant. Windsor, Ontario. Canada.

Publications:

Preliminary Design of a Fishfreezer in Durango City, Dgo. (in spanish) B.Sc. Thesis. Durango Technological Institute. Durango City, Dgo. México. 1978.

Importance of the State Equation in the Analysis of a Natural Gas Flow in Long Ducts with Friction, Heat Transfer and Level Changes. (in spanish) M.Sc. Thesis. National Polytechnic Institute. México City, México. 1984.

Martín-Domínguez, I.R. and McDonald, T.W. *Correlations for Some Saturated Thermodynamic and Transport Properties of Refrigerant R-11.* Memorias (Procc.) XVI Reunión Nacional de Energía Solar. 7-9 Oct. 1992, Oaxaca, Oax. ANES (Asociación Nacional de Energía Solar). pp.232-236 México.

Martín-Domínguez, I.R. and McDonald, T.W. *Correlations for Some Saturated Thermodynamic and Transport Properties of Refrigerant R-113.* Memorias (Procc.) XVI Reunión Nacional de Energía Solar. 7-9 Oct. 1992, Oaxaca, Oax. ANES (Asociación Nacional de Energía Solar). pp.237-241 México.

Martín-Domínguez, I.R. and McDonald, T.W. *Correlations for Some Saturated Thermodynamic and Transport Properties of Refrigerant R-22.* ASHRAE Transactions: Research. v.99 Pt.1 pp.344-348 1993.